FINAL REPORT

Methods to Reduce Lateral Noise Propagation from Seismic Exploration Vessels

Contract M07RS13346
Issued by the Minerals Management Service
U. S. Department of Interior

Proposal Objective:

Item 5:

"Reduce Lateral Noise Propagation from Seismic Exploration Vessels."

April 2009

Contractor:

Stress Engineering Services, Inc
PN 117168

Contact: Ray R. Ayers, Ph.D., P.E.
Phone: (281) 955-2900
E-mail: Ray.Ayers@Stress.com
13800 Westfair East Drive
Houston TX 77041

STRESS ENGINEERING SERVICES INC.

DISCLAIMER

This report has been reviewed by the Minerals Management Service and approved for publication. Approval does not signify that the contents necessarily reflect the views and policies of the Service, nor does mention of trade names or commercial products constitute endorsement or recommendation for use.

TABLE OF CONTENTS

PAGE NO.

APPENDICES:

LIST OF TABLES

PAGE NO:

LIST OF FIGURES

METHODS TO REDUCE LATERAL NOISE PROPAGATION FROM SEISMIC EXPLORATION VESSELS

Ray R. Ayers, PhD, P.E.
Stress Engineering Services, Inc.
Houston, Texas, USA

Warren T. Jones, PhD, P.E.
Consultant
Houston, Texas, USA

David Hannay, M.Sc.
JASCO Research, LTD.
Victoria, B.C., Canada

EXECUTIVE SUMMARY

Abstract

This paper covers the development of methods and equipment for reducing lateral noise propagation from seismic exploration vessels operating in the Alaskan Beaufort and Chukchi Seas. Oil exploration activities are currently taking place or are planned, and there is a need for creating methods and equipment to reduce lateral noise propagation from seismic exploration.

This project is supported by the U.S. Minerals Management Service, which has the responsibility and authority to ensure that oil and gas exploration and production activities are conducted in a safe and environmentally sound manner.

This research effort includes a literature synthesis and review to identify existing seismic exploration technologies (airguns) and involves developing promising methods and technologies that could potentially reduce the lateral propagation of sound from those airguns.

Three principal areas have been explored: (a) Attenuating lateral noise with air bubble curtains, like has been shown in the literature, or with some special bubble curtain material, acting as a more solid curtain-like barrier, (b) Making arrays more directional, and thus narrow the cone of sound, and (c) Changing the structure of the

airguns to reduce high frequency sound (noise) while maintaining the strong source signal needed for exploration purposes.

This paper (a) describes our preliminary findings in each of the above areas and (b) shows that deploying bubble curtains outboard of the seismic arrays towed by the same exploration vessel can potentially produce the sought-after noise reduction, while the minimizing impact on the traditional seismic exploration operations.

Introduction

A project is underway which is aimed at creating methods and equipment for reducing lateral noise propagation from seismic exploration vessels operating in the Alaskan Beaufort and Chukchi Seas where oil exploration activities are currently taking place or are planned.

The Minerals Management Service (MMS), an agency of the U. S. Department of Interior, has the responsibility and authority to ensure that oil and gas exploration and production activities have a minimal impact on the environment and are conducted in a safe and environmentally sound manner.

This MMS-funded research effort includes a literature synthesis and review to identify existing seismic exploration technologies associated with firing airgun arrays, and developing promising methods and technologies that could potentially reduce the lateral propagation of sound from those airguns. Included in the scope is evaluation, assessment and comparison of noise reduction technologies that could be used to reduce the lateral propagation of sound sources from seismic exploration vessels. Excluded in this project is an investigation of specific effects of acoustic noise on the various marine mammals.

The specific objective of this research is to discover and provide analytical proof-of-concept of a reliable cost-effective method and equipment to significantly reduce lateral noise from seismic airgun activities in the Alaskan Beaufort and Chukchi Seas. Implied

in this objective is that we want to minimize detrimental effects to the source signal while we are reducing lateral noise.

Conclusions and Recommendations

1. Of all of the concepts for lateral noise reduction considered, the simple air bubble curtain, produced by a streaming manifold on either side of the marine seismic exploration vessel, outboard of the airgun arrays, was found to be the most practical.

2. Fluid dynamics analyses and design of the air bubble curtain provided key sizing information for the manifolds, nozzles, air pressure and compressor horsepower requirements, and bubble parameters needed for the acoustic analysis.

3. Acoustic analysis results show that that deploying an air bubble curtain outboard of marine seismic vessels to reduce lateral noise could achieve a noise reduction of 20 dB or more.

4. Contrasted with deployment of more massive structural barrier systems, deployment of air manifolds – simple inexpensive hoses streaming on either side of the vessel - was relatively simple, and that the operational reliability of such manifolds should be relatively high.

5. The acoustic analysis needs to be expanded to a three-dimensional analysis, and the shallow-water seafloor effects should be included.

6. Other possible air bubble curtain arrangements, such as twin curtains on each side of the seismic vessel, should be explored to improve performance.

7. Where practical, key analysis assumptions having a large effect on system performance should be physically tested.

TYPICAL MARINE SEISMIC OPERATIONS

Following is a brief overview of the marine seismic operation as taken from Dragoset (2000) and Caldwell and Dragoset (2000). Please refer to those sources for a more complete explanation.

The primary method of producing a marine seismic source for subterranean oil/gas exploration is by firing an airgun (see Figure 1) underwater. The airgun is like a pneumatic cylinder “exploding” through a small orifice.

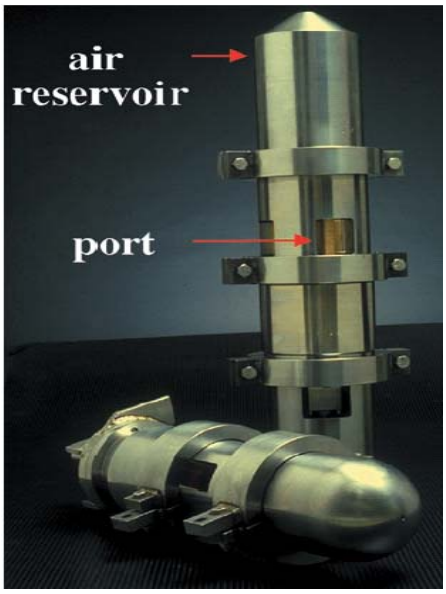

**Figure 1. Two typical internal shuttle airguns.
From Dragoset (2000).**

Airguns produce underwater sounds by rapidly releasing highly compressed air into the surrounding water. The pressurized bubble is initially small but starts to increase in size before undergoing damped oscillations. The resulting acoustic pressure wave is proportional to the pressure variation within the oscillating bubble. It has a high primary pressure peak corresponding to the initial release of air followed by a series of secondary peaks associated with the subsequent volume minima that occur as the air bubble oscillates in size. The secondary peaks are referred to as bubble pulses and these are undesirable from a seismic imaging perspective. The period between bubble pulses increases with the volume of the airgun chamber, and airgun arrays use this

feature to suppress bubble pulses by simultaneously firing multiple airguns with different volumes. The primary pulses occur at the same time so their pressures add coherently while the bubble pulses do not.

The acoustic signature (pressure wave) produced by a single airgun is like that shown in Figure 2:

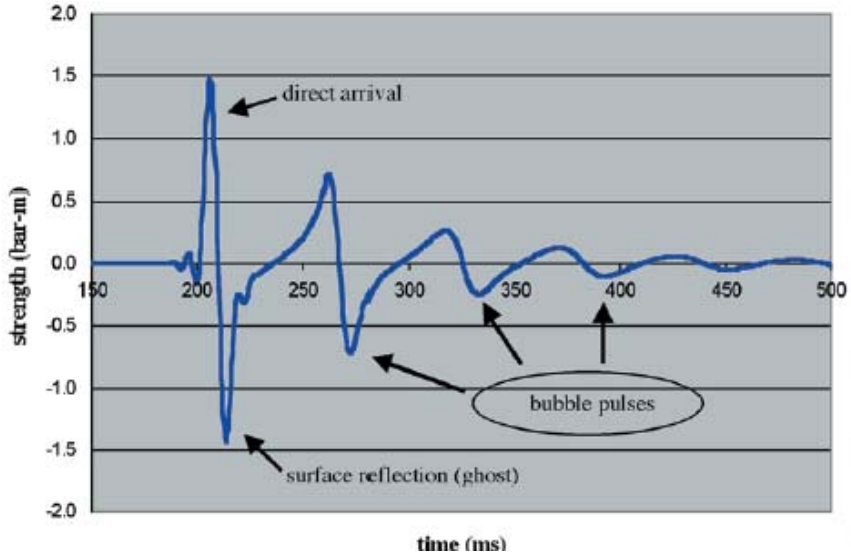

Figure 2. Signature of a single 40 cu. inch airgun as recorded by hydrophone. From Dragoset (2000).

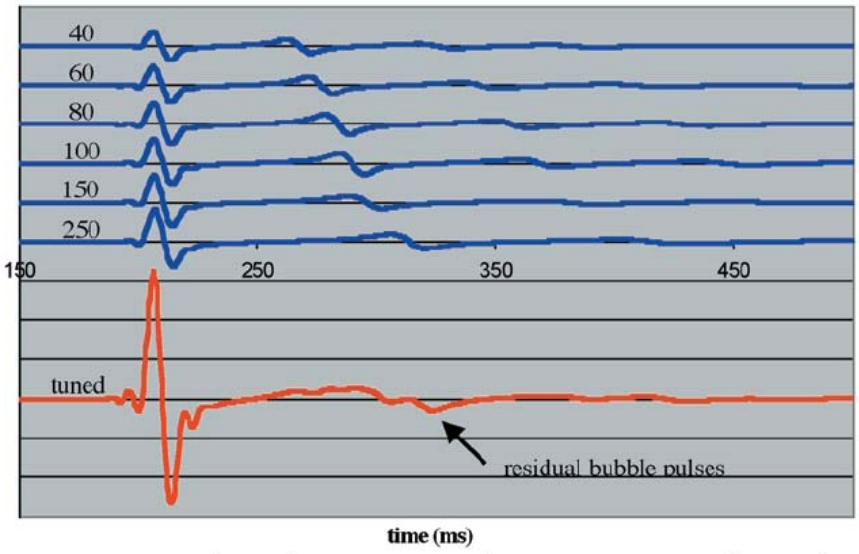

Figure 3. Concept of a "tuned" airgun array. From Dragoset (2000).

In Figure 3, blue-colored signatures come from individual guns whose volumes, in cubic inches, are shown on the left. If these six guns are placed in an array and fired simultaneously, they produce the red signature as measured at a hydrophone 305 m (1000 feet) below the array according to Dragoset (2000).

Following, in Figure 4, is a photographic overview of a marine seismic array and a sketch of the airgun configurations in the array.

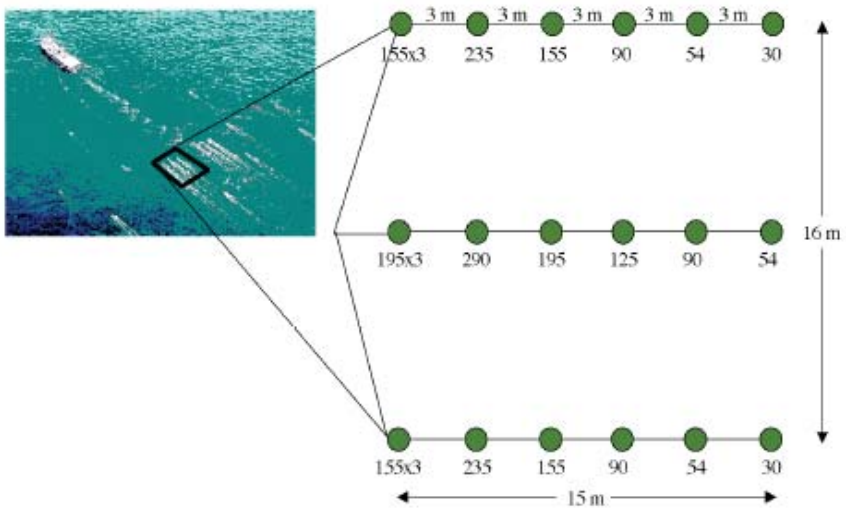

Figure 4. Plan view of a typical airgun array. Numbers below the gun stations (green circles) are gun volumes in cubic inches. From Dragoset (2000).

To complete our overview of marine seismic operations, Figure 5 shows a portion of the airgun arrays on deck similar to that deployed in the water in Figure 4:

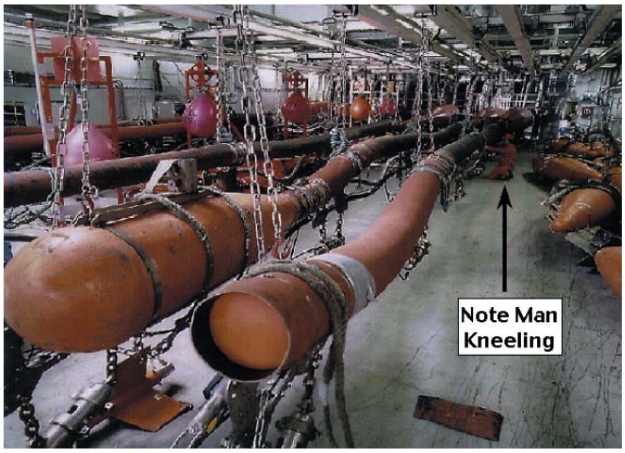

Figure 5. Portion of airgun array on deck. From Caldwell & Dragoset (2000).

The valuable purpose of the seismic exploration operation is to generate acoustic pulses like that shown in Figure 6.

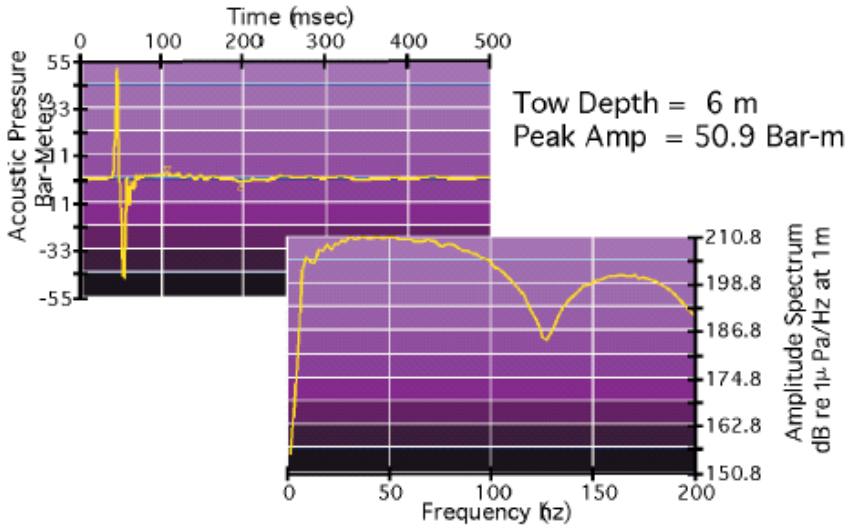

Figure 6. Back-calculated source signature and amplitude spectrum for a 3397 cubic inch array. From Caldwell & Dragoset (2000).

Based on the above overview information on marine seismic operations, it is possible to explain this noise reduction research project objective as attempting to reduce the lateral noise from seismic array without affecting peak amplitude of the source projecting through the seabed. Referring to the lower right-hand plot of Figure 6, we

wish to reduce the amplitude of the frequencies above approximately 100 Hz emanating laterally from the source.

TECHNICAL APPROACH

The technical approach we have taken involves:

1. Performing a brief literature investigation of currently used technologies for marine acoustic wave propagation as well as methods of noise reduction.

2. Using a previously developed analytical model of the physics of marine acoustic wave production and propagation. This analysis method is essential in performing analyses of the candidate concepts for noise reduction.

3. Using the Scientific Method (analysis, synthesis, and hypothesis) and other inventive methods including "old fashioned discovery" to identify candidate methods and equipment to reduce lateral noise for further evaluation.

4. Using engineering analysis and engineering judgment to rank-order the potential performance and potential reliability of the candidate lateral noise abatement techniques. Task 2 above will provide the analysis method(s) for estimating performance.

5. Proposing simple proof-of-concept testing methods to determine the best candidate method and equipment in terms of performance and reliability.

LITERATURE REVIEW

Our literature search immediately found two technical papers written by Bill Dragoset of Western Geophysical that provided an excellent introduction to airguns and airgun arrays used in marine seismic operations See Dragoset (2000) and Caldwell & Dragoset (2000). These papers satisfied our needs for describing currently-used

marine seismic operations. A second major finding was a 2007 Joint Industry report, Spence (2007) entitled “Review of Existing and Future Potential Treatments for Reducing Underwater Sound from Oil and Gas Industry Activities” written by Jesse Spence and others. We found that this JIP report contained a better literature search than we could generate from our smaller project funds, so these very-current and applicable search results satisfied our needs for a literature study. Of specific interest in the Joint Industry report was the air curtain concept for lateral noise reduction of marine seismic operations that was tested in Venezuela by Sixma (1996) and Sixma and Stubbs (1996).

SEARCH FOR NOISE REDUCTION OPTIONS

After the initial part of the literature search found papers on marine seismic noise control by Mr. William Dragoset, we contacted him and sought out advice. Mr. Dragoset has spent his career in marine seismic work for Western Geico, designing airgun arrays for seismic exploration of oil and gas. He told us to look in three areas to find potential areas for noise reduction:

1. Attenuate lateral noise with air bubble curtains, like has been shown in the literature, or with some special bubble curtain material, acting as a more solid barrier.

2. Make arrays more directional, and thus, narrow the cone of sound.

3. Change the design of airguns to reduce high frequency sound (noise) while maintaining the strong source signal needed for exploration.

But what are the attributes of a “good solution” for noise reduction of a marine seismic system? From personal experience of the primary author with developing airgun float systems for the RV Shell America, see Ayers (1988), the following attributes were determined to be the most appropriate:

- High reliability of any deployed noise reduction towed systems
- Low weight and volume to handle
- Easy to deploy, recover and store
- Low continuous horsepower requirement of any powered noise reduction system
- Low drag of deployed and towed in-the-water systems
- Low risk of physical interference with standard towed seismic arrays and listening systems.
- Low risk of detrimental acoustic interference with standard towed seismic arrays and listening systems.
- Minimum changes to the standard marine seismic system

With these attributes in mind, we focused on each the three areas for noise reduction above. We used traditional brainstorming to develop possible concepts to consider.

The preferred bubble curtain concept is shown in Figures 7 and 8.

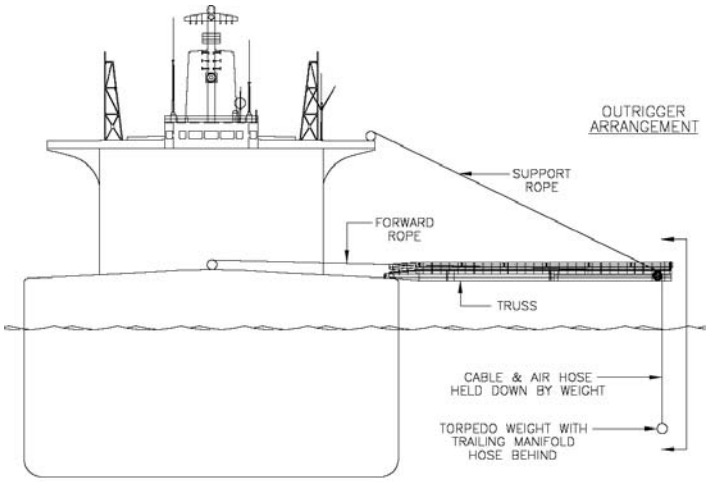

Figure 7. Front profile of bubble curtain outrigger arrangement.

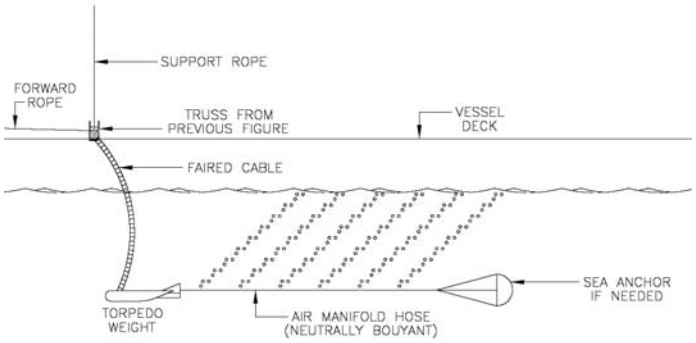

Figure 8. Side profile of bubble curtain concept.

Opportunities for Noise Reduction

We accepted the advice from Mr. Dragoset and came up with the following opportunities for noise reduction:

1. *A towed air bubble hose*, like that depicted in Figures 7 and 8 and tested in 1996 by Sixma (1996) is very simple to set up and operate, and it causes only minimal fluid drag, making the support system relatively light. This is a direction that is very promising. Bubble curtains are already being used to reduce noise from static noise sources. If a physical curtain, perhaps having bubbles imbedded, is used, the fluid frictional drag on the "flag" will require higher forces in the support structure, and could be fraught with flutter, creating additional drag. Durability of the curtain is an issue over time in use, and deployment and recovery of the curtain will be an issue not found in air bubbles, since there is no physical curtain.

2. *Making arrays more directional* is more the responsibility of the geophysical operator and its oil company client. Thus, we did not believe that we should interfere with that relationship. The MMS can suggest that the responsible people consider this potential opportunity. Even so, we considered towing a parabolic reflector to be deployed over the towed arrays. If such a reflector could be deployed successfully, the arrays can be focused. But deploying such a

structure, and towing it behind the vessel, along with the arrays and streamer cables, might be a very risky effort.

3. *Changing the structure of airguns* to add lateral noise reducers without affecting the required source signal would mean that the airgun manufacturers, Bolt and Sercel, would have to develop and test a totally new product – and such a development would be outside the scope and funding of this relatively small research project.

Steps Forward

In collaboration with Mr. John Ward of Shell, an interested industry participant in our project, we visited Noise Control Engineering, Inc. in Billerica MA, and commissioned some initial acoustic analysis work by Mr. Jesse Spence, whose work is cited above. Mr. Spence used the commercial software, Comsol(TM), to calculate the potential noise reduction of a:

(a) bubble curtain,
(b) physical curtain consisting of noise attenuation material, and
(c) parabolic reflector.

Based on the initial acoustic results, as well as the findings of Sixma (1996), it is clear that unless there is something inherently wrong with the structural, mechanical or acoustical requirements of operating an effective bubble curtain in conjunction with the seismic arrays and streamers, the bubble curtain should be the sole focus of further study in this project.

The project was then directed toward ascertaining that there are be no "show stoppers." Of all the concepts we considered, including those of Spence (2007), it was quite clear that this is the most operationally practical approach.

We further decided that since the Arctic Beaufort and Chukchi Seas are relatively shallow, say less than 61 m (200 feet) of water, we should consider allowing the towed air hoses (manifolds producing the bubbles) to drape down as deep as possible by proper weight/buoyancy adjustment, if this would be practical. The deeper the manifold, the higher the hydraulic power required for bubble generation.

The Sixma test reports, although providing useful and encouraging test results, did not provide sufficient bubble fluid dynamics information or acoustic analysis prediction results to properly design and evaluate an air bubble curtain. Thus our project needed to these areas in much greater detail:

- the fluid dynamics of bubble curtains
- the acoustic evaluation of the effectiveness of various bubble curtain designs.

Concerning the fluid dynamics analysis we specifically needed answers to the questions:

1. What is the expected bubble diameter and plume shape; and what is the variation in diameter and shape with water depth?
2. How should the air be introduced into the water column in order to create a bubble curtain in the correct location with respect to the airgun array? That is, should the manifold be horizontal, or vertical, or both? What is the length of the manifold and its position with respect to the ship and the airgun array?
3. Will “holes” occur in the bubble curtain? If so, how can they be prevented?
4. What size should the manifolds be and what air flow rate, pressure and compressor horsepower is necessary?
5. What is the equivalent acoustic impedance of the bubble curtain as contrasted with that of a physical curtain?

As we looked at our problem, we determined that it is a quasi-static condition, because the bubbles, once emitted from a moving manifold, are left behind in a nearly static water column. Further. We know from the prior Shell work, see Jones (1972), that there are forces working on the bubbles that tend to keep them small - say 6.4 mm diameter - so as they rise and the bubble wants to get larger, it breaks into other small bubbles instead. This is a fortunate result, because we need a "curtain" of many small bubbles on either side of our central seismic arrays.

Since the arrays are of the order of 15.2 m (50 feet) long, and they move forward at perhaps 5 knots (2.6 mps), and since the bubbles rise at perhaps 0.18 mps, our challenge is to design the layout of the submerged, neutrally-buoyant 'leaky' air hoses to produce the desired bubble curtains parallel to and just outboard of the arrays, just where they are needed to prevent un-damped acoustic waves in the lateral direction from penetrating the curtain and affecting the marine mammals.

We quickly recognized that the answers to our quasi-static problem for towed bubble curtains should also work as well for static applications like drilling and pile driving.

Following is a summary of the fluid mechanics of bubble curtains leading to a description of the bubble acoustic impedance characteristics needed as input for an acoustic analysis of the bubble curtain effectiveness. Following the fluid mechanics, the acoustic analysis results are presented.

BUBBLE CURTAIN FLUID DYNAMICS

This section summarizes a full report on the subject included as Appendix A of this report.

An air bubble curtain is developed by forcing air through orifices, or nozzles, in a manifold. Let the manifold be aligned with the *x*-axis of a coordinate system. The manifold (and *x*-axis) are located at a depth, *H*, below the water surface. The *z*-axis is pointed upward, and measures height above the nozzle exit. The *y*-axis is oriented to form a right-hand coordinate system.

Several simplifying assumptions are made. First, the water body is assumed to be of uniform density. Second, the air traveling from the seismic vessel to the manifold and along the manifold is assumed to be at the temperature of the sea water.

Even though air is exhausted through individual nozzles spaced some distance apart, the majority of the air bubble curtain can be treated as a two-dimensional plume above a line source of buoyancy. Large scale experiments performed by Jones (1972) confirmed the applicability of the plume equations to an air bubble curtain. Lee and Chu (2003) also take this approach in analyzing the dilution of effluent from ocean outfalls consisting of nozzles spaced along a manifold. The Lagrangian approach of Lee and Chu (2003) (indicated in Figure 9) is adapted, but in this case the "effluent" is air which varies in density as it rises to the surface.

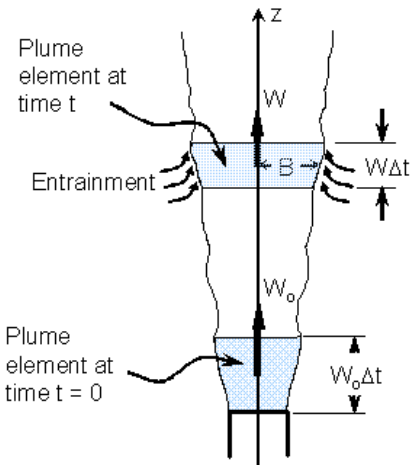

Figure 9. Lagrangian analysis of plume.

A "top hat" velocity profile is used for the velocity of the air-water mixture in the *z*-direction.

$$w = W \ if \ \ y \le B$$
$$= 0 \ otherwise \qquad \text{(a)}$$

where *W* and *B* are the velocity and half-width of an equivalent jet with a sharp boundary and uniform velocity, W, carrying the same mass flow and momentum flux as the actual plume.

Conservation of volume and mass flux requires

$$\begin{aligned} Q &= Q_a + Q_w \\ m &= m_a + m_w \\ m_a &= const \end{aligned} \qquad \text{(b)}$$

where subscript “a” refers to the air, subscript “w” refers to the water, and no subscript indicates the mixture. In general, mass flow rate *m* = *Q*. Conservation of momentum flux, *M*, requires

$$\frac{dM}{dt} = \frac{d}{dt}(\rho QW) = F = (\rho_w - \rho_a)gQ \qquad \text{(c)}$$

where *F* is the buoyancy flux. The entrainment hypothesis is used to provide for turbulent closure.

$$\frac{dQ}{dz} = \alpha W \qquad \text{(d)}$$

where α is the entrainment coefficient. Because flow in the plume is a boundary layer flow, the pressure is constant in the y-direction. Since air is treated as a perfect gas, the density of the air is given by

$$\rho_a = \frac{P}{RT} = \frac{\rho_w (H - z) + P_{atm}}{RT} \qquad \text{(e)}$$

Because this is a Lagrangian formulation,

$$\frac{dz}{dt} = W \qquad \text{(f)}$$

Because the speed of sound in an air-water mixture depends on the volume fraction of air, *s*, our goal is to use Equations (a) through (f) to determine

$$s = \frac{Q_a}{Q} \qquad \text{(g)}$$

The equations are non-dimensionalized, and Equation (f) is used to convert Equation (c) to a function of d/d*z*. The resulting equations to be solved are

$$\frac{d\overline{M}}{d\overline{z}} = \frac{\overline{\rho}_{ao}}{\overline{\rho}_a \overline{W}}$$
$$\frac{d\overline{m}}{d\overline{z}} = \alpha \overline{W} \qquad \text{(h)}$$

where the overbars represent a non-dimensional quantity. These two equations are solved using a fourth-order Runge-Kutta method for systems of equations as shown in Faires and Burden (1993). The non-dimensional volume fraction of air is then calculated from

$$\overline{s} = \frac{1}{1+\overline{\rho}_a}\left(\frac{\overline{m}}{\overline{m}_a} - 1\right) \qquad \text{(i)}$$

Time for the Lagrangian volume element to rise to a height *z* is calculated by a trapezoidal integration of Equation (f).

The usual equations for flow of a perfect gas through a nozzle or orifice are used to determine the mass flow rate of air as a function of pressure in the manifold. The number of nozzles per unit length determines the mass flow rate per unit length, m_a.

Manifold Dimensions

The method of Kreinin and Kafyrin (1979) is used to determine the manifold diameter required to maintain a uniform pressure within 2% over the length of the manifold.

All formulations to this point have been for a stationary manifold discharging air into still water. The assumption of still water may be accurate enough, but towing a manifold behind a seismic survey vessel traveling at 5 kts is far from stationary. So the question is, just what effect will the manifold traveling at 5 kts have on the formulation to this point.

Now consider the volume element in Figure 9. As soon as the element moves up away from the nozzle, it is completely disengaged from the traveling manifold. The only forces then acting on it are caused by its momentum traveling through the still water and its buoyancy. The vertical momentum is dissipated in a relatively short distance, based on Lee and Chu (2003). The horizontal momentum should also dissipate rapidly.

So not a lot of error is introduced by assuming that once the volume element leaves the nozzle, it travels vertically upward, with little or no horizontal motion.

Let t_s be the rise time (time between the air leaving the nozzle and reaching the surface) as given by integration of Equation (f). Let V_V be the speed of the vessel towing the airgun array and the manifolds. In the time t_s, the vessel travels a distance $L_s = V_V t_s$.

In Figure 10, the position of the manifold at time zero is indicated by the black outline. At time t_s, the manifold is shown in red, and the air-water curtain is indicated by the shaded area.

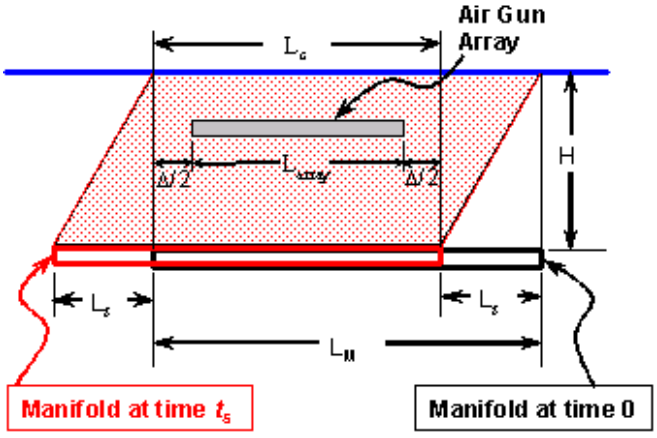

Figure 10. Determination of manifold length.

The length of the curtain, L_c, should be greater than the length of the airgun array, L_{array}. Define an extra length as shown, and the equation for the required manifold length is

$$L_M = L_{array} + \Delta + V_V t_s \qquad \text{(j)}$$

The manifold should be towed so that its leading edge is L_s + /2 ahead of the array.

Optimization

The above equations were programmed into an Excel workbook. The numerical integration was programmed as a user function in VBA. Besides properties of air and water, input included manifold depth *H*, vessel speed, array length, the extra length , the ratio of pressure at the end of the manifold to that at the beginning of the manifold, and the maximum speed of sound ratio, *c/cw* desired. Because the volume fraction of air in the plume varies with *z*, the ratio of the speed of sound in the plume to that in water varies with *z*. Number of orifices per foot of manifold and orifice diameter are also input

The Solver add-in was used to minimize the pneumatic horsepower (pressure times flow rate) in the manifold by varying the manifold pressure and diameter. Constraints were defined so that the solution satisfied the manifold pressure ratio and maximum c/cw ratio.

A table of solutions was generated by specifying various manifold depths, number and size of nozzles, and desired *c/cw* ratios. Specifying further design details is not justified in this first feasibility study, so engineering judgment was used to select the following configuration:

Depth of Manifold [H] (m)	Number of nozzles per ft [n] (1/m)	Diameter of nozzle exit [d] (mm)	Manifold Pressure [Pm] (kPa)	Diameter of manifold [Dman] (cm)	at Manifold End [Pend] (kPa)
18.3	9.8	3.2	402.7	22.8	394.6

Flow Rate (scmm)	Total Pneumatic HP at manifold (hp)	Rise Time (sec)	Manifold length (m)	Manifold Position in front of array (m)	Total Number of Nozzles (-)
139.7	423.1	15.5	61.3	43.0	603

Table 1. Design details for a manifold with 9.8 - 3.2 mm nozzles per m operating at a water depth of 18.3 m.

Figure 11 shows a graph of the average volume fraction vs. height above manifold for the bubble curtain design chosen for acoustic analysis.

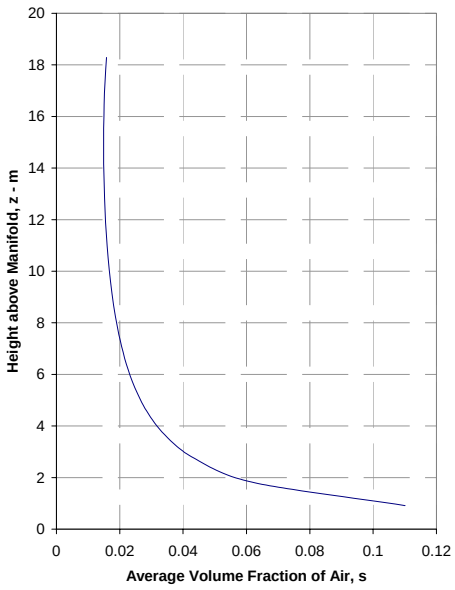

Figure 11. Key design parameter for the chosen bubble curtain.

ACOUSTIC ANALYSIS

This section summarizes a full report on the subject included as Appendix B of this report.

The purpose of the acoustic modeling study is to predict the absolute wave pressure reduction as a function of sound frequency due to sound propagation through a specific bubble curtain configuration.

The proposed bubble curtain manifolds are towed on either side of the array at a depth greater than the airguns. The released air bubbles will move upward from the manifolds due to buoyancy, and very little horizontally. Figure 12 depicts the relative positions of the manifolds and bubble curtains relative to a 3-string airgun array with 5 airguns in each string.

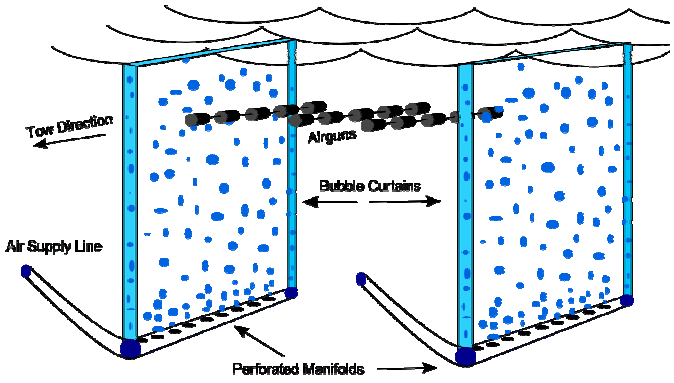

Figure 12: Positions of manifolds and curtains relative to a towed airgun array.

The manifold configuration that was analyzed is described as two 61.3 m (201 feet) -long manifolds deployed on either side of the airgun array and towed at 18.3 m (60 feet) depth. This scenario was chosen based on fluid-dynamic modeling described above that predicted the fractional volume of air in the water above the manifolds as a function of height above the manifolds. The bubble density also decreases perpendicularly across each curtain according to a square exponential decay function. The perpendicular distance off at which the bubble density reaches 1/e (~0.37) of its on-axis density is 2.4 m at 15.2 m depth and 0.58 m at 3.7 m depth.

Approach

Sound propagation and back-scattering in bubbly water has been studied extensively in problems encountered in acoustic oceanography and ultrasonic imaging. See Leighton

(1994). Even a very small fractional volume of air bubbles in water can significantly change the sound speed. The primary reason for this effect is that the compressibility of bubbly water is much greater than for regular water. Sound pressure waves incident on the boundaries of bubbly water layers can be reflected strongly due to the large change in sound speed and acoustic impedance across the boundaries. Bubbles also can absorb and scatter energy from acoustic pressure waves if the natural frequency of bubble oscillation is similar to that of the incident pressure wave. The natural resonant frequency of bubbles depends on their radii and depth. The resonance absorption effect is important only for large bubble sizes; bubble diameters corresponding to resonant frequencies 100 Hz and 500 Hz near the surface are respectively 3 cm and 6 mm. It is quite possible that these large bubble sizes could be produced by the bubble curtain system considered here.

Sound attenuation due to excitation of individual bubble oscillations is complex and depends on the distribution of bubble sizes in the bubbly liquid region. Although resonance absorption is likely an important effect, we have neglected it in this initial examination. Here we only consider the macroscopic effect of reduced acoustic impedance in the bubble curtain layer on the reflection and transmission coefficients through the layer. Leighton shows that when the frequency of the incident acoustic wave is much less than the bubble oscillation frequency then the sound speed C in the bubbly layer can be computed according to

$$C = C_w\left(1+\frac{\{VF\}}{2}\frac{C_w^2\rho_w}{C_a^2\rho_a}\right)^{-1} \qquad \text{(k)}$$

where C_w is the water sound speed, ρ_w is the water density, C_a is the air sound speed, ρ_a is the density of the air in the air bubbles and VF is the fractional volume occupied by air bubbles. For this study we have used a constant value for C_w of 1480 m/s. The air density varies with depth because the bubbles are compressed by underwater hydrostatic pressure. At standard temperature (NIST definition of 293.15 K) the density of air is given by ρ_a = 1.29 p/p_0 kg/m^3 where p/p_0 = (1+z/10.2) is the ratio of hydrostatic

pressure to atmospheric pressure in salt water and z is the depth in meters. The speed of sound in ideal gasses is independent of ambient pressure. The nominal speed of sound in air can be computed according to $C_a^2 = \gamma RT$ where $\gamma = 1.401$ is the ratio of specific heats for air at normal temperatures, $R = 286.9$ J/kg·K is the individual gas constant for air and T is the temperature in K, from Salomons (2001). At standard temperature $C_a = 343$ m/s.

The approach taken here involved modeling the reflection and transmission coefficients as a function of frequency through a homogenous planar layer of bubbly water. The layer has reduced sound speed and density relative to the surrounding water. The specific assumptions and parameters used for this modeling study were:

1. Bubble layer thickness of 4.3 m was chosen based on the off-axis distance at which the density factor had decreased to 1/e of its on-axis value at 5 m depth (corresponding to common airgun array operating depth).
2. Bubble density (air only) was specified as 1.92 kg/m^3 as computed per the discussion above at 5 m depth.
3. Bubble layer fractional air volume was set to 0.015 corresponding to the value from the fluid dynamic modeling at 5 m depth.
4. Bubble layer sound speed was computed with the following parameter values: C_w = 1490 m/s, ρ_w = 1020 kg/m^3, C_a = 343 m/s, ρ_a = 1.92 kg/m^3 and VF = 0.015. These parameters give curtain layer sound speed of C = 19.7 m/s.
5. Curtain layer density was chosen based on the sum of the products of relative fractions of water and air and their respective densities 1020 kg/m^3 and 1.92 kg/m^3 at 5 m depth. This gives a bubble curtain layer density of 1005 kg/m^3.

Thus a one-dimensional problem was evaluated in which a plane acoustic wave of frequency f is incident on a homogenous bubble layer from angle θ as shown in Figure 13. This analysis assumed infinite vertical extent of the curtain layer. Low frequency sound energy that would refract around the bottom of a finite bubble curtain was

neglected. Its amplitude and importance are likely low relative to the directly transmitted field that was fully considered. All sound paths that reflect from water surface and bottom and paths that reflect between the two air curtains have been neglected in this initial analysis.

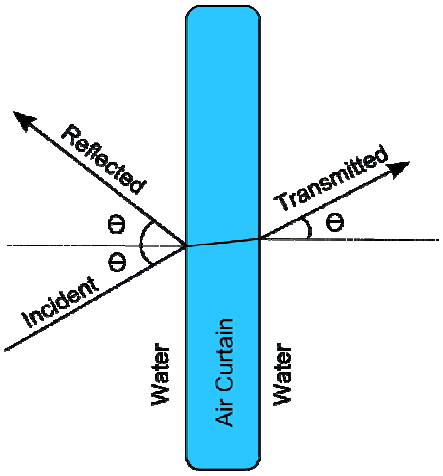

Figure 13: Diagram of Incident, Reflected and Transmitted Acoustic Paths.

The transmission coefficient *t* represents the ratio of amplitudes of the transmitted wave to the incident wave. This coefficient in decibels $TL = 20 \cdot \log(t)$ indicates how much signal attenuation will be produced by the bubble curtain. The transmission coefficient was computed using the well-known theoretical formula for plane wave sound transmission through a fluid layer having different acoustic impedance than the surrounding fluid on either side, e.g. Jensen et al. (2000), and Brekhovskikh (1980). This is an exact formulation for fluid layers that accounts for the boundary reflection and transmission coefficients and the infinite number of internal reflections within the bubble curtain layer. While absorption can be included by making the layer sound speeds complex, this was not done. The acoustic impedances of the water and bubble curtain layers were computed from their respective sound speeds and densities and from the angle of propagation in each layer. The angles of propagation were computed from Snell's law.

The transmission loss through the bubble curtain was computed as a function of frequency in 0.1 Hz steps between 1 Hz and 500 Hz using the method described above.

The results up to 100 Hz for incident angles 0°, 30°, 60° and 89° are shown in Figure 14.

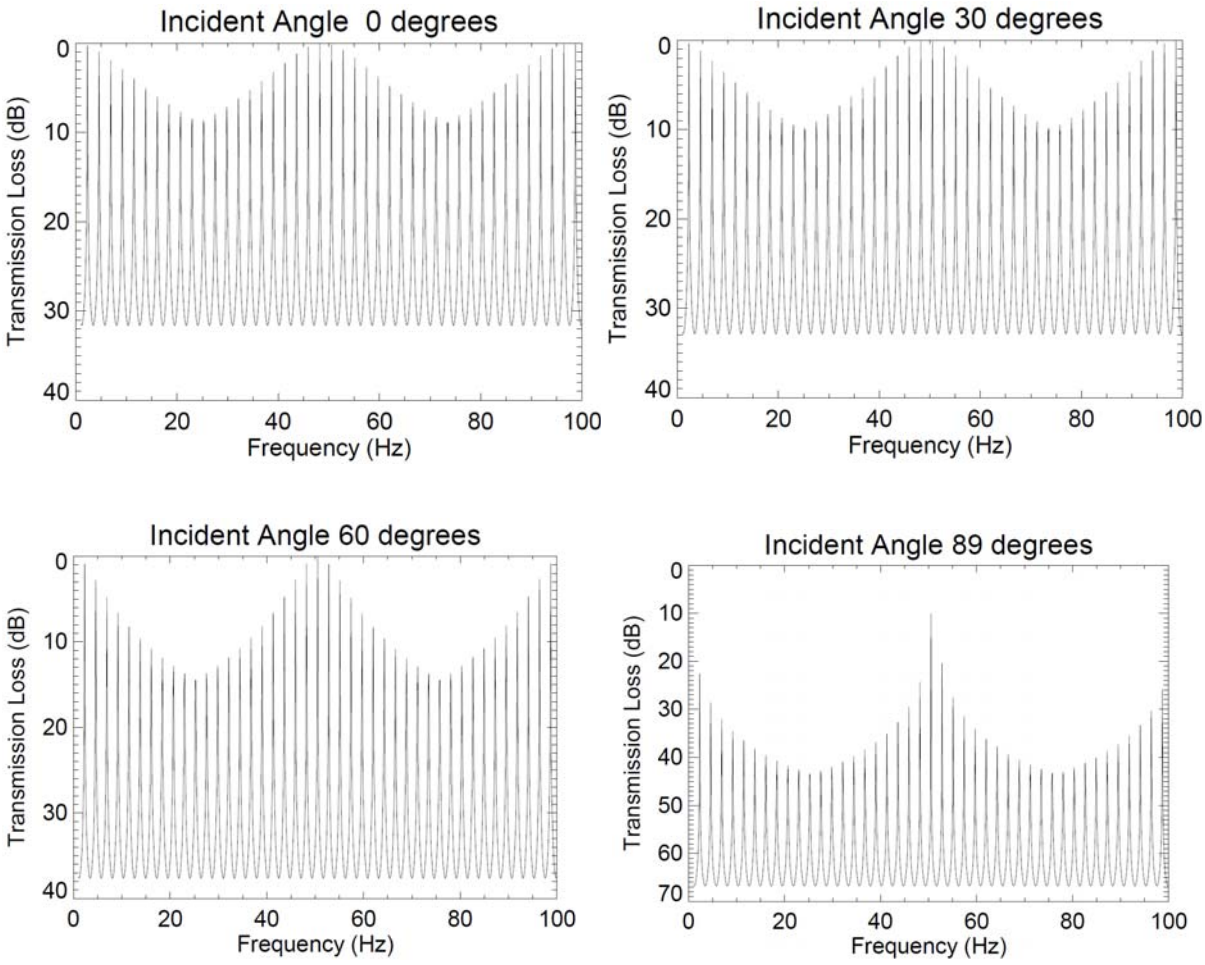

Figure 14: Transmission loss incurred by sound propagation through the bubble curtain bubble layer for four angles of incidence. The functions were computed at 0.1 Hz steps.

The linear transmission losses at several incidence angles were averaged over frequency between 1 Hz and 500 Hz and these average values are given in table 2.

Incidence Angle	Average TL
0°	21.5 dB
15°	21.7 dB
30°	22.5 dB
45°	23.9 dB
60°	26.4 dB
75°	31.3 dB
89°	51.8 dB

Table 2. Averaged transmission losses.

While Figure 14 shows transmission loss only to 100 Hz, the patterns continue similarly to 500 Hz.

Transmission loss was found to vary cyclically with frequency, with a period of approximately 2.3 Hz. This frequency corresponds with the ½-wavelength layer effect; a non-attenuating layer with thickness equal to a multiple of ½ wavelengths is acoustically invisible. The frequencies of zero loss are given by $f = nC/(2h)$ where n is an integer, C is the layer sound speed and h is the layer thickness. Here we had C = 19.74 m/s and h = 4.3 m so f = 2.295n Hz. The frequency of the loss minima do not change appreciably with incident angle because the wave propagation angles in the low speed bubbly curtain layer are near perpendicular to the boundaries for all incident angles. The angle is less than 0.8° for the shallowest incident angle 89°. The loss minima in Figure 4 do not always reach 0 dB. This is believed to be an artifact of insufficient resolution in discrete sampling of a periodic function. The minima peaks are so narrow that the true minima were not always sampled by the computational step size of 0.1 Hz. The average transmission loss in the frequency band 1 Hz to 500 Hz was 21.5 dB for plane sound waves incident perpendicularly (at 0° incidence angle) to the bubble curtain. The average loss increased with increasing incidence angle and reached 51.8 dB at 89°.

Acoustic Analysis Conclusions

Insofar as sound level reduction is concerned, the bubble curtain scenario examined here could reduce the spectral levels – noise - of airgun arrays by more than 20 dB.

The absolute reduction varied cyclically with frequency with a period of 2.3 Hz but did not have a systematic trend with frequency. This result was expected since we assumed no absorptive losses within the bubble curtain layer. Losses incurred by exciting individual bubble resonances were not addressed in this study and those would be in addition to the impedance loss mechanism considered here. Those resonant losses would be frequency dependent and influenced by the similarities between bubble resonant frequencies and the airgun array sound frequency spectrum. The bubble resonant frequencies are dependent on the bubble size distribution.

ACKNOWLEDGMENTS

The authors want to thank Mr. William Dragoset of Western Geophysical for the excellent technical advice given to the project team.

Appreciation is due to Mr. Jesse Spence of Noise Control Engineering, Inc. for his valuable initial work in assessing acoustic issues with noise reduction concepts.

Thanks is also due to Mr. John Ward of Shell, who has given us encouragement and advice throughout the whole project.

Finally the authors wish to thank the U.S. Minerals Management Service for project funding, and Mr. Joseph Mullin of the MMS for his project management assistance and encouragement.

REFERENCES

Ayers, Ray (1988), U.S. Patents 4,724,788, 4,974,995 5,046,443, 4,726,314 and 4,709,356.

Brekhovskikh, L.M. (1980), Waves in Layered Media Vol. 2 New York: Academic Press, 561 p. [Acoustics Institute, Academy of Sciences, USSR]

Caldwell, Jack and Dragoset, William (2000) “A Brief Overview of Seismic Air-Gun Arrays”, The Leading Edge, August.

Dragoset, William (2000), “Introduction to Air Guns and Air-Gun Arrays, The Leading Edge, August.

Faires, J. Douglas and Burden, Richard L (1993), Numerical Methods, PWS Publishing Company, Boston.

Jensen, F.B., W.A. Kuperman, M.B. Porter, H. Schmidt (2000), Computational Ocean Acoustics. New York: Springer Verlag.

Jones, Warren T. (1972), “Air Barriers as Oil-Spill Containment Devices,” Society of Petroleum Engineers Journal, Vol. 12 (2), pp. 126-142.

Kreinin, E. V. and Kafyrin, Yu. P. (1979), “Design of Isothermal Distributing Manifolds,” Khimicheskoe i Neftyanoe Mashinostroenie, Vol. 5, pp. 16-18.

Lee, Joseph H. W. and Chu, Vincent H. (2003), Turbulent Jets and Plumes, A Langrangian Approach, Kluwer Academic Publishers, Boston/Dordrecht/London.

Leighton, T.G. (1994), The Acoustic Bubble. San Diego: Academic Press, 1994. 613 p.

Salomons, E.M. (2001), Computational Atmospheric Acoustics, Kluwer Academic Publishers, the Netherlands.

Sixma, E. (1996), “Bubble Screen Acoustic Attenuation Test #1”. Western Atlas/Western Geophysical Report. Conducted for Shell Venezuela.

Sixma, E. and Stubbs, S. (1996), “Air Bubble Screen Noise Suppression Tests in Lake Maracaibo”. Sociedad Venexolana de Ingenieros Geofiscos, Congreso Venezolano de Geofisica.

Spence, Jesse, et al (2007), “Review of Existing and Future Potential Treatments for Reducing Underwater Sound from Oil and Gas Industry Activities”, Joint Industry Project Report”, by Noise Control Engineering, Inc.

APPENDIX A

Air Curtain Design for Attenuation of Air Gun Signals

December 2008

Consultant Report to
Stress Engineering Services, Inc.
Houston, TX

by

Warren T. Jones, Ph.D., P.E. (Inactive)

6202 N. Woods Ln
Katy, TX 77494

Tel: 281-391-2398
wjones984@comcast.net

TABLE OF CONTENTS

ABSTRACT

A study of methods and equipment for reducing lateral noise propagation from seismic exploration vessels indicated that an air bubble curtain represents a relatively simple system of attenuating seismic signals. In order to further evaluate such a system, it is necessary to determine sizes of manifolds and nozzles, manifold pressure, air volume flow rates, and how to locate manifolds with respect to the seismic air gun arrays.

Equations describing the flow of air in a rising plume of air bubbles, the flow of air through nozzles, and design of a pressure distributing manifold are combined into an optimization problem which minimizes the pneumatic horsepower required to produce a selected value of the speed of sound in the plume of air bubbles. Selecting different values for number and size of nozzles, depth, and maximum speed of sound in the plume produces a different optimal solution for size of manifold, air pressure, and volume flow rate. So a matrix of solutions is generated. Without going into a detail design, the “best” solution is a matter of engineering judgment.

The selected system has a 9-inch manifold towed at a depth of 60 feet below the surface. The manifold has 1/8 inch nozzles spaced 4 inches apart. Pneumatic horsepower and volume flow rate are 423 hp and 4933 scfm, respectively. The manifold is 201 feet long and should be towed 141 feet in front of the air gun array.

Air Curtain Design for Attenuation of Air Gun Signals

by

Warren T. Jones, Ph.D., P.E.(Inactive)

INTRODUCTION

Stress Engineering Services, Inc. is conducting a study of methods and equipment for reducing lateral noise propagation from seismic exploration vessels operating in the Alaskan Beaufort and Chukchi Seas [Ayers (2007)]. Early results of this study, including Spence (2008), indicated that an air curtain represents a relative simple system of providing attenuation of seismic signals. A sketch of the system under consideration is shown in Figure 1.

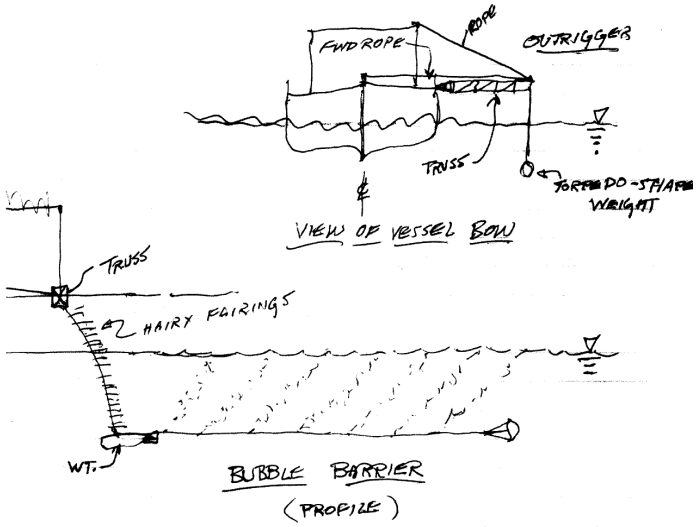

Figure 1 -Air Bubble Barrier Sketch

In order to proceed from a sketch to a design, several questions were posed as the basis for the present investigation [documented in Jones (2008)].

- What is the expected bubble diameter and plume shape; and what is the variation in diameter and shape with water depth
- How should the air be introduced into the water column in order to create a bubble curtain in the correct location with respect to the air gun array? That is, should the manifold be horizontal, or vertical, or both? What is the length of the manifold and its position with respect to the ship and the air gun array?
- Will holes occur in the bubble curtain? If so, how can they be prevented?
- What size should the manifolds be and what air flow rate and pressure is necessary?
- What is the equivalent acoustic impedance of the bubble curtain? This will allow selection of a material for proof-of-concept testing without the necessity of building a complete air curtain system.?

In other words, the objective of this project is to develop a feasibility design of a towed, air bubble barrier. Although the ultimate feasibility will be determined by the acoustic properties of the bubble barrier, no acoustic investigation is included here.

The next section of this report contains the Conclusions and Recommendations resulting from this study. The following section describes the equations used in answering the above equations. Following this is a short section describing the principles of Optimal Design and their application to design of air curtains. The last section presents and discusses the results of this study and the selection of a “best” design.

CONCLUSIONS AND RECOMMENDATIONS

Conclusions

An air bubble curtain is developed by forcing air from a manifold through nozzles. The air exits as a buoyant jet into the sea water, but within a short distance, the jet momentum is dissipated, and further motion is controlled by buoyancy. The rising stream of air is broken into bubbles by the turbulence caused by introducing the jet of air into the water. As a result of the balance between bubble breakup caused by the turbulence and bubble coalescence, all of the bubbles are about 1/4" inch in diameter. This phenomenal fact means that studies of individual bubbles rising in a column of water do not apply to the design of an air bubble curtain.

The only gaps in the air bubble curtain will occur near the manifold where the air from one nozzle has not yet merged with air from the adjacent nozzle. For nozzles spaced 3 or 4 inches apart, there will be a triangular gap with a height of 12 or 16 inches above the manifold. This gap is relatively small and will actually contain a small amount of air, so it is considered insignificant.

Equations developed for a two-dimensional, or line, plume previously have been found to apply to a buoyant flow exiting from a series of nozzles in a manifold into an ambient fluid. Here, “plume” means fluid motions produced by a continuous source of buoyancy. As the air rises, it entrains water into the flow, so the volume fraction of air in the plume decreases. But as the air rises, the pressure is reduced, and the volume of the air increases. As a result of these two opposing effects, the speed of sound and the specific acoustic impedance in the plume vary with height above the manifold.

The governing equations for a two dimensional plume have been combined with the equations for the compressible flow of air through a nozzle and the equations for the design of a pressure distribution manifold to create an optimization problem. By minimizing the pneumatic horsepower in the manifold (pressure times flow rate), an optimum solution is obtained based on specified configurations and constraints. Changing nozzle diameter, number of nozzles per ft along the manifold, or the manifold depth will produce a different optimal solution. In this way a matrix of solutions for different manifold depths below the surface was generated. Selection of a “best” design out of this matrix of solutions is based on engineering judgment.

The recommended “best” design is shown as Solution #58 in Table E - 2 of Appendix E and discussed under the heading “Discussion of Selected System” on page 25. The manifold for this system is located 60 ft below the surface. It has a diameter of 9”, a length of 201 ft, and 3 – 1/8 inch nozzles per ft. The maximum ratio of speed of sound in the air curtain to speed of sound in water of 0.07 is obtained with 423 hp and a flow rate of 4933 scfm.

Recommendations

Previous tests on air bubble barriers in the literature have concentrated on measuring signals and their attenuation with little attention to what was generating the air bubble barrier. Therefore, it is recommended that experimental measurements made during a Proof-of-Concept test include measurements of all variables pertaining to the air flow as well as those pertaining to attenuation of seismic signals.

Although not consider in this report, an air bubble barrier generates noise of its own. It is recommended that further investigation be conducted to determine the effect of air bubble barrier noise on marine life that the barrier is meant to protect.

The present analysis neglects the effect of a free water surface. Near the surface, water is no longer entrained into the rising plume. In this region, water falling from the mound created above the water surface meets the rising air-water mixture. The result is a horizontal current at the surface moving away from the plume centerline, so entrainment cannot occur. If the speed of sound in the plume near the surface turns out to be critical for sufficient attenuation of the seismic signal, a more detailed analysis of the plume in this region will be necessary.

AIR CURTAIN DESIGN

An air bubble curtain is developed by forcing air through orifices, or nozzles, in a manifold. Let the manifold be aligned with the x-axis of a coordinate system as shown in Figure 2. The manifold (and x-axis) are located at a depth, H, below the water surface. The z-axis is pointed upward, and measures height above the nozzle exit. The y-axis is oriented to form a right-hand coordinate system.

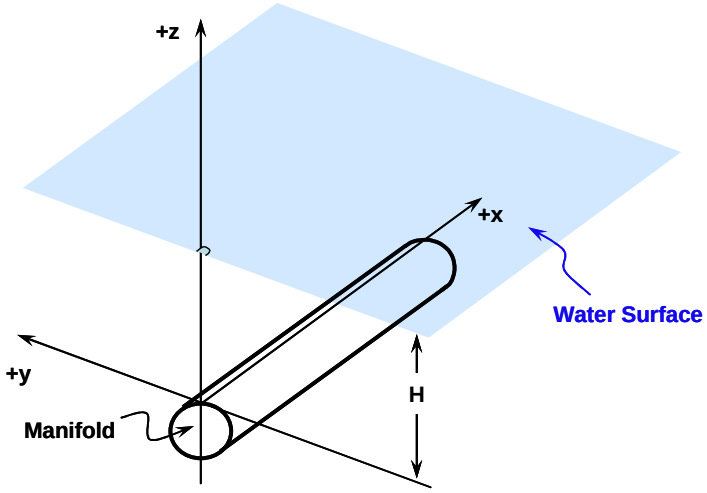

Figure 2 - Coordinate axes

Several assumptions will be made in order to simplify the following analysis as much as practical. First, the ocean is assumed to be of uniform density. The following equations can be adapted to a stratified ocean or to an ocean with continuously varying density. However, for this first feasibility analysis, the ocean density and temperature are assumed to be constant.

Another simplifying assumption is that the air traveling from the ship to the manifold and along the manifold is at the temperature of the sea water. If the manifold is far enough away from the air compressor, the air could well be approaching the sea water temperature. But it could also be different. Accounting for actual air temperature at the entrance to the manifold will await a detailed, final design analysis.

Characteristics of an Air Bubble Curtain

Circulation patterns in the water and velocity profiles in and around an air bubble curtain are shown in Figure 3. This is a view looking along the manifold in the positive x direction. As the bubbles rise, they entrain water, and the vertical average velocity profile of the air-water mixture is well represented by a Gaussian profile, as shown. The air in the mound of air-water mixture at the surface escapes into the atmosphere, and the water runs downhill, creating a surface velocity as shown on the right side of the figure. The magnitude of this velocity is important when an air bubble curtain is used as a breakwater, or to contain an oil spill. However, for the purpose of attenuating air gun signals, the volume fraction of the air in the rising plume is the most important characteristic.

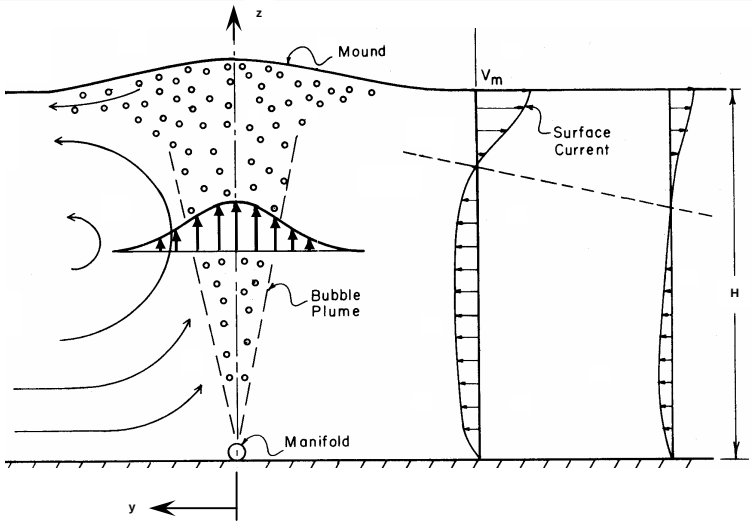

Figure 3 - Circulation Patterns and Velocity Profiles

Bubble Size

Jones (1972) conducted large scale experiments on an air bubble curtain in 7 ft of water in the 6-ft wide test section of a current tank. Based on observations (not measurements) in still water, the majority of the air bubbles in the rising plume were on the order of ¼ inch in diameter. Only a comparatively few bubbles were larger – on the order of ¾- to 1-inch.

The explanation for this is found in the work done by Towell, Strand et al. (1965) on sparged towers. They observed that when air was introduced through a sparger (a nozzle containing multiple orifices) at the bottom of a column of water in a Plexiglas tube, the air bubbles were all approximately ¼-inch in diameter no matter what type of sparger was used or what size orifices were in the sparger. The bubble size remained constant over the entire 10-foot height of the water column. This is in direct contradiction to the notion that a bubble of gas should expand as it rises in a column of liquid. High speed photography was used to explain this paradox. Individual bubbles were observed during the process of coalescing with other bubbles and breaking up. The fact that the size was independent of elevation is explained by a balance between breakup and coalescence. Small bubbles touch and coalesce until a bubble size is reached that is unstable in the turbulence created by the rising bubble plume. The intensity of turbulence in the center of the plume depends only on the flow rate of the air, so it is approximately the same at all elevations.

Towell, Strand et al. (1965) found the bubble size to be independent of air flow rate, and explained this as follows. The higher air flow rates result in higher coalescence rates, but the intensity of turbulence is also higher, resulting in a higher rate of breakup. This balances the increased coalescence rate and keeps the bubble size constant.

This explanation agrees with all the observations made during the air barrier tests of Jones (1972); no matter what the air flow rate was, the bubble size was always about the same. The only exception occurred at very low air flow rates where the bubbles were not close enough to coalesce or create much turbulence. This constant bubble size explains why previous investigations of the use of air barriers as breakwaters found no effect of orifice size on the surface current produced.

Gaps in Curtain of Bubbles

At air flow rates commonly used in air curtains, the bubbles are continually coalescing and breaking up. So the bubbles remain in close proximity to each other at all times. Visual observation in the tests of Jones (1972) confirmed that there were no gaps, or holes, in the curtain of bubbles.

However, near the manifold, there will be gaps between nozzles where the air from one nozzle has not yet merged with air from the adjacent nozzle. Both the width and height of this gap will depend on the nozzle spacing.

Consider a series of nozzles discharging air into the water as shown in Figure 4. The nozzles have a circular exit and are spaced a distance L_N apart. Above a certain height, the circular jets of air merge, and from there to the surface, the effect is that of a two-dimensional, or line plume. [See “Plume Equations” on page 8.]

The rate of spreading for a circular buoyant jet may be used to calculate the height, h, where air from adjacent nozzles merge. From dimensional analysis and experiments, Lee and Chu (2003) give the half-width of a jet as

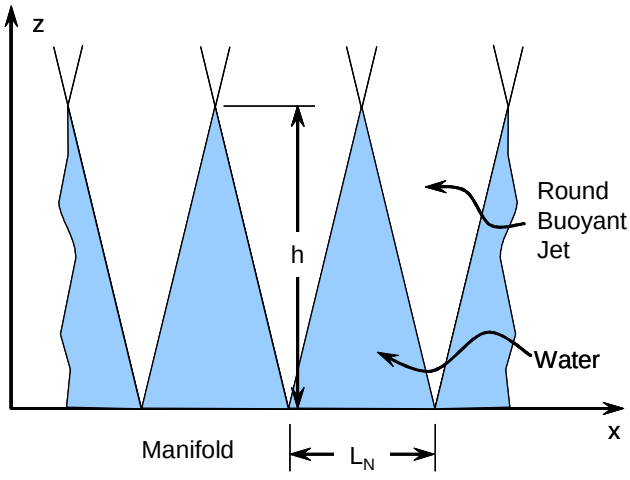

Figure 4 – Gaps in the Bubble Curtain at the Manifold

$$b\lambda = 1.19(0.105)z = 0.125z \tag{1}$$

where b is the half-width of the Gaussian velocity profile, and λ is a factor to account for the air spreading faster than the average velocity spreads. Setting $b\lambda$ equal to one-half the distance between nozzles, L_N, allows the distance h to be calculated as

$$h = 4L_N \tag{2}$$

So there is a triangle of water with base L_N and height $4L_N$ between nozzles. However, it is not pure water; there is some air in it. The width of a Gaussian profile extends from $-\infty \quad to \quad +\infty$. The half-width b of the Gaussian velocity profile is the distance from the centerline to where the velocity is $1/e$ times the centerline velocity. So there will be some air in this triangle between nozzles.

For nozzles space 3 or 4 inches apart, the height h is 12 or 16 inches. Allowing for the fact that there will be some air in this triangle, the effect of this gap on the overall performance of the air curtain is insignificant.

Speed of Sound and Specific Impedance in the Air-Water Mixture

Attenuation of an air gun signal traveling through an air bubble curtain occurs because the speed of sound in the curtain is less than the speed of sound in sea water. Therefore, to begin an investigation of air curtain design, it is necessary to define the speed of sound in the air bubble curtain.

In general, the speed of sound, c, in any kind of material is given by

$$c = \sqrt{\frac{g}{\beta\rho}} \tag{3}$$

where g is the acceleration of gravity, β is the compressibility of the material, and ρ is the density of the material.

Domenico (1982) gives the following equations for compressibility and density of an air-water mixture

$$\begin{aligned} \beta &= (1-s)\beta_w + s\beta_a \\ \rho &= (1-s)\rho_w + s\rho_a \end{aligned} \tag{4}$$

where the subscripts w and a refer to water and air, respectively, and s is the volume fraction of air in the flow. The result of substituting Equations (4) into Equation (3) is the same as Equation (3) of Costigan and Whalley (1997) which matched their experimental results.

The density and compressibility of water are taken as constants. The density of air is given by the perfect gas relationship

$$P = \rho_a RT \tag{5}$$

where P is the pressure, T is the temperature in ^{o}R, and R is the gas constant for air = 53.36 ft-lb$_f$/lb$_m$-^{o}R. The compressibility of air is given by [see Appendix A]

$$\beta_a = \frac{1}{P} \tag{6}$$

If Q_a is the volume flow rate of air and Q is the volume flow rate of the air water mixture, then

$$s = \frac{Q_a}{Q} \tag{7}$$

Substituting Equation (4) into Equation (3) gives the speed of sound in the air curtain. Using the values of β_w and ρ_w for water and $s = 0$ gives the speed of sound in water, c_w. In the following, the ratio of c to c_w will be used as a measurement of the efficiency of the air barrier curtain.

$$\frac{c}{c_w} = \sqrt{\frac{\beta_w \rho_w}{\left[(1-s)\beta_w + s\beta_a\right]\left[(1-s)\rho_w + s\rho_a\right]}} \tag{8}$$

Specific Impedance I is defined as

$$I = c\rho$$

Using Equations (3) and (4), the specific impedance for the air curtain can be written as

$$I = \sqrt{\frac{(1-s)\rho_w + s\rho_a}{(1-s)\beta_w + s\beta_a}} \tag{9}$$

Using the values of β_w and ρ_w for water and $s = 0$ gives the specific impedance of the sea water I_w, and the ratio I/I_w is given by

$$\frac{I}{I_w} = \sqrt{\frac{\beta_w}{\rho_w}\frac{(1-s)\rho_w + s\rho_a}{(1-s)\beta_w + s\beta_a}} \tag{10}$$

Nozzle-Manifold Geometry and Flow Rates

Before delving into the fluid mechanics of the rising air-water mixture in the bubble plume, a few definitions are in order. Let

- n = Number of nozzles per unit length
- q_o = Volume flow rate through a single nozzle
- Q_o = Volume flow rate per unit length
- m_o = Mass flow rate through a single nozzle
- m_a = Mass flow rate of air per unit length

Then

$$\begin{aligned} Q_o &= n\,q_o \\ m_a &= n\,m_o \end{aligned} \tag{11}$$

The spacing of the nozzles, L_N, is given by

$$L_N = \frac{1}{n} \tag{12}$$

Let

Q_{oT} = Total flow rate into manifold

L_M = Length of manifold

Then

$$Q_{oT} = nq_o L_M = Q_o L_M \tag{13}$$

It should be noted that Q_{oT} is the total volume flow rate into the manifold at the pressure, P, and temperature, T, of the air. The volume flow rate at standard conditions is given by

$$Q_{oT} \ in \ scfm = Q_{oT} \frac{P}{P_{std}} \frac{T_{std}}{T} \tag{14}$$

where "scfm" is standard cubic feet per minute and Q_{oT} is expressed in cubic feet per minute. The usual definition of "standard conditions" is atmospheric pressure and a temperature of 68 ^{o}F = 527.69 ^{o}R..

Plume Equations

Jones (1972) found that previous investigators used equations developed for a two-dimensional, or line, "plume" to describe an air bubble curtain used as a breakwater. Here, "plume" means fluid motions produced by continuous sources of buoyancy - for example, the hot air rising over a forest fire. Since 1972 more investigations, both theoretical and experimental, of the fluid mechanics of buoyancy-driven flows have been accomplished. An excellent source for the results of these investigations is the book by Lee and Chu (2003).

Even though air is exhausted through individual nozzles spaced a distance L_N apart, the majority of the air bubble curtain can be treated as the two-dimensional plume above a line source of buoyancy. The large scale experiments of Jones (1972) confirmed the applicability of the 2-D plume equations to the generation of a horizontal surface current by an air bubble curtain. Lee and Chu (2003) also take this approach in analyzing the dilution of effluent from ocean outfalls consisting of nozzles spaced along a manifold. Unfortunately, their analyses are all for effluents having a constant density which is very close to that of water. Fortunately, their formulation is directly applicable to an "effluent" of air having a density which varies with height above the manifold and which is greatly different from that of water.

A 2-D plume can be generated by discharging air through a continuous slot in the top of a manifold. The equivalent slot width, $2B_o$, which discharges the same mass and volume of air per unit length as n nozzles per unit length of diameter d is

$$2B_o = n\frac{\pi d^2}{4} \tag{15}$$

Lagrangian Analysis

The velocity profile in a rising plume has a Gaussian distribution as indicated in Figure 3. However, analysis of the air-water mixture in the plume is considerably simplified by the use of a "top-hat" profile

$$\begin{aligned} w &= W \ if \ |y| \le B \\ &= 0 \ otherwise \end{aligned} \qquad (16)$$

where W and B are the velocity and half-width of an equivalent jet with a sharp boundary and uniform velocity, W, carrying the same mass flow and momentum flux as the actual plume.

Consider the Lagrangian plume element indicated in Figure 5. As it exits from the nozzle, it has a velocity W_o a half-width B_o, and a length in the z-direction of $W_o\Delta t$, where Δt is a small time increment. At time t, it has risen to a height z above the nozzle, and it has a velocity W, a half-width B, and a length in the z-direction of $W\Delta t$.

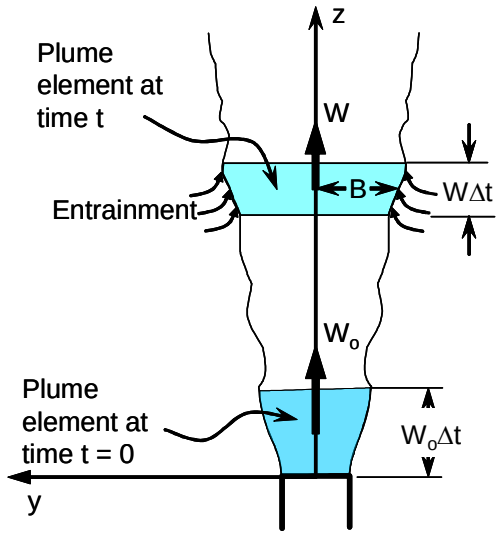

Figure 5 – Lagrangian Formulation

Governing Equations

Because this is a Lagrangian formulation,

$$\frac{dz}{dt} = W \qquad (17)$$

Conservation of mass per unit length of manifold requires that

$$\begin{aligned} Q &= Q_a + Q_w \\ m &= m_a + m_w \\ m_a &= const \end{aligned} \qquad (18)$$

where subscript "a" refers to the air, subscript "w" refers to the water, and no subscript indicates the mixture. In general, mass flow rate $m = \rho Q$. Conservation of momentum flux, M, requires

$$\frac{dM}{dt} \equiv \frac{d}{dt}(\rho Q W) = F \equiv (\rho_w - \rho_a) g Q \qquad (19)$$

where F is the buoyancy flux.

The entrainment hypothesis is used to provide for turbulent closure. The entrained volume flux, Q_e, is taken to be proportional to the velocity W so that

$$Q_e = \alpha W \Delta z$$

where α is the coefficient of entrainment. Because the entrained fluid consists entirely of water

$$dQ_w = Q_e = \alpha W \Delta z = \alpha W^2 \Delta t$$

where the second equality is a result of Equation (17). Dividing by Δz and Δt and taking the limit gives

$$\frac{dQ_w}{dz} = \alpha W \quad or \quad \frac{dQ_w}{dt} = \alpha W^2 \tag{20}$$

Because flow in the plume is a boundary layer flow, the pressure is constant in the y-direction. Since air is treated as a perfect gas, the density of the air is given by

$$\rho_a = \frac{P}{RT} = \frac{\rho_w (H - z) + P_{atm}}{RT} \tag{21}$$

From the second of Equations (4) on page 6,

$$\rho = \rho_w - s(\rho_w - \rho_a)$$

Using Equation (7) gives

$$\rho_w - \rho = \frac{Q_a}{Q}(\rho_w - \rho_a)$$

and noting that $Q_a = m_a/\rho_a$,

$$\rho_w - \rho = \frac{m_a}{Q}\left(\frac{\rho_w}{\rho_a} - 1\right)$$

Substituting this into the definition of the buoyancy flux F in Equation (19) gives

$$F = m_a g\left(\frac{\rho_w}{\rho_a} - 1\right) \tag{22}$$

Non-dimensionalization

Define scaling factors λ such that $\xi = \lambda_\xi \overline{\xi}$ where ξ is any variable and an overbar represents a non-dimensional value. Substituting into Equations (17) and (19) - (21) gives

$$\frac{\lambda_z}{\lambda_t} = \lambda_W \qquad \frac{\lambda_M}{\lambda_t} = \lambda_F$$
$$\lambda_M = \lambda_\rho \lambda_Q \lambda_W \qquad \frac{\lambda_Q}{\lambda_t} = \lambda_W^2 \tag{23}$$
$$\lambda_P = \lambda_\rho \lambda_z \qquad \lambda_\rho = \frac{\lambda_P}{\lambda_{RT}}$$

Note that Equations (18) result in an identity and the second of Equations (20) gives a redundant relationship. Equations (23) are 6 equations in 9 unknowns, so 6 of the unknowns can be determined in terms of the other three. Distances, densities, and buoyant forces will be O{1} by selecting the following:

$$\boxed{\begin{aligned} \lambda_z &= H \\ \lambda_\rho &= \rho_w \\ \lambda_F &= F_o = (\rho_w - \rho_{ao}) g Q_{ao} \end{aligned}} \tag{24}$$

With these definitions, the remaining scaling factors can be determined as

$$\boxed{\begin{aligned} &\lambda_W = \left(\frac{F_o}{\rho_w}\right)^{1/3} \qquad \lambda_t = H\left(\frac{\rho_w}{F_o}\right)^{1/3} \qquad \lambda_Q = H\left(\frac{F_o}{\rho_w}\right)^{1/3} \\ &\lambda_P = \rho_w H \qquad \lambda_{RT} = H \end{aligned}} \tag{25}$$

Substituting the scaling factors into the governing equations gives

$$\frac{d\bar{z}}{d\bar{t}} = \overline{W} \tag{26}$$

$$\begin{aligned} \overline{Q} &= \overline{Q}_a + \overline{Q}_w \\ \overline{m} &= \overline{m}_a + \overline{Q}_w \\ \overline{m}_a &= const \end{aligned} \tag{27}$$

$$\frac{d\overline{M}}{d\bar{t}} \equiv \frac{d}{dt}(\overline{\rho}\,\overline{Q}\,\overline{W}) = \overline{F} \tag{28}$$

$$\frac{d\overline{Q}_w}{d\bar{z}} = \alpha \overline{W} \quad or \quad \frac{d\overline{Q}_w}{d\bar{t}} = \alpha \overline{W}^2 \tag{29}$$

$$\overline{\rho}_a = \frac{\overline{P}}{\overline{R}\,\overline{T}} = \frac{1 - \bar{z} + \overline{P}_{atm}}{\overline{R}\,\overline{T}} \tag{30}$$

Noting that $\frac{d}{dt} = \frac{d}{dz}\frac{dz}{dt}$, Equations (26) and (28) may be combined to give

$$\frac{d\overline{M}}{d\bar{z}} = \frac{\overline{F}}{\overline{W}} \tag{31}$$

Differentiate the second of Equations (27), remembering that m_a is a constant, to give

$$\frac{d\overline{m}}{d\bar{z}} = \frac{d\overline{Q}_w}{d\bar{z}} \tag{32}$$

Then the first of Equations (29) becomes

$$\frac{d\overline{m}}{d\bar{z}} = \alpha\,\overline{W} \tag{33}$$

The buoyancy flux F is determined in Equation (22). Dividing both sides by $\lambda_F = F_o$, remembering that $Q_{ao} = m_a/\rho_{ao}$, and rearranging gives

$$\overline{F} = \frac{\overline{\rho}_{ao}}{\overline{\rho}_a}\frac{1-\overline{\rho}_a}{1-\overline{\rho}_{ao}} \approx \frac{\overline{\rho}_{ao}}{\overline{\rho}_a} \tag{34}$$

Since the density of air is so much smaller than the density of water, the factor $\kappa \equiv \frac{1-\overline{\rho}_a}{1-\overline{\rho}_{ao}} = \frac{\rho_w - \rho_a}{\rho_w - \rho_{ao}}$ is very close to 1. Substituting numerical values for the density of water and the density of air as a function of z [as given by Equation (21)] shows that as z varies from 0 to 200 ft, κ varies from 1.0 to 1.0075. Hence the approximate equality in Equation (34).

Noting that $W = M/m$, the non-dimensional governing equations are

$$\frac{d\overline{m}}{d\bar{z}} = \alpha\,\overline{W} \tag{33}$$

$$\frac{d\overline{M}}{d\bar{z}} = \frac{\overline{\rho}_{ao}}{\overline{\rho}_a\overline{W}} \tag{35}$$

$$\overline{\rho}_a = \frac{\overline{P}}{\overline{R}\,\overline{T}} = \frac{1-\bar{z}+\overline{P}_{atm}}{\overline{R}\,\overline{T}} \tag{30}$$

$$\overline{W} = \frac{\overline{M}}{\overline{m}} \tag{36}$$

The first two of these equations are a system of differential equations in M and m which define an initial value problem. The second two define quantities appearing on the right hand side of the first two.

Once this system of equation has been solved numerically, the quantities of interest for this study must be determined. Substitute $Q = m/\rho$ into the first of Equations (18), and apply the scaling factors from Equations (24) and (25). The result is

$$\overline{Q} = \frac{\overline{m}_a}{\overline{\rho}_a} + \overline{m}_w \tag{37}$$

The volume fraction of air, s, is defined by Equation (7) on page 7 as

$$s = \frac{Q_a}{Q} = \frac{\overline{Q}_a}{\overline{Q}} = \overline{s} \tag{7}$$

Noting that the first term on the right-hand-side of Equation (37) is $\overline{Q}_a$, s can be written as

$$\overline{s} = \frac{1}{1 + \overline{\rho}_a \left(\dfrac{\overline{m}}{\overline{m}_a} - 1 \right)} \tag{38}$$

Note that the dimensional s in Equation (7) and the non-dimensional $\overline{s}$ in Equation (38) will have the same numerical value. Once the value of s is determined, Equations (8) and (10) on page 7 give the plume acoustic properties of interest.

Another property which will turn out to be of interest is the time required for the Lagrangian volume element to reach the surface, t_s. This is obtained by numerical integration of Equation (26).

$$\overline{t}_s = \int_0^1 \frac{d\overline{z}}{\overline{W}} \tag{39}$$

The dimensional value is then

$$t_s = \lambda_t \overline{t}_s = H \left(\frac{\rho_w}{F_o} \right)^{1/3} \overline{t}_s \tag{40}$$

Relationship of Top Hat and Actual Velocity Profiles

Dimensional analysis and laboratory measurements of mean velocities in a turbulent buoyant plume have shown the flow to be self-similar and well represented by a Gaussian profile. That is,

$$w = w_m e^{-\frac{y^2}{b^2}} \tag{41}$$

where w_m is the maximum, or centerline, velocity and b is the width of the profile. Dimensional analysis shows b to be proportional to height above the nozzles, and experiments have shown

$$b = 0.116z \tag{42}$$

Note that when $y = b$, $w = e^{-1}w_m$.

Equating the mass and momentum flux of the Top Hat velocity profile and the actual profile gives the following relations [Lee and Chu (2003)]

$$\begin{aligned} w_m &= 2W \\ b &= \frac{B}{\sqrt{2}} \end{aligned} \tag{43}$$

The concentration, or volume fraction, of air in the rising plume has been found to follow a self-similar Gaussian distribution, similar to that for velocity

$$s = s_m e^{-\frac{y^2}{(\lambda b)^2}} \tag{44}$$

where b = width of the velocity profile, and

$$\lambda = 1.35 \tag{45}$$

The maximum value of s_m in Equation (44) is given in terms of average $\bar{s}$, Equation (38), by

$$s_m = 1.25\bar{s} \tag{46}$$

Specific Momentum Flux and Characteristic Length of Buoyant Jet Flow

A jet is the flow produced by a continuous source of momentum. A plume is the flow produced by a continuous source of buoyancy. In our case, as air exits from the nozzle at a relatively high velocity, it is a continuous source of both momentum and buoyancy, and so we have a buoyant jet. Lee and Chu (2003) show through dimensional analysis and experimental results that the majority of the flow produced by a buoyant jet is controlled by buoyancy.

In order to quantify exactly which part of the flow is controlled by buoyancy, it is necessary to compare the momentum flux with the buoyancy flux. The specific momentum flux (that is, momentum flux per unit mass) at the nozzle exit is given by

$$M_{so} = \frac{M_o}{\rho_{ao}} = Q_{ao} w_o \tag{47}$$

where w_o is the velocity of the air at the nozzle exit. Similarly, the specific buoyancy flux is

$$F_{so} = \frac{F_o}{\rho_{ao}} = \frac{(\rho_w - \rho_{ao})}{\rho_{ao}} g Q_{ao} \tag{48}$$

The characteristic length of a two-dimensional buoyant jet is given by

$$l_s = \frac{M_{so}}{F_{so}^{2/3}} \tag{49}$$

Experiments have shown that the flow in a two dimensional buoyant jet is plume-like for

$$\frac{z}{l_s} \geq 4 \tag{50}$$

"Plume-like" means that above 4 characteristic lengths, the initial momentum of the jet exiting the nozzles is completely dissipated, and only buoyancy controls the flow.

Compressible Fluid Flow Through the Nozzles

The manifold and nozzles essentially are in an infinite heat sink – the ocean. Assume the air in the manifold has been in transit long enough to reach the ocean temperature. The nozzles are short, so take the flow through the nozzles to be an isentropic flow of a perfect gas [Obert (1948), Binder (1951), Beychok (2008)].

Let k = the ratio of specific heats, equal to 1.4 for air.

P_M = Pressure in the manifold

P_o = External pressure at the nozzle exit

T_{sw} = Temperature of the air in the manifold = temperature of the seawater in ^oR

R = the gas constant = 53.36 ft-lb_f/lb_m-^oR for air.

Then, for subsonic velocities, the mass flow rate through a single nozzle, m_0, is

$$m_o = C_{dss} a P_M \sqrt{\frac{2g}{RT_{sw}}\left(\frac{k}{k-1}\right)\left[r_p^{2/k} - r_p^{(k+1)/k}\right]} \qquad \text{Subsonic} \tag{51}$$

where a is the exit area of the nozzle, C_{dss} is the subsonic discharge coefficient, and the pressure ratio, r_p, is defined as

$$r_p \equiv \frac{P_o}{P_M} \tag{52}$$

Using the isentropic pressure-density relationship

$$\frac{P}{\rho^k} = Const \tag{53}$$

it may be shown that there exists a critical pressure ratio, r_{pc}, for which the mass flow rate based on the velocity given by Equation (51) reaches a maximum.

$$r_{pc} = \left(\frac{2}{k+1}\right)^{\frac{k}{k-1}} \tag{54}$$

This velocity at the critical pressure ration, r_{pc}, is the sonic velocity, and no matter how far r_p is decreased below r_{pc}, the velocity does not increase. In our case, no matter how much P_m is increased, the exit velocity will not increase. However, as P_m is increased, the mass flow rate, m_o, continues to increase, and is given by

$$m_o = \frac{C_{ds} a P_m}{\sqrt{T_{sw}}} \sqrt{\frac{gk}{R}\left(\frac{2}{k+1}\right)^{\frac{k+1}{k-1}}} \qquad \text{Sonic Flow} \qquad (55)$$

where C_{ds} is a sonic discharge coefficient, which is highly dependent on the exact shape of the nozzle or orifice through which a gas is flowing.

Volume flow rate through the nozzle is then given by

$$q_o = \frac{m_o}{\rho_{ao}} \qquad (56)$$

where ρ_{ao} is the density of the air at the nozzle exit. Exit velocity is

$$w_o = \frac{q_o}{a} \qquad (57)$$

Air density in the manifold is determined from the perfect gas law. If the air is at the seawater temperature, T_{sw}, then

$$\rho_{aM} = \frac{P_M}{R T_{sw}} \qquad (58)$$

Manifold Design

Kreinin and Kafyrin (1979) give equations for the design of isothermal distributing manifolds. These equations will be used to determine the minimum manifold diameter necessary to limit the pressure drop between the first nozzle and the last nozzle.

The manifold inlet Reynolds number is given by

$$\mathrm{Re}_{in} = \frac{V_{in} D}{\upsilon} \qquad (59)$$

where V_{in} is the air velocity at the beginning of the manifold

D is the manifold diameter

υ is the kinematic viscosity of the air at the manifold inlet.

As stated by Edwards (2003), the viscosity of air, μ, is a function primarily of temperature. It varies very little with pressure. The Sutherland formula for viscosity is

$$\mu = \mu_o \left(\frac{a}{b}\right)\left(\frac{T}{T_o}\right)^{3/2} \tag{60}$$

where $a = 0.555T_o + C$

$b = 0.555T + C$

μ_o = reference μ at reference temperature T_o

C = Sutherland's constant.

For standard air, $C = 120$

$T_o = 524.07\ ^oR$

$\mu_o = 0.01827\ cp$

Kinematic viscosity, υ, is given by

$$\upsilon = \frac{\mu}{\rho} \tag{61}$$

V_{in} is given by the total volume rate of air flow divided by the manifold area. Using Equation (13) and the usual formula for the area of a circle, Re_{in} can be written as

$$\mathrm{Re}_{in} = \frac{4nq_o}{\pi\upsilon}\frac{L_M}{D} \tag{62}$$

Define a quantity η as

$$\eta = \frac{\mathrm{Re}_{in}}{16}\frac{D}{L_M} = \frac{nq_o}{4\pi\upsilon} \tag{63}$$

Then a friction factor F can be defined as

$$F^2 = \left|\frac{2}{\eta}(1+\eta) - \frac{\alpha_M}{2}\right| \tag{64}$$

where $\alpha_M = 2\ \ for\ \mathrm{Re} \le 2300$ and $\alpha_M = 1.05 - 1.1\ for\ \mathrm{Re} > 2300$.

The total exit area of all the nozzles is given by

$$a_\Sigma = nL_M\frac{\pi d^2}{4} \tag{65}$$

where d is the nozzle diameter. The ratio of the nozzle area to the manifold area is

$$\hat{a}_\Sigma = \frac{a_\Sigma}{\pi D^2 / 4} \tag{66}$$

If $F\hat{a}_\Sigma$ is small, then the ratio of the pressure at the end of the manifold to the pressure at the beginning of the manifold is given by

$$\frac{P_{end}}{P_{in}} = 1 - (F\hat{a}_\Sigma)^2 \tag{67}$$

From Equation (66), it is obvious that P_{end}/P_{in} depends on the ratio of total nozzle exit area to manifold cross section area.

Calculation of Manifold Length

All formulations to this point have been for a stationary manifold discharging air into still water. The assumption of still water may be accurate enough, but towing a manifold behind a seismic survey vessel traveling at 5 kts is far from stationary. So the question is, just what effect will the manifold traveling at 5 kts have on the formulation to this point.

The answer is ultimately found in the Lagrangian formulation described in "Lagrangian Analysis" on page 9. However, the analysis described in Appendix B provides some guidance. Appendix B analyzes a single, isolated bubble of air, ¼-inch in diameter, ejected at high velocity (100 fps) from a manifold traveling at 5 kts. This analysis has no direct application to the design of a towed manifold for the production of an air curtain. But it does illustrate how rapidly the horizontal and vertical velocity of this isolated bubble is reduced.

The trajectory of the bubble is shown in Figure 6. This plot shows that the bubble moves less than 0.002 ft in the direction of manifold travel. At the same time, the bubble has risen about 0.02 feet above the manifold nozzle exit. The results shown in this bubble trajectory confirm that the motion of a manifold moving at a velocity of 5 kts may be neglected.

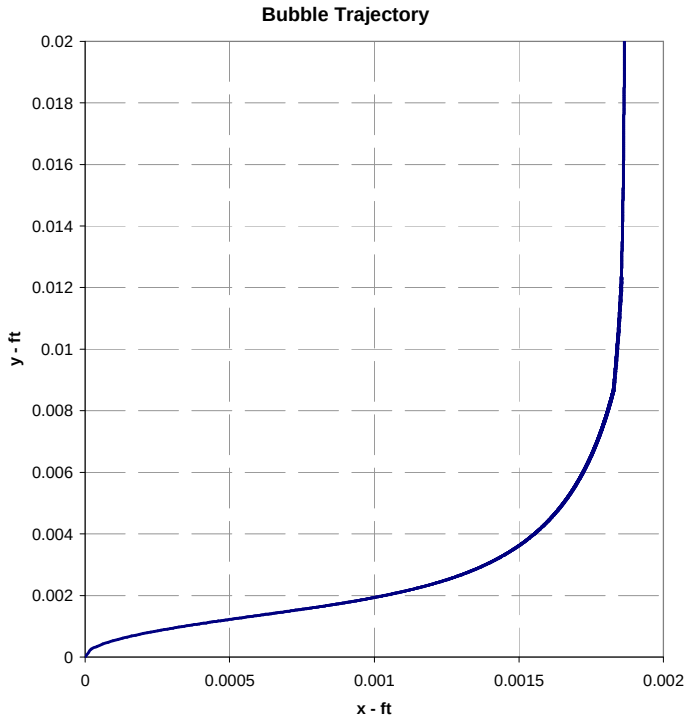

Figure 6 - Isolated Bubble Trajectory

Now consider the volume element in Figure 5. Just as for the single isolated bubble, as soon as the element moves up away from the nozzle, it is completely disengaged from the traveling manifold. The only forces then acting on it are caused by its momentum traveling through the still water and its buoyancy. Equation (50) on page 15 shows the vertical momentum is dissipated in a relatively short distance. And since the volume element of the jet is much larger than the ¼-inch bubble in Appendix B, the horizontal momentum should also dissipate rapidly.

So not a lot of error is introduced by assuming that once the volume element leaves the nozzle, it travels vertically upward with little or no horizontal motion.

Let t_s be the rise time (time between the air leaving the nozzle and reaching the surface) as given by Equation (40) on page 13. Let V_V be the speed of the vessel towing the air gun array and the manifolds. In the time t_s, the vessel travels a distance L_s, or

$$L_s = V_V t_s \tag{68}$$

In Figure 7, the position of the manifold at time zero is indicated by the black outline. At time t_s, the manifold is shown in red, and the air-water curtain is indicated by the shaded area.

The length of the curtain, L_c, which extends unbroken from the manifold to the surface is given by

$$L_c = L_M - L_s \tag{69}$$

Define an extra length Δ so that L_c is greater than the length of the air gun array, L_{array}

$$L_c = L_{array} + \Delta \tag{70}$$

Combining the above equations gives the equation for the required manifold length.

$$L_M = L_{array} + \Delta + L_s \tag{71}$$

The manifold should be towed so that its leading edge is $L_s + \Delta/2$ ahead of the array.

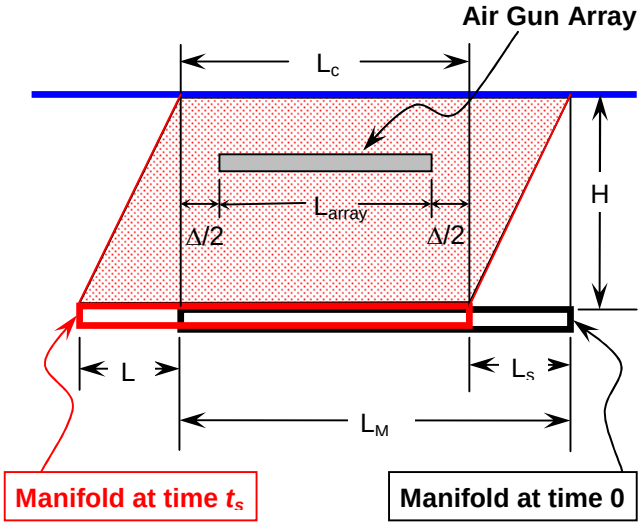

Figure 7 – Required Manifold Length

In Figure 7, the leading and trailing edge of the bubble curtain are shown as straight lines from the manifold at time t_s to the surface at a point over the ends of the manifold at time 0. The shape of the leading and trailing edges would be straight lines if the velocity of rise were constant. But integration of Equations (31) - (34) shows that the velocity is not constant, but in fact, it increases as the bubbles rise.

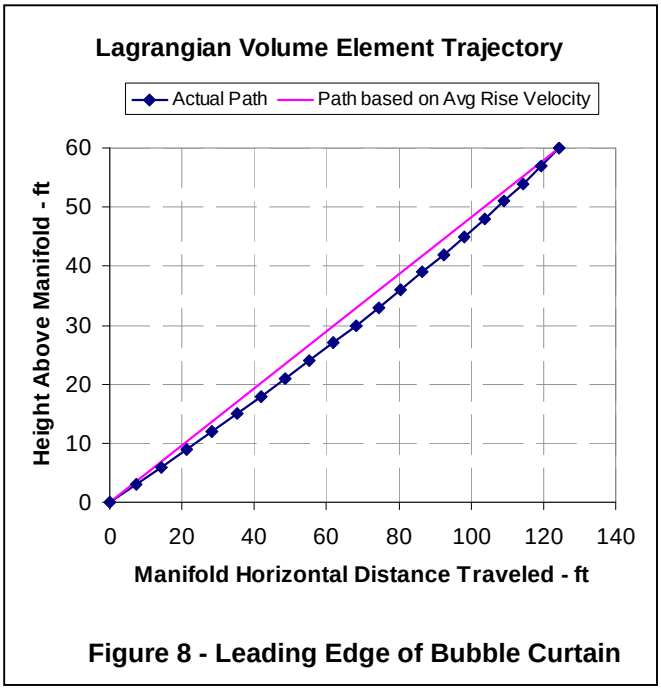

Figure 8 - Leading Edge of Bubble Curtain

However, as shown in Figure 8, the straight line is a good approximation for the leading and trailing edges of the bubble curtain. The trajectory calculated from the forward speed of the vessel and the time t to reach a height z is shown by blue curve with data points. The red curve represents the trajectory if the bubbles rose at a constant velocity. The difference in the horizontal direction between the two curves is relatively small, the maximum being 6 feet at a height of 33 feet above the manifold. Even with this difference, the use of L_c as defined in Figure 7 is conservative because it does not depend on the shape of the leading edge, but only on the location where the bubble curtain reaches the surface.

OPTIMAL DESIGN

All the equations necessary for the design of an air curtain have been stated in the previous sections. But the sheer number of equations and the interdependencies involved make any effort to arrive at a reasonable design very difficult. Fortunately, optimization methods exist for attacking just this sort of problem.

Principles

A brief summary of optimal design, adapted from Papalambros and Wilde (1988), follows.

The goal of design optimization is to improve a design so as to achieve the best way of satisfying the original need, within the available means.

A more rigorous statement is that design optimization involves:

- The selection of a set of variables to describe the design alternatives
- The selection of an objective, or criterion, expressed in terms of the design variables, which we seek to minimize or maximize
- The determination of a set of constraints, expressed in terms of the design variables, which must be satisfied by any acceptable design
- The determination of a set of values for the design variables, which minimize (or maximize) the objective, while satisfying all the constraints

The set of design variables is collectively known as the "*State Variable*"; it is an array of the independent variables chosen to describe the design alternatives. When the values of these variables are known (or assumed), everything else about the system can be calculated.

The objective of the design is known as the "objective function", and it is a function of the State Variable.

The constraints are represented by functional relations among the design variables (the State Variable) such as

$h(\boldsymbol{x}) = 0$

$g(\boldsymbol{x}) >= 0$

where $\boldsymbol{x}$ is the State Variable and $h()$ and $g()$ represent functions. As indicated by the equations, there are *equality constraints* and *inequality constraints*.

Application to Air Curtain Design

The principles stated above can be easily implemented in an Excel workbook using the Excel Solver add-in. Certain input quantities are required, such as water properties, air properties, depth of manifold below surface, number and diameter of nozzles, etc. With these values known, the state vector is taken to be composed of manifold pressure and manifold diameter.

$$State\ Vector = \begin{bmatrix} P_M \\ D \end{bmatrix} \tag{72}$$

Using the input values and P_M, the air flow through a nozzle can be calculated; the plume equations then determine the value of the air volume fraction in the plume; and the speed of sound ratio and specific impulse ratios can be calculated. Using D and the quantities already calculated, the pressure drop in the manifold can be calculated.

The objective function to be minimized is taken to be the pneumatic power of the flow in the manifold, that is, pressure times flow rate:

$$Power = P_M Q_{oT} \tag{73}$$

An equality constraint is used to determine the manifold diameter, D. The calculated ratio of the pressure at the end of the manifold, P_{end}, to the pressure at the beginning of the manifold, P_{in}, is set equal to some allowable value, chosen by the user. In this case the allowable value was chosen to be 0.98.

$$\frac{P_{end}}{P_{in}} - \left(\frac{P_{end}}{P_{in}} \right)_{Allowable} = 0 \tag{74}$$

Obviously, the manifold pressure must be greater than or equal to the external pressure or there will be no flow. At the same time, the pressure at the end of the manifold must also be greater than the external pressure. In fact, it should be some specified value greater than the external pressure. This minimum allowable pressure differential is chosen to be 2 psi.

In order to attenuate the air gun noise, the velocity of sound in the bubble plume, c, must be less than the velocity of sound in water, c_w. So the ratio c/c_w is constrained to be less than some selected value of $(c/c_w)_{max}$.

Thus the set of inequality constraints is

$$\begin{aligned} Manifold\ \text{Pr}essure - External\ \text{Pr}essure &\geq 0 \\ \left(Manifold\ End\ \text{Pr}essure - External\ \text{Pr}essure\right) - Allowable\ Differential &\geq 0 \\ \left(\frac{c}{c_w} \right)_{\max} - \frac{c}{c_w} &\geq 0 \end{aligned} \tag{75}$$

Equations (72) through (74) present a well-defined optimization problem. However, the calculations for the plume involve numerical solution of the Equations (30), (33), (35), and (36) on page 12.

The numerical solution was achieved by using a fourth-order Runga-Kuta routine for systems of initial value differential equations [Faires and Burden (1993)]. This routine was programmed as a user function in VBA. Integration is performed from the manifold to the surface ($\bar{z} = 0\ to\ 1$). At each step, the c/cw ratio is calculated, and compared with the maximum c/cw ratio already obtained. At conclusion of the integration, the function returns the maximum c/cw ratio for use in the last constraint of Equation (75).

This completes the definition of the optimization problem. These equation have been programmed into the Excel workbook, Air Curtain Design.xls. This workbook is described in more detail in Appendix C, and comparisons of the workbook formulas for calculation of air flow rates with experimental results is described in Appendix D.

RESULTS

Naturally, results depend on values of the input quantities. Sheet "Input" of the Air Curtain Design.xls workbook, containing all input values, is shown in Appendix C. Before presenting results, it is worthwhile to call attention to some of these input values.

Values for all the properties of air are standard values. The density of the sea water is taken to be constant at 64 lb_m/ft^3 and its temperature is taken to be 40 ^oF.

The manifold is envisioned to be similar to a "fire hose", so that it can be rolled up in its flattened configuration. When deployed, air pressure expands it to a circular shape. This concept does not allow for nozzles of any length, so the "nozzles" are treated as orifices. Accordingly, the nozzles discharge coefficients are taken to be 0.65.[J. E. Gasho & Associates (unknown)]

The vessel speed is taken to be 5 kts, or 8.4 fps, and the array length is taken to be 50 ft. The extra length Δ [see Figure 7] is taken to be 10 ft.

The minimum pressure drop ratio in the manifold is taken to be 0.98; that is, the pressure at the end of the manifold has dropped only 2% below the pressure at the beginning of the manifold. Also the minimum pressure differential at the end of the manifold is taken to be 2 psi. That is, the pressure at the end of the manifold is at least 2 psi greater than the external pressure. Later detailed design will have to seriously evaluate these input values, because the manifold diameter and length depend heavily on both.

With all other input values established, it is necessary to choose the depth of the manifold, H; the diameter, d; and number per foot, n, of the nozzles (orifices); and a desired maximum value of the c/cw ratio. Using the Solver add-in of Excel, a manifold pressure and diameter are determined which meet all constraints and minimize the pneumatic horsepower. Thus there is a solution for each combination of these variables.

So a matrix of solutions has been generated. At the end of each Solver minimization process, significant results were copied onto a row in the matrix. The complete matrix is contained in Sheet "SolutionSummary" of the workbook and presented in its entirety in Appendix E.

Selection of a "Best" Design

This investigation is based achieving a c/c_w ratio as small as possible, without actual calculation of the resulting attenuation of the air gun pressure signal. No details of the manifold deployment system were investigated, so no calculations of pressure loss from the air compressor to the beginning of the manifold and the first nozzle were made. No heat transfer calculations were made, so the actual air temperature in the manifold was assumed. In addition, no investigation into air compressor specifications was conducted.

Within these limitations, "the best" design can be defined as that which produces the largest volume of air, using the least horsepower, and with the smallest manifold diameter, all of which are mutually exclusive. As in any design problem, the design designated as "the best" in this investigation is a result of compromise among conflicting requirements. Without the further detailed specification of various parts of the system to produce the air curtain, picking the "best" design is a matter of engineering judgment.

Pneumatic horsepower and manifold diameter were chosen as the primary variables of interest. Secondary variables included volume flow rate, manifold length, and towing position with respect to the air gun array. To illustrate the application of engineering judgment to the matrix of solutions, consider Figure E - 1 from Appendix E, reproduced below as Figure 9.

This figure shows pneumatic hp and manifold diameter plotted against the maximum c/c_w ratio for a manifold depth of 200 ft, the maximum depths of the Beaufort and Chukchi Seas. Solutions are plotted for various number and diameter of nozzles.

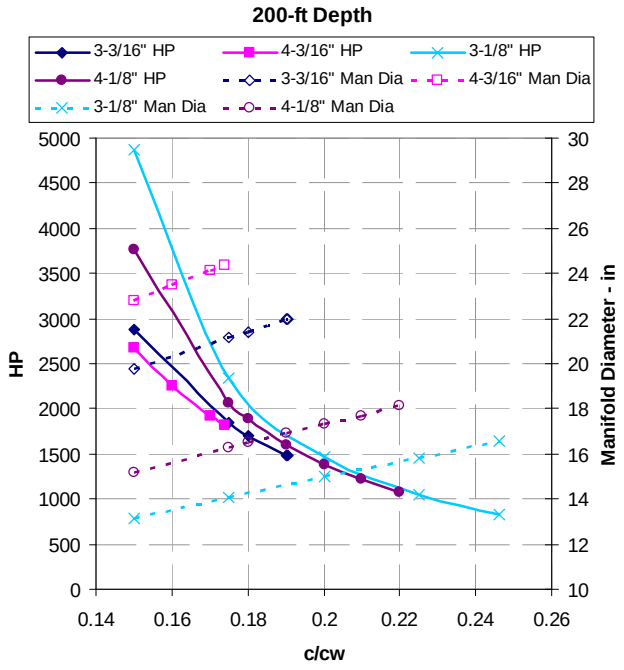

Figure 9 - HP and Diameters required for 200' Depth

Immediately obvious is the fact that all the solid hp curves have values greater than about 1000 hp. It is not possible to accept a higher maximum value of c/c_w in order to require less hp because the lowest point on each hp curve has reached the minimum pressure differential constraint at the end of the manifold. Lower hp can only be achieved by allowing pressure in the manifold at its end to be less than 2 psi greater than the external pressure!

Ideally, the maximum c/cw ratio would be less than 0.1; that is, the speed of sound in water would be at least 10 times the speed of sound in the plume. None of the values in this figure approach this value.

The manifold diameter curves (dotted) in this figure range from 13 to over 24 inches. Note that as the require hp decreases, the required manifold diameter increases. Also, as the total area of the nozzles per ft increases, the manifold diameter increases. Thus requirements for small hp and small diameter are mutually exclusive.

As can be seen in Table E - 5 and Table E - 6 of Appendix E, flow rates range from 13,200 to 56,100 scfm and manifold lengths range from 380 to 680 ft.

Figure 9 has illustrated trends in the solutions. However, it is also obvious that the requirements for the primary variables, hp and diameter, are too large for such an air curtain system to be practical. In addition, the secondary variables are too large to be practical. So shallower depths were investigated. Figures similar to Figure 9 for other depths are included in Appendix E.

Table 1 shows the range of manifold diameters in the solution matrix for each nozzle size. Obviously the larger nozzle size requires a larger manifold diameter. The same effect is obtained when the number of nozzles per foot is increased.

Table 1

MANIFOLD DIA RANGE		
Nozzle Dia	Manifold Dia	
	Min	Max
(in)	(in)	(in)
0.125	7.108	18.289
0.1875	10.493	24.365

So required horsepower can be reduced by increasing either the nozzle size or the number of nozzles per foot. But reduced horsepower comes at the cost of increased manifold diameter and all the associated practical handling problems.

The recommended system is shown as Solution #58, highlighted in orange, in Table E - 2 of Appendix E. This design is for a manifold having 3 – 1/8" nozzles per ft at a depth of 60 ft producing a maximum c/c_w ratio of 0.07. Such a system requires 423 hp, a flow rate of 4933 scfm, and a manifold diameter of 9". Manifold length is 201 ft, and it should be towed 141 ft in front of the air gun array.

The hp and manifold diameter plot from Figure E - 5 is reproduced here as Figure 10. The recommended system is represented by a point at $c/c_w = 0.7$ on the light blue curves which have an "x" for each data point.

A similar system is that of Solution #64 in Table E - 2 of Appendix E, also shown in Figure 10. This manifold has 4 -1/8" nozzles per ft, requires 367 hp, 4924 scfm, a manifold diameter of 10.4", and produces a maximum c/c_w ratio of 0.07. Solution #58 is recommended over this system because the manifold diameter is about an inch and a half smaller. The power required for Solution #58 is about 50 hp more, but 50 hp may be "cheaper" than handling and deploying a larger manifold. Manifold length is the same for both cases.

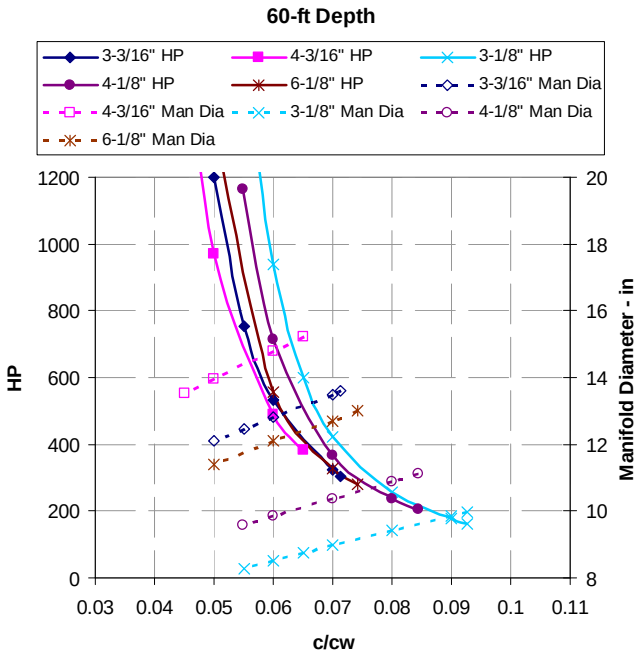

Figure 10 - HP and Diameters required for 60' Depth

Detail investigation of the pressure signal attenuation properties of the air curtain produced by the selected manifold may call for different compromises among the conflicting requirements for the design. For example, it may be worth using a compressor with more horsepower in order to get better signal attenuation. For the present, the selected "best" design represents a realistic starting point for more detailed investigation.

Discussion of Selected System

The variation in volume fraction of air as a function of height above the manifold for Solution #58 is shown in Figure 11. At the nozzle exit, the volume fraction of air is 1.0. As this figure shows, at a height, *z*, of 3 ft above the nozzle exit, the average volume fraction has already been reduced to 11%. This reduction is due to the water entrained in the upward flow. The fraction continues to decrease to a minimum of about 1.5% at *z* = 48 ft, and then slightly increases from there to the surface. This increase is due to the

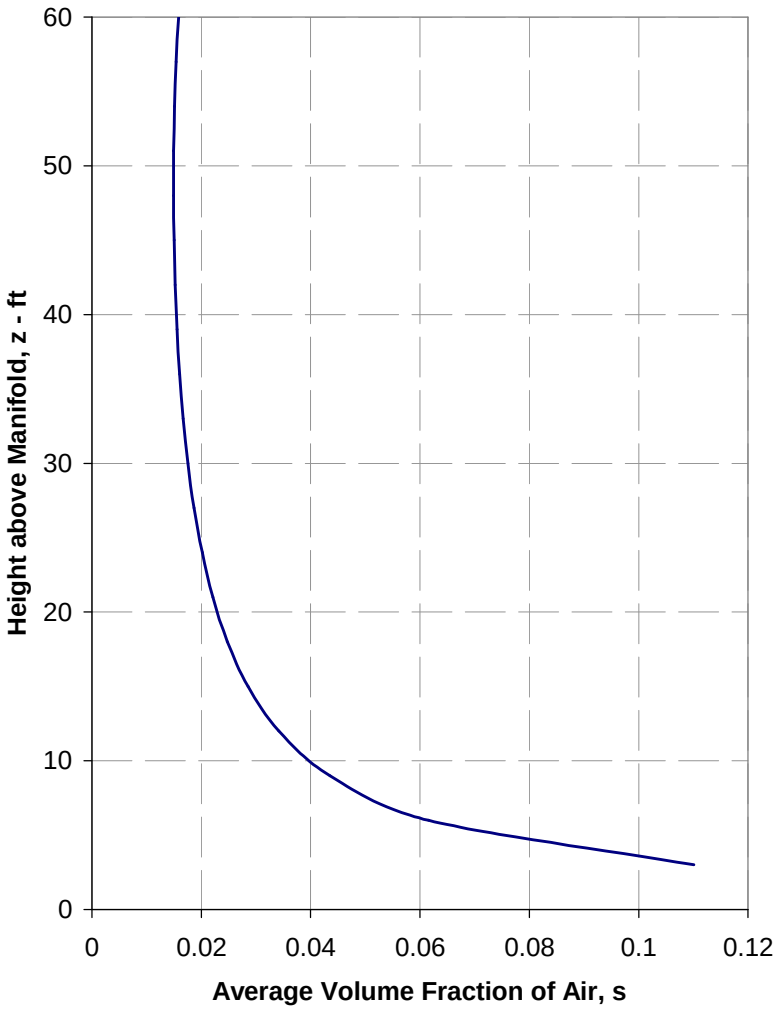

Figure 11 – Average Volume Fraction of Air, Solution #58

expansion of the air having a greater effect than the entrainment of water into the flow.

The variation in the speed of sound ratio, c/c_w, as a function of height above the manifold for Solution #58 is shown in Figure 12. At 3 ft above the manifold, it is 0.035; it reaches a maximum value of 0.07 at a

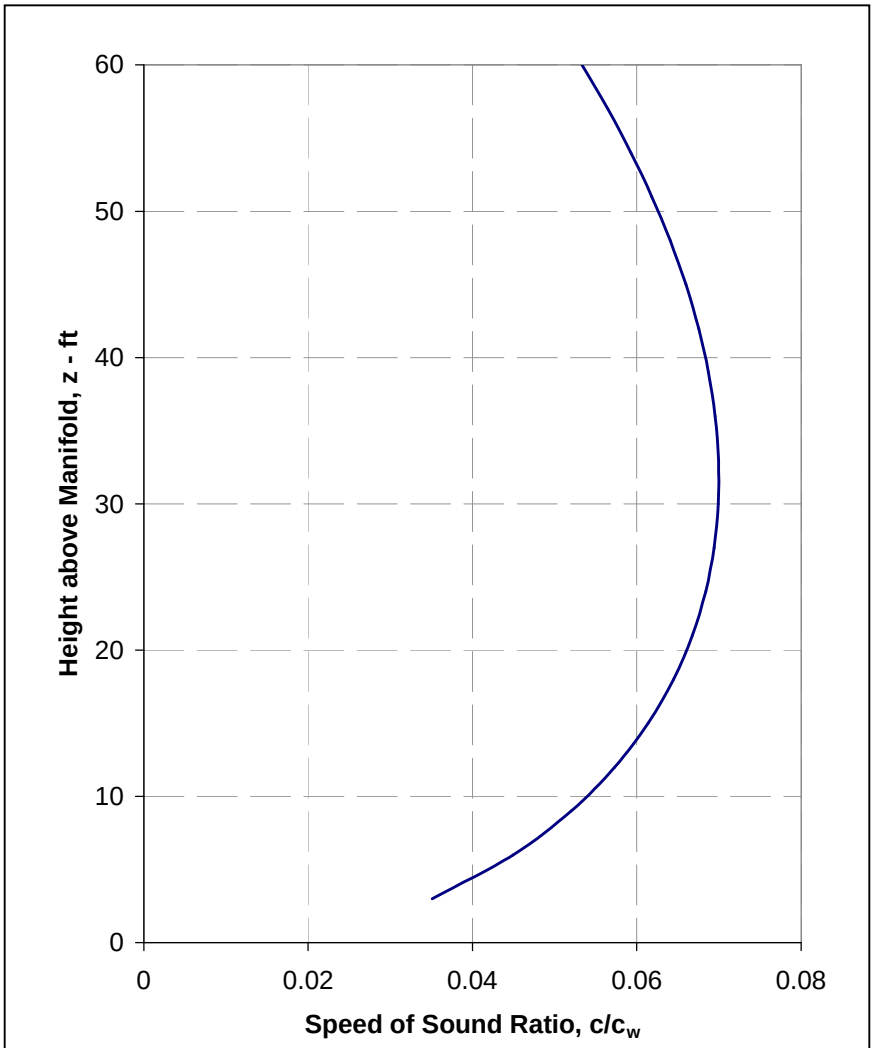

Figure 12 – Speed of Sound Ratio, Solution #58

height of 31.7 ft above the manifold; and decreases to 0.053 at the surface.

This relatively wide variation occurs even though the average volume fraction of air, s, is almost constant from mid-depth to the surface. However, when the formula for calculating c/c_w, shown in Equation (8) on page 7 is considered, it is obvious that the dependence on z is a complex one. The variation in s is shown in Figure 11. At the same time both compressibility, β_a, [Equation (6) and the second equality in Equation (21)] and density, ρ_a, [Equation (21)] of the air vary with z. The result is shown in the figure.

The variation in the specific acoustic impedance, I/I_w, as a function of height above the manifold for Solution #58 is shown in Figure 13. As shown at the end of Appendix C, this curve is simply ρ/ρ_w times the c/c_w curve, So the shape of the curves in Figure 13 and Figure 12 is very similar, and the values are close.

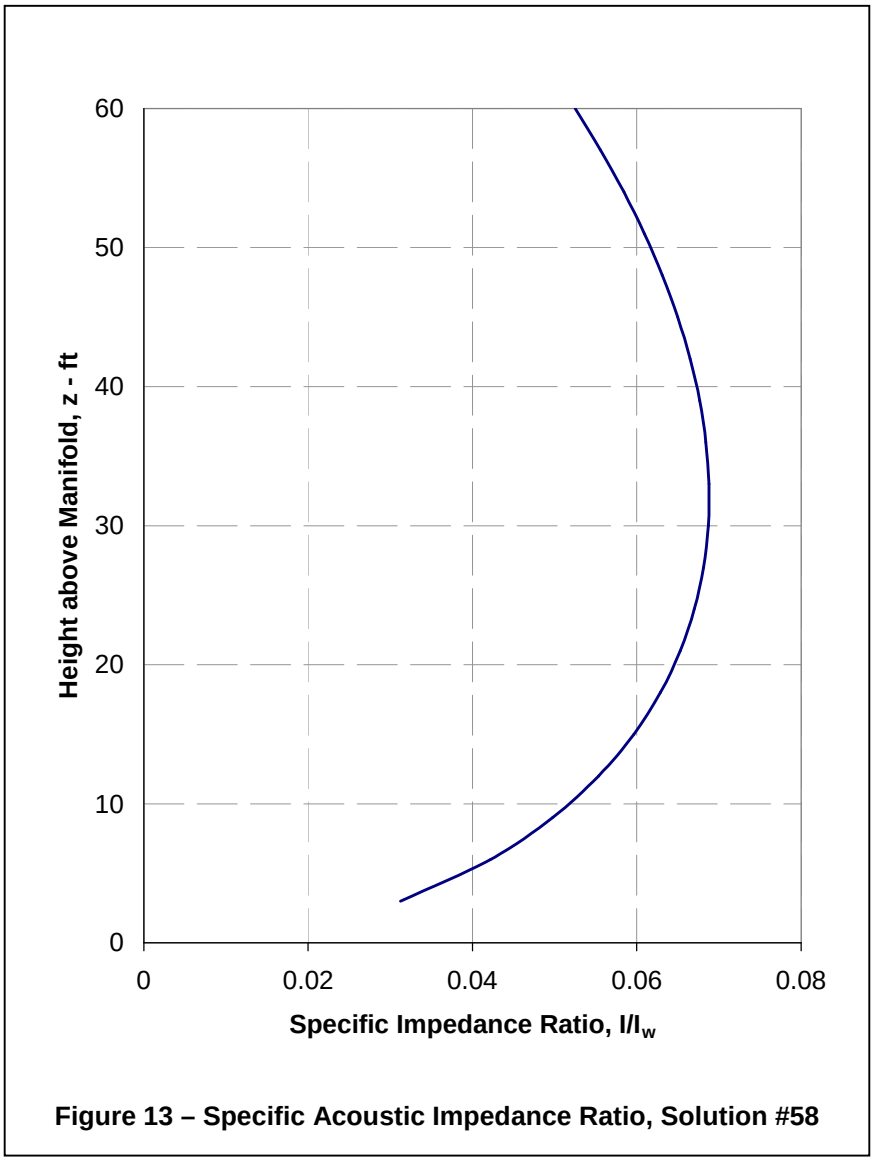

Figure 13 – Specific Acoustic Impedance Ratio, Solution #58

REFERENCES

Anonymous (1996), "Bubble Screen Acoustic Attenuation Test #1 Conducted for Shell Venezuela", Western Geophysical, Western Atlas International, Inc, Houston, TX.

Ayers, Ray R. (2007), "Methods to Reduce Lateral Noise Propagation from Seismic Exploration Vessels", PN 117168, Stress Engineering Services, Inc. proposal to the Minerals Management Service, Houston, Texas.

Beychok, Milton R. (2008), Gas Discharge to the Atmosphere from a Pressure Source, http://www.air-dispersion.com/usource.html, (accessed October 20, 2008).

Binder, R. C. (1951), Advanced Fluid Dynamics and Fluid Machinery, Prentice-Hall, Inc., New York.

Costigan, G. and Whalley, P. B. (1997), "Measurements of the Speed of Sound in Air-Water Flows," Chemical Engineering Journal, Vol. 66, pp. 131-135.

Domenico, S. N. (1982), "Acoustic Wave Propagation in Air-Bubble Curtains in Water - Part I: History and Theory," Geophysics, Vol. 47 (3), pp. 345-353.

Edwards, Ken (2003), Gas Viscosity, http://www.lmnoeng.com/Flow/GasViscosity.htm, (accessed October 10, 2008).

Faires, J. Douglas and Burden, Richard L (1993), Numerical Methods, PWS Publishing Company, Boston.

J. E. Gasho & Associates, Inc. (unknown), Application Engineering Basics, http://www.jegasho.net/rotron%20pages/orifice%20flow%20calculation.htm, (accessed October 30, 2008).

Jones, Warren T. (1972), "Air Barriers as Oil-Spill Containment Devices," Society of Petroleum Engineers Journal, Vol. 12 (2), pp. 126-142.

Jones, Warren T. (2008), Email to R. R. Ayers, "Bubble Curtain Mitigation of Lateral Noise Propagation from Seismic Exploration Vessels", September 22.

Kreinin, E. V. and Kafyrin, Yu. P. (1979), "Design of Isothermal Distributing Manifolds," Khimicheskoe i Neftyanoe Mashinostroenie, Vol. 5, pp. 16-18.

Lee, Joseph H. W. and Chu, Vincent H. (2003), Turbulent Jets and Plumes, A Lagrangian Approach, Kluwer Academic Publishers, Boston/Dordrecht/London.

Obert, Edward F. (1948), Thermodynamics, McGraw-Hill Book Company, Inc., New York.

Papalambros, Panos Y. and Wilde, Douglass J. (1988), Principles of Optimal Design, Modeling and Computation, Cambridge University Press, New York.

Sixma, E. and Stubbs, Scott (1996), "Air Bubble Screen Noise Suppression Tests in Lake Maracaibo", Congreso Venezolano de Geofisica, Sociedad Venezolana de Ingenieros Geofisicos.

Spence, Jesse (2008), "Seismic Array Directionality Study", Technical Memo 08-035, Noise Control Engineering, Inc.

Sutherland, John W. (2002), Forces Acting on Airborne Particles, http://www.mfg.mtu.edu/cyberman/environment/air/forces/forces.html, (accessed September 20, 2008).

Towell, G. D., Strand, C. AP., et al. (1965), "Mixing and Mass Transfer in Large Diameter Bubble Columns", A.I.Ch.E.-A.Chem.E. Symposium Series No. 10, pp. 10:97-10:105.

Appendix A

Compressibility of Air

Appendix A

Compressibility of Air

Compressibility, β, is given by

$$\beta = -\frac{dv/v}{dP} \tag{A-1}$$

where v is specific volume and $v = 1/\rho$.

As the air rises toward the surface after leaving the nozzle, it is in essentially an infinite heat sink, the ocean, and turbulence ensures that the air is well mixed with the sea water. So temperature of the air should remain constant at the sea water temperature. To calculate its compressibility, write the perfect gas equation as

$$Pv = RT \tag{A-2}$$

Take the differential of both sides and set $dT = 0$ since the process is isothermal.

$$Pdv + vdP = 0 \tag{A-3}$$

Solving for dv/v and substituting into Equation (A-1) gives

$$\beta_a = \frac{1}{P} = \frac{1}{P(z)} \tag{A-4}$$

The second equality is included to indicate that the pressure of the air rising toward the surface is a function of height above the nozzle, z.

Domenico (1982) quotes the relationship $\beta_a = 1.0086/P$ obtained from the American Institute of Physics Handbook as the actual relationship for air. Since this is a feasibility study, the perfect gas relationship of Equation (A-4) is accurate enough.

Appendix B

Isolated Bubble Trajectory

Appendix B

Isolated Bubble Trajectory

Consider an isolated, single bubble ejected from a manifold being towed at a speed of u_o. as shown in the adjacent sketch. At the instant the bubble exits from the nozzle, it is traveling in the x-direction at a speed of u_o and in the z direction at a velocity of w_o.

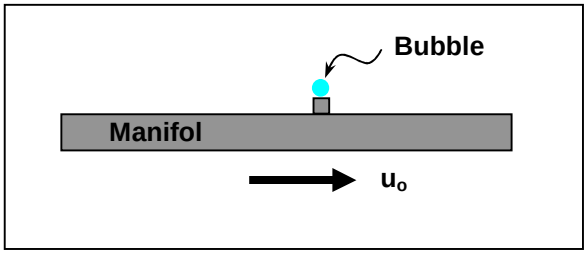

The bubble is a sphere with a ¼-inch diameter, in accordance with the predominant bubble size in a buoyant plume of air exiting into water. For simplicity, assume the bubble does not change shape or expand with lessening pressure. With these assumptions, the bubble is essentially a solid body.

Equations of Motion

A free body of the bubble is shown in the adjacent sketch. The bubble has a weight W and is acted upon by a buoyant force F_B. Because of its velocity in the x direction, there is a horizontal drag force, F_{DH}, exerted on the bubble. Because of its velocity in the z direction, there is a vertical drag force, F_{DV}, exerted on the bubble.

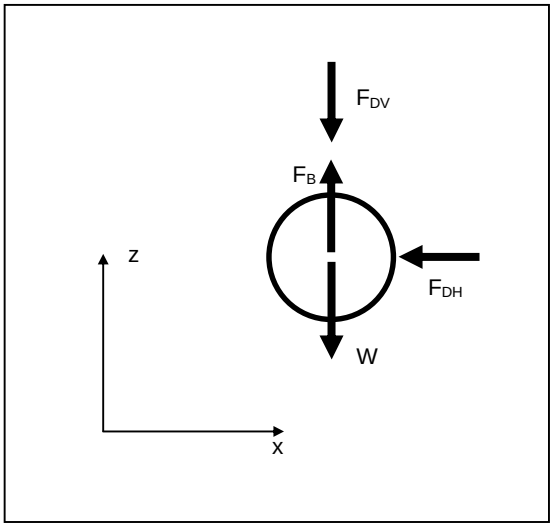

The equations of motion are given by

$$m\ddot{x} = -F_{DH}$$
$$m\ddot{z} = F_B - W - F_{DV} \qquad \text{(B-1)}$$

and initial conditions for $x(t)$ and $z(t)$ are

$$x(0) = 0$$
$$\dot{x}(0) = u_o$$
$$z(0) = 0 \qquad \text{(B-2)}$$
$$\dot{z}(0) = w_o$$

Various quantities involved in these equations are

$$m = \frac{w_a}{g}\frac{\pi D^3}{8} \qquad A = \frac{\pi D^2}{4} \qquad W = w_a \frac{\pi D^3}{8}$$
$$F_B = w_{sw}\frac{\pi D^3}{8} \qquad \rho_{sw} = \frac{w_{sw}}{g} \qquad \text{(B-3)}$$
$$F_{DH} = \frac{1}{2}\rho_{sw} C_{DH} A\dot{x}^2$$
$$F_{DV} = \frac{1}{2}\rho_{sw} C_{DV} A\dot{z}^2$$

where w_a and w_{sw} are the specific weight of air and seawater, respectively

D is the bubble diameter

C_{DH} and C_{DV} are the drag coefficients in the horizontal and vertical directions.

Substituting into Equations (B-1) gives

$$\ddot{x} = -\frac{w_{sw}}{w_a}\frac{C_{DH}}{D}\dot{x}^2$$
$$\ddot{z} = \frac{w_{sw} - w_a}{w_a}g - \frac{w_{sw}}{w_a}\frac{C_{DV}}{D}\dot{z}^2 \qquad \text{(B-4)}$$

These two second order differential equations may each be written as two first order differential equations with their associated initial conditions

$$\begin{aligned}
\dot{x} &= u && , \quad x(0) = 0 \\
\dot{u} &= -\frac{w_{sw}}{w_a}\frac{C_{DH}}{D}u^2 && , \quad u(0) = u_o \\
\dot{z} &= w && , \quad z(0) = 0 \\
\dot{w} &= \frac{w_{sw} - w_a}{w_a}g - \frac{w_{sw}}{w_a}\frac{C_{DV}}{D}w^2 && , \quad w(0) = w_o
\end{aligned} \qquad \text{(B-5)}$$

Non-dimensional Equations of Motion

Because of the velocity squared terms, a numerical solution is appropriate. In order to carry out a numerical solution, these equations need to be non-dimensionalized. So let

$$\begin{aligned}
x &= \lambda_x \hat{x} \\
z &= \lambda_z \hat{z} \\
t &= \lambda_t \hat{t}
\end{aligned} \qquad \text{(B-6)}$$

where the λs are scaling factors and hats represent the non-dimensional quantity. Substituting Equations (B-6) into Equations (B-5) and setting $\lambda_x/D = \lambda_z/D = g\lambda_t^2/\lambda_z = 1$ leads to the following definition of the scaling factors

$$\begin{aligned}
\lambda_x &= \lambda_z = D \\
\lambda_t &= \sqrt{\frac{D}{g}} \\
\lambda_v &= \sqrt{Dg}
\end{aligned} \qquad \text{(B-7)}$$

where λ_v is the scaling factor for velocity. The non-dimensional system of equations becomes

$$\begin{aligned}
\frac{d\hat{x}}{d\hat{t}} &= \hat{u} && , \quad \hat{x}(0) = 0 \\
\frac{d\hat{u}}{d\hat{t}} &= -\frac{w_{sw}}{w_a} C_{DH} \hat{u}^2 && , \quad \hat{u}(0) = \hat{u}_o \\
\frac{d\hat{z}}{d\hat{t}} &= \hat{w} && , \quad \hat{z}(0) = 0 \\
\frac{d\hat{w}}{d\hat{t}} &= \frac{w_{sw} - w_a}{w_a} - \frac{w_{sw}}{w_a} C_{DV} \hat{w}^2 && , \quad \hat{w}(0) = \hat{w}_o
\end{aligned} \tag{B-8}$$

Numerical Integration

The simplest numerical integration scheme was chosen for implementation in an Excel workbook – Euler Numerical Integration. The second of Equations (B-8) can be written as

$$\begin{aligned}
&\frac{\hat{u}_{i+1} - \hat{u}_i}{\hat{t}_{i+1} - \hat{t}_i} = -C_1 C_{DHi} \hat{u}_i^2 \\
&where \\
&C_1 = \frac{w_{sw}}{w_a}
\end{aligned} \tag{B-9}$$

This equation may be rearranged to solve for $\hat{u}_{i+1}$ in terms of $\hat{u}_i$. Similar operations on the other Equations (B-8) give

$$\begin{aligned}
&\hat{u}_{i+1} = \hat{u}_i - C_1 C_{DHi} \hat{u}_i^2 \Delta\hat{t} \\
&\hat{x}_{i+1} = \hat{x}_i + \hat{u}_i \Delta\hat{t} \\
&\hat{w}_{i+1} = \hat{w}_i + \left(C_2 - C_1 C_{DVi} \hat{w}_i^2\right) \Delta\hat{t} \\
&\hat{z}_{i+1} = \hat{z}_i + \hat{w}_i \Delta\hat{t} \\
&where \\
&C_2 = \frac{w_{sw} - w_a}{w_a} \\
&\Delta\hat{t} = \hat{t}_{i+1} - \hat{t}_i
\end{aligned} \tag{B-10}$$

Initial conditions provide values for time step zero ($i = 0$). Then calculation of values at successive time steps from these equations is straightforward.

The drag coefficient, C_D, for a spherical particle is defined in terms of the Reynolds number, Re, as shown in Sutherland (2002).

$$C_D = \frac{24}{\mathrm{Re}} \quad , \quad \mathrm{Re} < 1$$
$$C_D = \frac{24}{\mathrm{Re}}\left(1 + \frac{\mathrm{Re}^{2/3}}{6}\right) \quad , \quad 1 < \mathrm{Re} < 1000 \qquad \text{(B-11)}$$
$$C_D = 0.5 \quad , \quad 1000 < \mathrm{Re} < 2x10^5$$

Results

Equations (B-10) and (B-11) were programmed in an Excel workbook, Bubble Trajectory.xls. A $\Delta\hat{t}$ of 0.0001 was chosen and the resulting non-dimensional quantities converted back to dimensional quantities using the scaling parameters in Equations (B-6) and (B-7). The resulting time step was $2.54x10^{-6}$ sec.

The manifold velocity, u_o, was taken to be 5 kts = 8.44 fps. The air exit velocity, w_o, was arbitrarily taken to be 100 fps.

Displacements and velocity in the x-direction as a function of time are shown in Figure B - 1. Note that the velocity in the x-direction is essentially zero in less than 0.01 seconds and the displacement in the x-direction remains constant thereafter. In 0.01 seconds, the manifold has moved 0.084 feet.

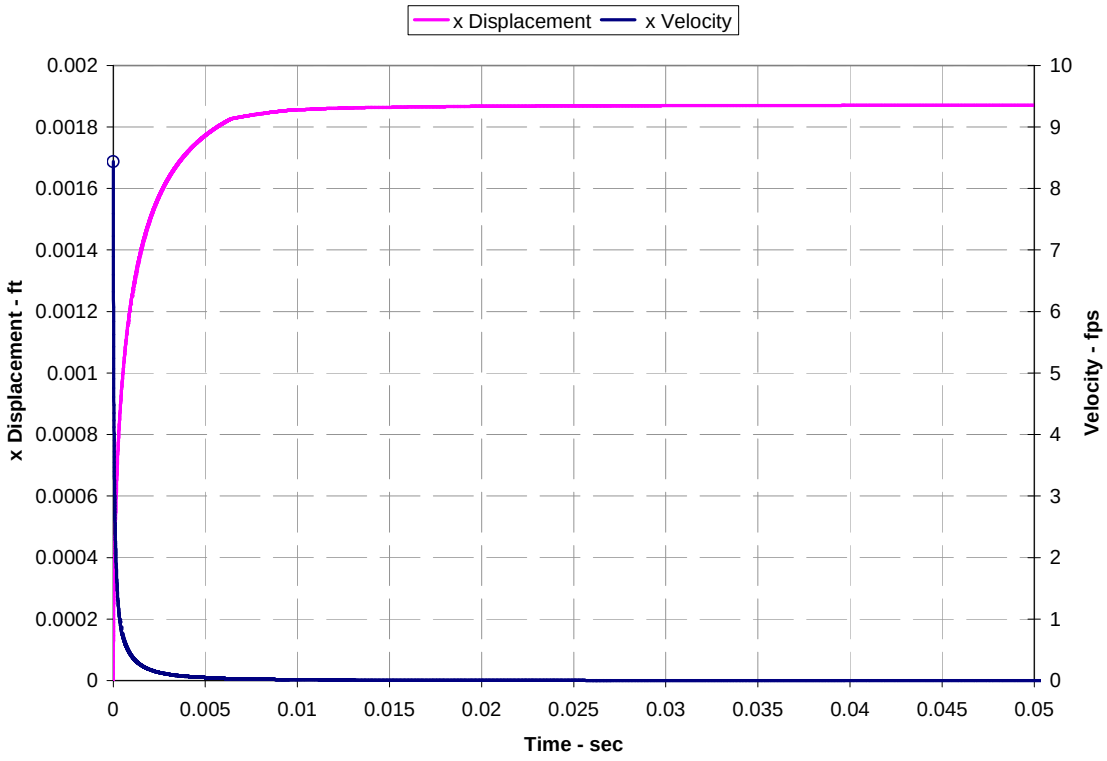

Figure B - 1 Displacement and Velocity in the x Direction

Displacements and velocity in the x-direction as a function of time are shown in Figure B - 2.

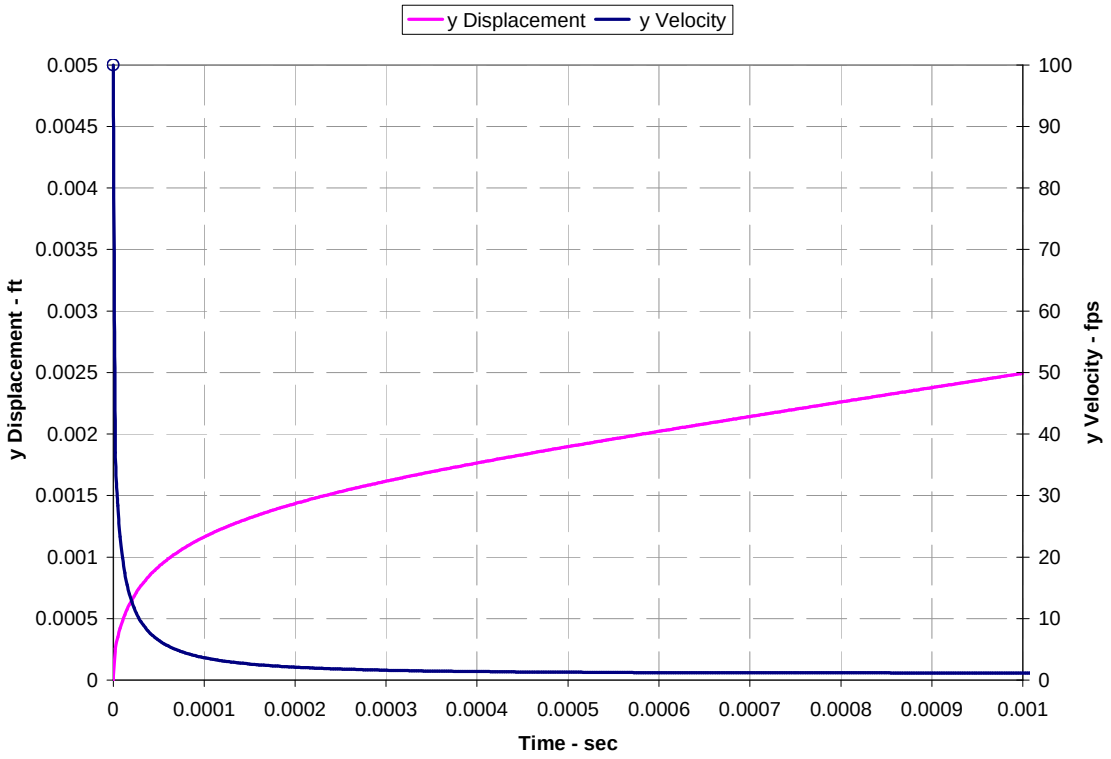

Figure B - 2 Velocity and Displacement in the y-Direction

Note that the initial velocity in the y-direction of 100 fps has decreased to what appears to be a constant value in 0.0004 seconds. At this time, the y displacement is 0.0018 ft. Actually, the y velocity continues to decrease and eventually reaches a constant value of 1.15 fps at 0.002 seconds, at which time the y displacement is 0.0037 ft. The value of 1.15 fps agrees well with bubble terminal rise velocities of about 30 - 33 cm/sec = 0.98 - 1.1 fps quoted in the literature.

Using time as a parametric value, the bubble trajectory may be plotted as shown in Figure B - 3.

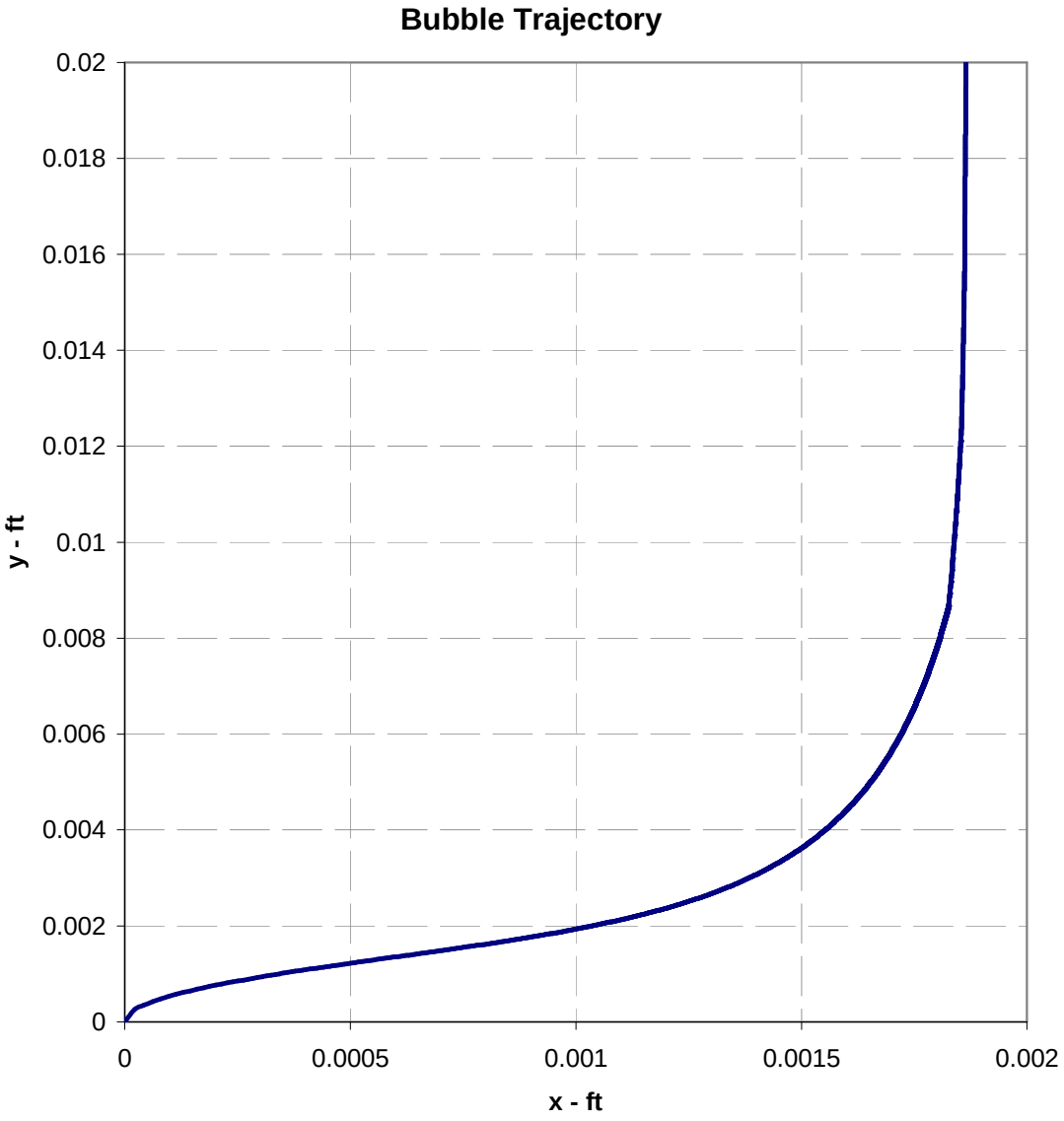

Figure B - 3 Bubble Trajectory

This plot shows that the bubble moves less than 0.002 ft in the direction of manifold travel. At the same time, the bubble has risen about 0.02 feet above the manifold nozzle exit.

The results shown in this bubble trajectory confirm that the motion of a manifold moving at a velocity of 5 kts may be neglected.

Appendix C

Excel Workbook Air Curtain Design.xls

Appendix C

Excel Workbook Air Curtain Design.xls

This workbook consists of four worksheets and three chart sheets containing plots of the data in the fourth worksheet. Each of the sheets is described on the following pages.

In addition, Visual Basic for Applications (VBA) code is contained in the usual Excel objects and in three modules. Documentation is contained in the comments in the code.

This workbook evolved over the course of this investigation. The emphasis has been on developing the correct method to evaluate the feasibility of the air bubble curtain. Therefore, this workbook contains vestiges of previous methods deemed unsuitable or inefficient. It is NOT user friendly, and is not necessarily the most efficient arrangement of the calculations described below. However, it is reasonably efficient, so no further work was done to improve either the efficiency or the user friendliness.

Numerical values and plots shown in the following figures are for the selected “best” design, Solution #58 of Appendix E.

AIR CURTAIN DESIGN	Created: Warren T. Jones, Ph.D. 10/3/08 4:05 PM
Input	Last Revision: 11/30/08 3:07 PM

Properties of Air

Atmospheric pressure [Patm]	14.7	psi =	2116.8	lb/ft^2	
Gas Constant [GCR]	53.36	ft-lb/lbm-°R			
Specific Heat Ratio [k]	1.4				
Standard Conditions: Temperature [Tstd]	68	°F =	527.69	°R	
Standard Conditions: Pressure [Pstd]	14.7	psi =	2116.8	lb/ft^2	
Sutherland's Formula: To [RefT]	524.07	°R			
Sutherland's Formula: C [SutherlancConst]	120				
Sutherland's Formula: a[aFactor]	410.8589				
Sutherland's Formula: b[bFactor]	397.328				
Sutherland's Formula: m_o[muo]	0.01827	cp			

Properties of Water

Density of water [rhow]	64	lbm/ft^3			
Compressibility of water [Betaw]	2.10E-08	ft^2/lb			
Seawater Temperature [Tsw]	40	°F =	499.69	°R	

Gravity, Nozzle, and Plume Properties

Acceleration of gravity [g]	32.1739	ft/sec^2			
Sub-sonic Nozzle Coefficient [cdss]	0.65				
Sonic Nozzle Coefficient [cds]	0.65				
2-D Entrainment factor [EntFac] =	0.103				
2-D Velocity spreading factor [VelSpreadFac] =	0.116				
Ratio concentration to velocity width [lambda]	1.35				
Lagrangian Spreading Coefficient [Lbeta]	0.145				

Design of Air Curtain

Vessel Speed [Vv]	5	kts =	8.445	fps	
Array Length [Larray]	50	ft			
Excess Length [Lexcess]	20	ft			
Depth of Manifold [H]	60	ft			
Maximum Number of Nozzles/ft [Maxn]	3				
Maximum Nozzle dia [Maxd]	0.125	in =	0.010417	ft	
Max Speed of Sound Ratio [Maxcocw]	0.07				
Minimum Pressure Drop Ratio in Manifold [PendoPinAllow]	0.98				
Minimum Pressure Differential at Manifold End [PendDiffAllow]	2	psi			

Calculated Quantities

Water Pressure at manifold [Po]	5956.8	psfa =	41.366667	psia			
Speed of Sound in water [cw]	4895.305798	fps					
Specific Impedance of water [SpecImp_w]	9737.693318	$lb\text{-}sec/ft^3$ =	1.530E+06	$N\text{-}sec/m^3$ =	1.530E+06	rayls	
Critical Pressure Ratio [rpc]	0.528281788						
Max Pm for sonic velocity at nozzle [Pmmax]	11275.80041	psf =	78.30417	psi			
k/(k-1) [kokm1]	3.5						
k/(k+1) [kokp1]	0.583333333						
(k-1)/k [km1ok]	0.285714286						
(k+1)/k [kp1ok]	1.714285714						
(k+1)/(k-1) [kp1okm1]	6						
Viscosity of air [mu_cp]	0.017589323	cp					
Viscosity [VisAir]	3.676E-07	$lb\text{-}sec/ft^2$					

Plot Parameters

Number of Plot Points [NumPlotPts]	20
Number of integration steps [NumSteps]	20000
Number of output steps [NumOut]	1000

Figure C - 1 Sheet "Input"

Sheet "Input"

This sheet in shown in Figure C - 1. Input quantities are arranged in groups. Properties of air and water are input in the first two groups. Gravity, Nozzle and Plume properties are input in the third group. Design variables are in the fourth group. Calculated quantities which do not depend on anything but these input values are shown next. At the bottom of the sheet, the group "Plot Parameters" contains values for the numerical integration of the simultaneous differential equations and the plots in the three chart sheets.

Input supplied by the user is shown in the yellow cells outlined in blue. An identifying label is shown to the left of each input cell along with the Excel name for that cell enclosed in square brackets. The values shown in these yellow cells were used throughout this investigation. The orange cells in the "Design of Air Curtain" group are those variables which were varied to produce the matrix of solutions described below under Sheet "SolutionSummary"

AIR CURTAIN DESIGN	Created: Warren T. Jones, Ph.D.	10/3/08 5:16 PM
Design Calculations	Last Revision:	12/20/08 12:48 PM

Depth of Manifold	60	ft		
Number of nozzles per ft [n]	3	1/ft		
Diameter of nozzle exit [d]	0.125	in =	0.010417	ft

State Vector

Manifold Pressure [Pm]	58.402125	psia =	8409.906	psfa
Diameter of manifold [Dman]	8.98653346	in =	0.748878	ft

Plume and Flow Calculations

Nozzle pressure ratio [rp]	0.70830756			
Nozzle spacing [NozSpac]	4	in		
Area of 1 nozzle [a] =	8.5221E-05	ft^2		
Air density in manifold [Rhoam]	0.31540942	lbm/ft^3		
Air density at exit of nozzle [Rhoao]	0.22340688	lbm/ft^3		
Mass flow rate through 1 nozzle [ma]	0.01025174	lbm/sec		
Volume Flow Rate through 1 nozzle [qo]	0.0458882	ft^3/sec =	2.753292	cfm
Nozzle exit velocity [wo]	538.460236	fps		
Volume flux per unit length [Qo]	0.13766461	$ft^3/sec/ft$ =	8.259877	cfm/ft
Density difference at manifold exit [DelRhoo]	63.7765931	lbm/ft^3		
Buoyancy flux per unit length [Fo]	282.48	lb/sec^3		
Rise Time [ts]	15.4867546	sec	282.4798	
Manifold length [Lm]	201	ft		
Speed of Sound Ratio [cocw]	0.07			

Pressure Drop in Manifold Calculations

Manifold area [Aman] =	0.4404654	ft^2
Vin [Vin] =	62.821252	ft/sec
Kinematic Viscosity of air[KinVisAir] =	3.75E-05	ft^2/sec
Re_{in} [Rein] =	1.25E+06	
Eta [Eta] =	292.13796	
$alpha_M$ [alpham] =	1.075	
Factor F [F] =	1.2121659	
Sum of nozzle exit areas [Suma] =	0.0513884	ft^2
a_πHat [SumaHat] =	0.1166683	
Fa_πHat [FSumaHat] =	0.1414214	
P_{end}/P_{in} [PendoPin] =	0.98	

Equality Constraints - Should be = 0

Pend/Pin - Allowable Pend/Pin = 1.2538E-10

Minimize

Power = 423.1037 hp

Inequality Constraints - Should be >= 0

Manifold pressure - external pressure =	17.0354584	psi
(Pend - Po) - Allowable Diff =	13.8674159	psi
Max c/cw - c/cw =	0	

Optimum Solution

go' [goprime]	9,184.77	ft/sec^2
Fr_o	55.04971	
Momentum Flux [Mo]	16.56046	lbm/sec^2
Characteristic length [ls]	0.385	ft

Required Flow rate and Pressure at manifold

0.07	**= Max c/cw**
60	**ft = Manifold Depth**
58.4	**psia at entrance**
57.2	**psia at end**
4933.79	**scfm = 1660.2 cfm at manifold**
423.1	**Total pneumatic HP at manifold**
201.00	**ft = Manifold length**
141	**ft = Manifold Position in front of air gun array**
603	**Total Number of Nozzles**

Plane jet flow is plume-like for z >	**1.539**	**ft**
Velocity width at surface	**13.92**	**ft**
Visual plume width at surface	**17.4**	**ft**
Concentration width at surface	**18.79**	**ft**

Scaling Factors and Non-Dimensional Quantities

lambdaF	282.4798	lb/sec^3	madot	0.0307552	lbm/ft-sec
lambdam	6298.933	lbm/ft-sec	CapWo	538.46024	fps
lambdaP	3840	psf	Mo_bar	0.0016028	
lambdaQ	98.42083	ft^2/sec	Wo_bar	328.25991	
lambdaRhc	64	lbm/ft^3	ma_bar	4.883E-06	
lambdaRT	60	ft	Patm_bar	0.55125	
lambdat	36.57762	sec	rhoao_bar	0.0034907	
lambdaW	1.640347	fps	RT_bar	444.39097	
lambdaz	60	ft	betaw_bar	8.056E-05	
lambdac	1.640347	fps	cw_bar	2984.3107	
ambdabeta	0.00026	ft^2/lb	g_bar	717.43637	

Figure C - 2 Sheet "Design"

Sheet "Design"

Sheet Description

This sheet is shown in Figure C - 2. All calculations for the design are done from this sheet. Bold headings separate various regions. The State Vector is shown at the top, with a light blue background for the cells. The Solver Add-In varies the values in these cells in order to satisfy the constraints and minimize the power shown in the light green cell on the right.

Immediately below the State Vector are the Plume and Flow Calculations, and to their right are the Pressure Drop in the Manifold Calculations. Equality and Inequality Constraints are shown below the Plume and Flow Calculations.

Various quantities of interest in evaluating optimal designs based on the Input in Figure C - 1 are listed between the two double lines in bold print. In normal print are quantities of general fluid dynamics interest which do not necessarily enter into an evaluation of the suitability of this design. One item of both optimal design interest and fluid dynamics interest is the height above which the flow is plume-like. The topmost bold item on the left side of the page below the first double line is "Plane jet flow is plume-like for z > 2.788 ft." That means that for all heights above the manifold greater than about 2-3/4 ft, the flow in the bubble curtain is driven solely by buoyancy.

Scaling factors for the non-dimensionalization of the differential equations are shown below the second double line. Also shown there are values of various non-dimensional quantities used in the solution of the differential equations.

Two buttons are also located on this page with captions of "Update Plots" and "Optimum Solution." The "Update Plots" button calculates and updates the table on Sheet "PlotData" which is used to create the charts contained in the last three sheets of the workbook: "cht_s", "cht_cRatio", and "cht_Iratio." The "Optimum Solution" button is used to initiate execution of the VBA routines used in obtaining an optimum solution.

Calculation Algorithms

For any value of manifold pressure, P_m, in the State Vector, the following algorithm is used to calculate the cells under the heading "Plume and Flow Calculations"

- The nozzle pressure ratio, r_p, is calculated from Equation (52) on page 15.
- The nozzle spacing is calculated from Equation (12) on page 8. (This step is not necessary for the following steps – it's included just for easy reference.)
- The area of one nozzle, a, is calculated from $\pi d^2/4$
- Air density in the manifold, ρ_{aM}, is calculated from Equation (58) on page 16.
- Since the "nozzles" in the manifold will likely be just holes, they are treated as orifices. So air density at the exit of the nozzle, ρ_{ao}, is calculated from the perfect gas relationship and the pressure and temperature in the water at the manifold depth.
- If $r_p > r_{pc}$ as given by Equation (54) on page 15, then the subsonic mass flow rate is calculated from Equation (51) on page 15; otherwise the sonic mass flow rate is calculated from Equation (55) on page 16.
- The flow rate through one nozzle, q_o, is calculated by Equation (56) on page 16.
- The nozzle exit velocity, w_o, is calculated from Equation (57) on page 16.
- The volume flux per unit length, Q_o, is calculated from Equation (11) on page 7.
- The density difference at the manifold exit is simply the water density, ρ_w, minus the air density at the nozzle exit, ρ_{ao}.

- Buoyancy flux per unit length at the nozzle exit, F_o, is calculated from the right-hand equality in Equation (19) on page 9 using the air density at the nozzle exit, ρ_{ao}.
- The rise time, t_s, is the value calculated in the table on Sheet "PlotData" (shown with an orange background in Figure C - 4).
- The manifold length, L_M, is calculated from Equations (68) though (71) on page 19.
- The Speed of Sound Ratio is the maximum value of c/c_w and is calculated by the User Function MaxSpeed2 (described below)
- The objective function is the pneumatic horsepower given by Equation (73) on page 21.

The calculations just described only involve the first variable in the State Vector, P_m. However, several quantities calculated above are also involved in calculating the Pressure Drop Ratio in the manifold, namely a, ρ_{aM}, Q_o, and L_M. For any value of manifold diameter, D_{Man}, in the State Vector, the following algorithm is used to calculate the cells under the heading "Pressure Drop in Manifold Calculations"

- The manifold area, A_{man}, is calculated from $\pi D^2/4$.
- The velocity entering the manifold V_{in}, is calculated from $Q_o L_m/A_{man}$
- Kinematic viscosity of the air in the manifold is given by Equations (60) and (61) on page 17
- Calculation of the remaining quantities ending with P_{end}/P_{in} follow Equations (62) through (67).

Button "Update Plots"

Clicking this button executes the VBA subroutine SolveSys(bWRITE As Boolean) with bWRITE set equal to TRUE. This subroutine reads the required non-dimensional values currently in Sheets "Design" and "Input" and calls the Runga-Kutta integration routine, RKsys2. Because the argument bWRITE is TRUE, the table on Sheet "PlotData" is updated during the course of numerical integration.

User Function MaxSpeed2

This function calculates the maximum value of the speed of sound ratio, c/c_w, occurring from the manifold to the surface. To do this, it calls the VBA subroutine SolveSys(bWRITE As Boolean) with bWRITE set equal to FALSE. With bWRITE = FALSE, nothing is written out, This is a necessary requirement, because user functions cannot modify the contents of any cell except the cell in which the call to the user function is located. This function returns the maximum value of c/c_w for use in the third constraint shown in Equation (75) on page 21. In order to ensure that this function is evaluated every time the Solver add-in changes the values in the State Vector, this user function has arguments P_M and D_{Man}. So whenever the Solver add-in varies values in the State Vector, this function is recalculated.

Button "Optimum Solution"

The following algorithm is executed by clicking on the "Optimum Solution" button.

1. Begin an iteration loop
2. Execute the Solver. The Solver varies the State Vector to determine the values which minimize the pneumatic hp. During these calculations, the rise time, t_s, has a value equal to that in the table on Sheet "PlotData"
3. Recalculate the rise time by calling SolveSys(TRUE). This updates the table on Sheet "PlotData" and the rise time on Sheet "Design" is equal to the rise time calculated in this table.
4. If the new rise time differs from the old rise time by less than some value (selected to be 10^{-8} in this case), exit the loop.
5. Go to step 1.

Because the majority of the bubble curtain is driven by buoyancy, the rise time does not vary very much, even with large changes in manifold pressure, P_M. Therefore, this iteration scheme converges very rapidly. Most solutions were obtained on the second pass, and none required more than three passes.

Sheet "SolutionSummary"

This sheet contains the matrix of solutions discussed in the body of this report. Values of key items from Sheet "Design" for each solution have been copied and pasted into this sheet. No calculations are done in this sheet; it is simply a storage place for the various solutions. Details of the sheet can be seen in Appendix E.

Sheet "PlotData"

This sheet contains data to be plotted in the chart sheets. This data is obtained through the non-dimensional solution of the simultaneous, non-dimensional differential equations and through calculations made on this sheet. These calculations are arranged in one table which is too large to print out onto a single sheet of paper, so it is described in the following figures.

	Non-Dimensional Integration				Non-Dimensional Calculated		
i	zi_bar	Mi_bar	mi_bar	t_bar	Wi_bar	rhoai_bar	si_bar
0	0	0.001603	4.88261E-06	0	328.2599	0.003491	1
1	0.05	0.025141	0.011690211	0.023176517	2.150585	0.003378	0.1100723
2	0.1	0.049472	0.022811926	0.046329558	2.168684	0.003266	0.0615219
3	0.15	0.074442	0.034029024	0.069285729	2.1876	0.003153	0.0435297
4	0.2	0.100092	0.04534557	0.092040173	2.207313	0.003041	0.0342041
5	0.25	0.126467	0.056765807	0.114588028	2.227879	0.002928	0.0285386
6	0.3	0.153619	0.068294303	0.136924157	2.249367	0.002816	0.0247645
7	0.35	0.181603	0.079936006	0.159043097	2.271857	0.002703	0.0220985
8	0.4	0.210483	0.091696296	0.18093901	2.295436	0.002591	0.0201411
9	0.45	0.240329	0.103581041	0.202605649	2.320207	0.002478	0.0186676
10	0.5	0.271223	0.115596667	0.224036298	2.346284	0.002366	0.0175428
11	0.55	0.303254	0.12775024	0.245223723	2.373802	0.002253	0.0166811
12	0.6	0.336527	0.140049562	0.266160096	2.402913	0.002141	0.0160265
13	0.65	0.371162	0.152503291	0.286836916	2.433798	0.002028	0.0155419
14	0.7	0.407299	0.165121083	0.307244912	2.466666	0.001916	0.0152026
15	0.75	0.445099	0.177913779	0.327373921	2.501767	0.001803	0.0149931
16	0.8	0.484755	0.190893621	0.347212743	2.539399	0.001691	0.0149049
17	0.85	0.526497	0.204074545	0.36674896	2.579923	0.001578	0.0149359
18	0.9	0.5706	0.217472541	0.385968707	2.623781	0.001465	0.0150894
19	0.95	0.617405	0.231106142	0.404856378	2.671522	0.001353	0.0153755
20	1	0.667333	0.244997062	0.423394248	2.72384	0.00124	0.0158123

Figure C - 3 Non-Dimensional Quantities

Figure C - 3 shows the non-dimensional quantities. The columns under the "Non-Dimensional Integration" heading are written by the Subroutine SolveSys() described above. The columns under the "Non-Dimensional Calculated" heading are calculated on this sheet using Equations (36), (30), and (38) on pages 12 and 13 of the body of this report.

Figure C - 4 shows the dimensional quantities calculated using the scaling factors in Equations (24) and (25) on page 11 of the body of this report. The cell highlighted in orange is the dimensional value of rise time which is referenced on the Sheet "Design" and used in the iteration loop under the heading 'Button "Optimum Solution"' above.

Figure C - 5 shows the calculations of the speed of sound and specific acoustic impedance ratios using the second equality in Equation (21) on page 10 and Equations (6), (8), and (10) on pages 6 and 7.

	Dimensional						
i	z (ft)	M (lbm/sec^2)	m (lbm/ft-sec)	t (sec)	W (ft/sec)	rhoa (lbm/ft^3)	s (-)
0	0	993.62779	0.0307552	0	538.46023	0.2234069	1
1	3	15585.939	73.635863	0.8477419	3.5277057	0.216206	0.110072
2	6	30669.894	143.6908	1.6946251	3.5573949	0.2090051	0.061522
3	9	46149.97	214.34655	2.5343072	3.5884234	0.2018043	0.043530
4	12	62051.566	285.62872	3.3666106	3.620759	0.1946034	0.034204
5	15	78402.948	357.56403	4.1913575	3.6544945	0.1874025	0.028539
6	18	95235.5	430.18126	5.00836	3.6897431	0.1802017	0.024764
7	21	112584.19	503.51157	5.8174182	3.7266335	0.1730008	0.022099
8	24	130488.13	577.58885	6.6183187	3.765312	0.1657999	0.020141
9	27	148991.33	652.45007	7.4108328	3.8059446	0.1585991	0.018668
10	30	168143.47	728.1357	8.194715	3.848721	0.1513982	0.017543
11	33	188001.04	804.69024	8.9697006	3.8938595	0.1441973	0.016681
12	36	208628.64	882.16285	9.7355033	3.9416123	0.1369965	0.016027
13	39	230100.61	960.60806	10.491812	3.9922736	0.1297956	0.015542
14	42	252503.21	1040.0867	11.238288	4.0461884	0.1225947	0.015203
15	45	275937.31	1120.667	11.974559	4.1037659	0.1153939	0.014993
16	48	300522.05	1202.4262	12.700216	4.1654954	0.108193	0.014905
17	51	326399.55	1285.4519	13.414805	4.2319687	0.1009922	0.014936
18	54	353741.47	1369.845	14.117817	4.3039111	0.0937913	0.015089
19	57	382757.99	1455.7222	14.808683	4.3822234	0.0865904	0.015376
20	60	413710.54	1543.2202	15.486755	4.4680441	0.0793896	0.015812

Figure C - 4 Dimensional Quantities

	Additional Calculated Values					
i	P lb/ft^2	Air bubble Compres-sibility ft^2/lb	Speed of Sound, c ft/sec	Speed of Sound Ratio, c/c$_w$ -	Specific Acoustic Impedance, I lb-sec/ft^3	Specific Acoustic Impedance Ratio, I/I$_w$ -
0	5956.8	1.68E-04				
1	5764.8	1.73E-04	171.88373	0.0351119	304.4018	0.03126
2	5572.8	1.79E-04	220.05851	0.044953	410.8956	0.042196
3	5380.8	1.86E-04	254.5585	0.0520005	484.3928	0.049744
4	5188.8	1.93E-04	280.55861	0.0573118	539.0536	0.055357
5	4996.8	2.00E-04	300.46005	0.0613772	580.6654	0.059631
6	4804.8	2.08E-04	315.61271	0.0644725	612.3099	0.06288
7	4612.8	2.17E-04	326.86925	0.066772	635.8753	0.0653
8	4420.8	2.26E-04	334.81144	0.0683944	652.6243	0.06702
9	4228.8	2.36E-04	339.85845	0.0694254	663.4542	0.068133
10	4036.8	2.48E-04	342.32467	0.0699292	669.0313	0.068705
11	3844.8	2.60E-04	342.4533	0.0699554	669.8671	0.068791
12	3652.8	2.74E-04	340.43699	0.0695436	666.364	0.068431
13	3460.8	2.89E-04	336.43129	0.0687253	658.8458	0.067659
14	3268.8	3.06E-04	330.56369	0.0675267	647.5766	0.066502
15	3076.8	3.25E-04	322.93991	0.0659693	632.7748	0.064982
16	2884.8	3.47E-04	313.64842	0.0640713	614.6227	0.063118
17	2692.8	3.71E-04	302.76372	0.0618478	593.2736	0.060925
18	2500.8	4.00E-04	290.34879	0.0593117	568.8567	0.058418
19	2308.8	4.33E-04	276.45695	0.0564739	541.4814	0.055607
20	2116.8	4.72E-04	261.13316	0.0533436	511.2401	0.052501

Figure C - 5 Ratios

Some other data appear on this sheet which have no significance as far as evaluating the feasibility of the air curtain, and so they are not shown here. One set of data does deserve mention, however. Using one particular set of input data, the non-dimensional differential equations were integrated numerically with different number of steps, and the solutions compared. Eventually, 20,000 steps were chosen. The non-dimensional values obtained by doubling the number of steps to 40,000 were the same to 3 significant figures. Values obtained with 80,000 steps were the same as obtained with 40,000 steps to 4 significant figure. Since solution times increased with the number of steps, 20,000 steps seemed to be a reasonable compromise between accuracy and solution time.

Sheet "cht_s"

The values of *z* and *s* shown in Figure C - 4 are plotted on this sheet. Significance of this plot is discussed in the body of the report.

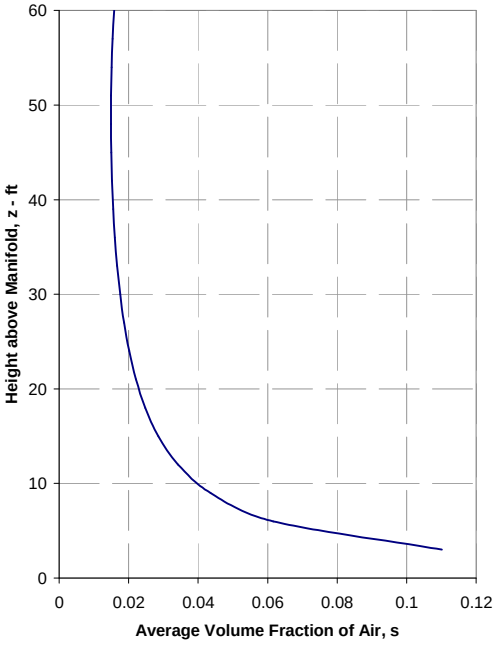

Figure C - 6 Volume Fraction of Air

Sheets "cht_cRatio" and "cht_Iratio"

These two sheets plot the speed of sound ratio, c/c_w, and the specific acoustic impedance ration, I/I_w, [shown in Figure C - 5] as a function of height above the manifold, z. Significance of these plots is discussed in the body of the report.

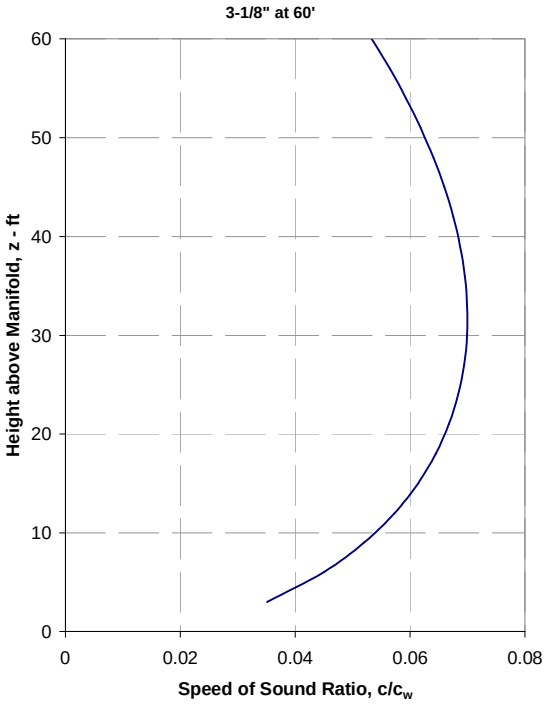

Figure C - 7 Speed of Sound

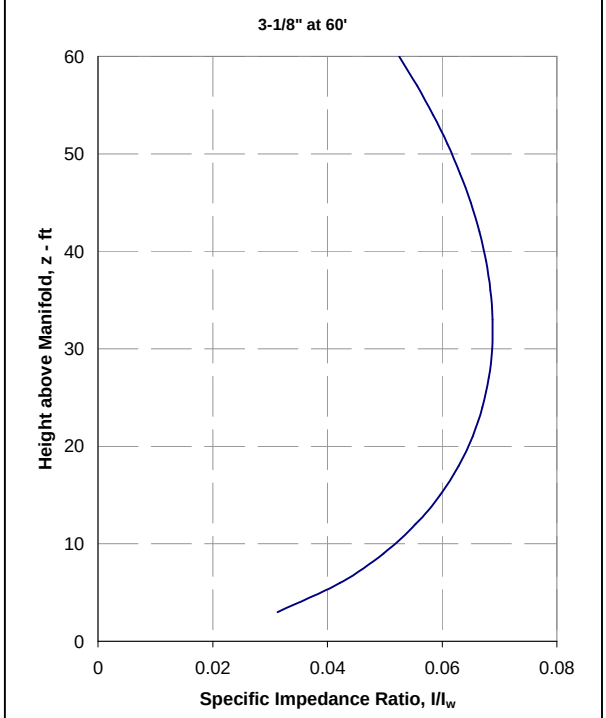

Figure C - 8 Specific Acoustic Impedance

Note that the Specific Acoustic Impedance curve looks almost identical to the Speed of Sound curve. In fact, it varies slightly from the c/c_w curve.

Specific impedance I is defined as $I = c\rho$, so

$$\frac{I}{I_w} = \frac{\rho}{\rho_w}\frac{c}{c_w}$$

Examination of the complete data set shown in Figure C - 5 shows that $\frac{\rho}{\rho_w} = \frac{I/I_w}{c/c_w}$ varies from 0.894 at $z = 3$ ft to 0.984 at $z = 60$ ft. Thus the Specific Acoustic Impedance curve is the Speed of Sound curve multiplied by a number varying from about 0.9 to 0.98. Therefore, the shape of the curves in the above two figures are similar, and the casual observer will not notice any difference in the numerical values plotted.

Appendix D

Comparison with Experiments

Appendix D

Comparison with Experiments

Sixma and Stubbs (1996) of Shell Venezuela and Western Geophysical investigated shot generated noise observed in Lake Maricaibo and the use of bubble screens to suppress unwanted noise and reflections peculiar to that region. As a precursor to the field test, Western Geophysical conducted tests to determine the attenuation properties of a bubble screen. Thanks to Shell Oil USA, the Western Geophysical report to Shell Venezuela, Anonymous (1996), has been made available to the present investigation.

The tests were conducted in Western Geophysical's test site near Houston in a 25-foot deep pit with a manifold on bottom located between an air gun and a hydrophone, each at 12 feet above bottom. Waveforms, amplitude spectra, and attenuation spectra are presented in the report for various combinations of orifice size and air supply pressure and flow rate. Percent air saturation is quoted, but no mention is made of how it was determined.

Equations presented in the section, "Compressible Fluid Flow Through the Nozzles" on page 15 in the body of this report were copied from the workbook Air Curtain Design.xls into a new Excel workbook along with pertinent input quantities. The resulting worksheet to calculate flow rates based on supply pressure is shown in Figure D- 1.

Input quantities which were explicitly stated in the Western Geophysical report are shown with a yellow background; those cells containing assumed values are shown with an orange background. For example, it is assumed that the pit was filled with fresh water at 85 ^{o}F. In the Comparison table at the bottom of the figure, the supply pressures and flow rates quoted in the Western Geophysical report are shown with a yellow background.

The remaining cells in the Comparison table contain the formulas for calculating compressible flow through nozzles for the three orifice sizes used in the Western Geophysical tests.

No description is given of the shape of the nozzles used. As shown in J. E. Gasho & Associates (unknown), the discharge coefficients can have a wide range of values, depending on the nozzle shape. So for a first approximation, both the subsonic and sonic discharge coefficients were taken to be 1.0.

AIR CURTAIN DESIGN COMPARISON
Western Geophysical

Created: Warren T. Jones, Ph.D 10/25/08 11:41 AM
Last Revision: 11/14/08 2:05 PM

Properties of Air

Atmospheric pressure [Patm]	14.7	psi =	2116.8 lb/ft^2
Gas Constant [GCR]	53.36	ft-lb/lbm-^{o}R	
Specific Heat Ratio [k]	1.4		
Standard Temperature [Tstd]	68	^{o}F =	527.69 ^{o}R
Conditions Pressure [Pstd]	14.7	psi =	2116.8 lb/ft^2

Properties of Water

Density of water [rhow]	62.4	lbm/ft^3
Compressibility of water [Betaw]	2.10E-08	ft^2/lb
Seawater Temperature [Tsw]	85	^{o}F = 544.69 ^{o}R

Gravity and Plume Properties

Acceleration of gravity [g]	32.1739	ft/sec^2
Sub-sonic Nozzle Coefficient [cdss]	1	
Sonic Nozzle Coefficient [cds]	1	

Design of Air Curtain

Depth of Manifold [H]	25	ft
Number of Nozzles per ft [n]	3	1/ft
Length of Manifold [LM]	33	ft

Calculated Quantities

Water Pressure at manifold [Po]	3676.8	psfa =	25.53333 psia
Critical Pressure Ratio [rpc]	0.528282		
Max Pm for sonic velocity at nozzle [Pmmax]	6959.922	psf =	48.33279 psi
k/(k-1) [kokm1]	3.5		
(k+1)/k [kp1ok]	1.714286		
(k+1)/(k-1) [kp1okm1]	6		

Comparison

	Western Geophysical Data - Table 1 p. 10											
Pm	P	Q	Nozzle pressure ratio [rp]	Air density in manifold [Rhoam]	Air density at exit of nozzle [Rhoao]	Mass Flow rate [m]	Volume Flow Rate through 1 nozzle [qo]	Nozzle exit velocity [wo]	Volume flux per unit length [Qo]	Total Flow Rate	Total Flow Rate	Ratio Meas/Calc
psfa	psia	scfm	-	lb$_m$/ft^3	lb$_m$/ft^3	lbm/sec	ft^3/sec	fps	cfm/ft	cfm	scfm	-
1/64 Orifice	=	0.015625	in =	0.001302	ft	area =	1.33E-06	ft^2				
4464	31	7	0.823656	0.153589	0.133714	0.000106	0.000791	594.1043	0.142398	4.69912	7.907445	0.885242
6480	45	13	0.567407	0.222951	0.148738	0.000196	0.001317	989.1809	0.237091	7.824014	13.16586	0.987402
7920	55	16	0.464242	0.272496	0.157515	0.00024	0.001525	1145.498	0.274558	9.060414	15.24641	1.049427
8928	62	18	0.411828	0.307177	0.162999	0.000271	0.001662	1247.837	0.299087	9.869874	16.60853	1.08378
13824	96	25	0.265972	0.475629	0.184687	0.000419	0.002271	1705.242	0.40872	13.48776	22.69653	1.10149
3/64 Orifice	=	0.046875	in =	0.003906	ft	area =	1.2E-05	ft^2				
4752	33	74	0.773737	0.163498	0.136124	0.00111	0.008151	680.148	1.467188	48.41722	81.47408	0.908264
6192	43	113	0.593798	0.213042	0.146818	0.001674	0.011405	951.678	2.052922	67.74643	114.0003	0.991225
7632	53	141	0.481761	0.262587	0.155856	0.002084	0.013369	1115.587	2.406501	79.41453	133.6348	1.055114
9072	63	165	0.405291	0.312132	0.163746	0.002477	0.015126	1262.18	2.722724	89.8499	151.1949	1.091306
10368	72	184	0.35463	0.356722	0.170114	0.002831	0.01664	1388.494	2.995204	98.84175	166.326	1.106261
3/32 Orifice	=	0.09375	in =	0.007813	ft	area =	4.79E-05	ft^2				
4320	30	228	0.851111	0.148634	0.132467	0.003447	0.026022	542.8341	4.683921	154.5694	260.1017	0.87658
4752	33	295	0.773737	0.163498	0.136124	0.004438	0.032604	680.148	5.868754	193.6689	325.8963	0.905196

Figure D- 1 - Excel Workbook for Calculating Flowrates

The last column in the Comparison table shows the ratio of the measured flow rate to the calculated flow rate. This ratio is in fact the definition of the discharge coefficient for a nozzle, so if discharge coefficients of 1.0 are used in the calculations, this column gives the value of discharge coefficient which would result in the calculated flow matching the measured flow exactly.

For each nozzle size, the lowest two pressures result in subsonic flows. The highest three pressures for the 1/64" and 3/64" are sonic. The table indicates a subsonic discharge coefficient of about 0.9$^+$ and a sonic discharge coefficient of about 1.0$^+$ would match the measured flow. These results were obtained by adjusting the length of the manifold. A length less than the 33 ft used here would result in both subsonic and sonic discharge coefficients being greater than 1.0, which is impossible.

The calculated flow rates using the new values of discharge coefficient and the measurements of flow rates presented in the Western Geophysical report are in general agreement as shown in Figure D- 2 and Figure D-3

In Figure D- 2, the solid curves are drawn through the measured flow rates as listed in Table 1 of the Western Geophysical report; the data points represent flow rates calculated from the workbook shown in

Figure D- 1. A direct comparison of the measured and calculated value for each value of supply pressure is shown in Figure D-3.

Agreement is excellent on the 1/64" nozzle. For the 3/64" nozzle, calculated results for the two highest pressures (and flow rates) fall below the measured values. The largest difference is with the 3/32" nozzle. Calculated flow rates for both values of pressure lie well above the measured values.

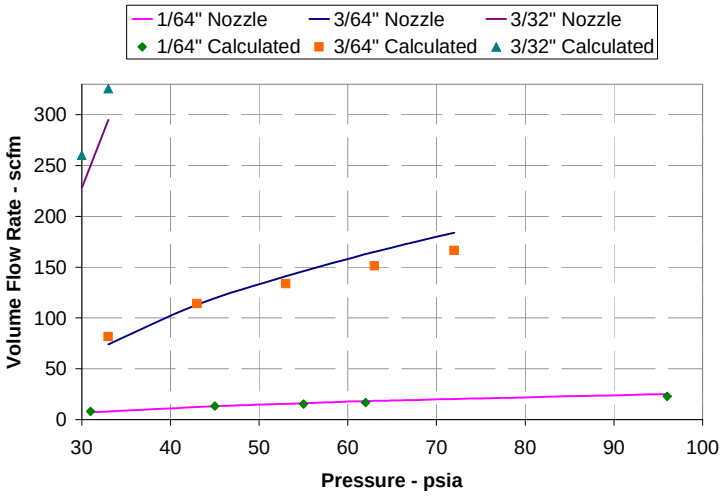

Figure D- 2 - Flow Rates

This discrepancy at high flow rates (with the largest nozzles) can be explained by the absence of pertinent information in the Western Geophysical report. The pressures stated in the report are undoubtedly supply pressures measured at the regulator on the bank of high pressure air bottles located on the pier. Nothing is stated about the size or length of the conduit for the air from this regulator to the manifold at the bottom of the pit.

Consider the highest flow rate listed in Figure D- 1. Assuming the conduit is the same diameter as the manifold, 2", the pressure head loss in 26 ft of conduit would be about 1.5 psi for a flow rate of 295 scfm [see the friction loss nomograph in the J. E. Gasho web site, J. E. Gasho & Associates (unknown)]. Decreasing the manifold pressure from 33 to 31.5 psi results in a calculated flow rate of 295.8 scfm, an almost exact match for the measured value.

So if at least 26' of conduit existed between the supply and the manifold in 25' of water, then the highest calculated flow rate is not greater than the measured flow rate as indicated in Figure D- 2 and Figure D-3.

Of course, at lower flow rates, friction loss between the supply and the manifold would be less. So the supply pressure and manifold pressure would be closer in value, and smaller differences would exist between the measured flow rate and the value calculated using the supply pressure.

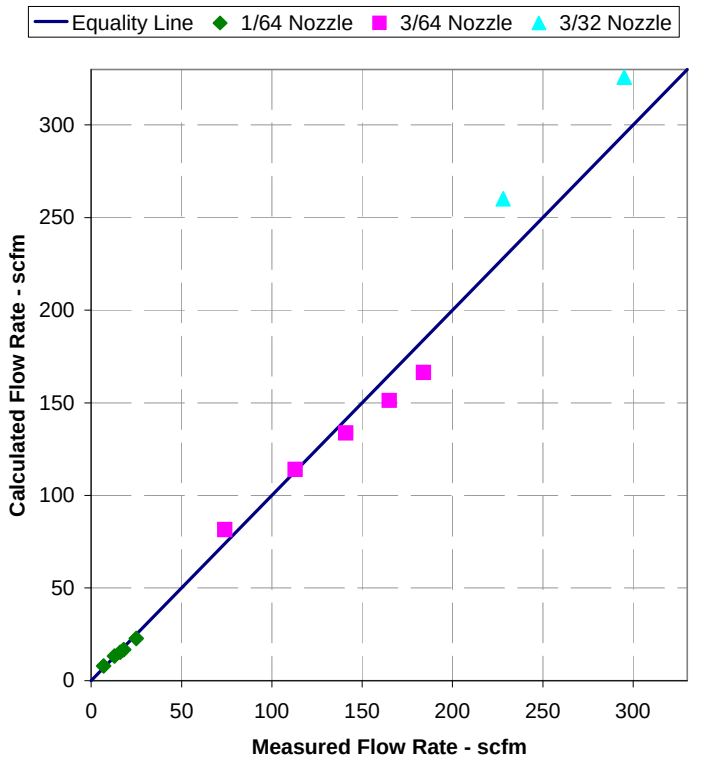

Figure D-3 Calculated vs Measured Flow Rates

Appendix E

Solution Matrix

The solution matrix contained in the Sheet “SolutionSummary” of the Air Curtain Design.xls workbook is shown on the following pages in Table E - 1 through Table E - 6. The headings on the columns are self-explanatory.

These tables are followed by plots of the pneumatic hp and manifold diameter vs. maximum *c/cw* ratio in Figure E - 1through Figure E - 10.

Appendix E

Solution Matrix

Table E - 1

AIR CURTAIN DESIGN	Created: Warren T. Jones, Ph.D.	10/29/08 11:05 AM
Solutions Summary	Last Revision:	12/19/08 9:42 AM

Solution #	Max Speed of Sound Ratio c/c_w (-)	Non-Dim Height, z/H, at Max c/cw (-)	Depth of Manifold [H] (ft)	Number of nozzles per ft [n] (1/ft)	Diameter of nozzle exit [d] (in)	Manifold Pressure [Pm] (psia)	Diameter of manifold [Dman] (in)	Pressure at Manifold End [Pend] (psia)	Flow Rate (scfm)	Total Pneumatic HP at manifold (hp)	Rise Time (sec)	Manifold length (ft)	Manifold Position in front of array (ft)	Total Number of Nozzles (-)	Pressure Diff at Manifold Beginning (psi)	Pressure Diff at Manifold End (psi)
1	0.0797597	0.503	70	3	0.1875	48.786848	14.331	47.8	5582.1	361.1	18.55	227	167	681	2.98	2.00
2	0.07	0.5009	70	3	0.1875	52.594654	13.67657	51.5	7662.8	534.4	16.18	207	147	621	6.78	5.73
3	0.06	0.49735	70	3	0.1875	64.207413	12.992926	62.9	11298.3	961.9	13.74	187	126	561	18.40	17.11
4	0.0727281	0.50185	70	4	0.1875	48.786848	16.022888	47.8	6983.8	451.8	16.85	213	152	852	2.98	2.00
5	0.07	0.50125	70	4	0.1875	49.599492	15.793269	48.6	7653.1	503.3	16.19	207	147	828	3.79	2.80
6	0.06	0.4979	70	4	0.1875	55.983493	15.004	54.9	11272.9	836.8	13.75	187	126	748	10.17	9.05
7	0.055	0.4953	70	4	0.1875	63.851954	14.553	62.6	14044.4	1189.0	12.52	176	116	704	18.04	16.76
8	0.0639201	0.49985	70	6	0.1875	48.786848	18.76923	47.8	9590.5	620.4	14.72	195	134	1170	2.98	2.00
9	0.06	0.49845	70	6	0.1875	50.272125	18.377257	49.3	11247.7	749.7	13.76	187	126	1122	4.46	3.46
10	0.05	0.4927	70	6	0.1875	60.576533	17.308923	59.4	18020.5	1447.4	11.30	166	105	996	14.77	13.55
11	0.1	0.5048	70	3	0.125	49.532974	10.396325	48.5	3273.8	215.0	23.44	268	208	804	3.72	2.73
12	0.09	0.5037	70	3	0.125	53.005561	9.990977	51.9	4200.6	295.2	21.01	248	187	744	7.19	6.13
13	0.08	0.50205	70	3	0.125	60.999265	9.5507946	59.8	5552.1	449.1	18.59	227	167	681	15.19	13.97
14	0.07	0.4994	70	3	0.125	82.161927	9.1145571	80.5	7711.6	840.1	16.14	207	146	621	36.35	34.71
15	0.065	0.4974	70	3	0.125	103.87529	8.8670597	101.8	9249.0	1273.9	14.91	196	136	588	58.06	55.99
16	0.0944345	0.5045	70	4	0.125	48.786848	11.750386	47.8	3745.1	242.3	22.09	257	197	1028	2.98	2.00
17	0.09	0.504	70	4	0.125	49.828018	11.538127	48.8	4195.5	277.2	21.02	248	188	992	4.02	3.02
18	0.08	0.5025	70	4	0.125	54.235309	11.054308	53.2	5566.6	400.3	18.60	228	167	912	8.42	7.34
19	0.07	0.5001	70	4	0.125	65.657642	10.526208	64.3	7689.5	669.4	16.16	207	146	828	19.85	18.53
20	0.065	0.4983	70	4	0.125	78.186911	10.26618	76.6	9261.0	960.1	14.94	197	136	788	32.38	30.81
21	0.06	0.49585	70	4	0.125	100.37384	9.9734426	98.4	11308.3	1505.0	13.70	186	126	744	54.56	52.56
22	0.082842	0.50335	70	6	0.125	48.786848	13.690965	47.8	5093.1	329.5	19.30	233	173	1398	2.98	2.00
23	0.08	0.5029	70	6	0.125	49.514405	13.540545	48.5	5556.6	364.8	18.61	228	167	1368	3.70	2.71
24	0.075	0.502	70	6	0.125	51.371747	13.205578	50.3	6471.0	440.8	17.40	217	157	1302	5.56	4.53
25	0.07	0.50075	70	6	0.125	54.431991	12.893972	53.3	7667.6	553.4	16.18	207	147	1242	8.62	7.53
26	0.0755553	0.51505	65	3	0.1875	46.519274	13.979654	45.6	5141.2	333.3	17.19	216	155	648	2.93	2
27	0.07	0.51385	65	3	0.1875	48.330918	13.613803	47.4	6197.8	417.4	15.87	205	144	615	4.74	3.78
28	0.065	0.5124	65	3	0.1875	51.190417	13.23949	50.2	7408.6	528.5	14.68	194	134	582	7.60	6.58
29	0.06	0.5105	65	3	0.1875	56.339749	12.890317	55.2	9062.6	711.5	13.48	184	124	552	12.75	11.62
30	0.055	0.5079	65	3	0.1875	66.259018	12.532297	64.9	11337.5	1046.8	12.27	174	114	522	22.67	21.34
31	0.055	0.50855	65	4	0.1875	56.070386	14.472143	54.9	11307.8	883.5	12.29	174	114	696	12.48	11.36
32	0.06	0.511	65	4	0.1875	50.669012	14.885534	49.7	9045.7	638.7	13.49	184	124	736	7.08	6.07

Table E - 2

AIR CURTAIN DESIGN	Created: Warren T. Jones, Ph.D. 10/29/08 11:05 AM
Solutions Summary	Last Revision: 12/19/08 9:42 AM

Solution #	Max Speed of Sound Ratio c/c_w (-)	Non-Dim Height, z/H, at Max c/cw (-)	Depth of Manifold [H] (ft)	Number of nozzles per ft [n] (1/ft)	Diameter of nozzle exit [d] (in)	Manifold Pressure [Pm] (psia)	Diameter of manifold [Dman] (in)	Pressure at Manifold End [Pend] (psia)	Flow Rate (scfm)	Total Pneumatic HP at manifold (hp)	Rise Time (sec)	Manifold length (ft)	Manifold Position in front of array (ft)	Total Number of Nozzles (-)	Pressure Diff at Manifold Beginning (psi)	Pressure Diff at Manifold End (psi)
33	0.065	0.51275	65	4	0.1875	47.829587	15.327987	46.9	7436.5	495.7	14.69	195	134	780	4.24	3.28
34	0.0689038	0.51385	65	4	0.1875	46.519274	15.604227	45.6	6410.6	415.6	15.61	202	142	808	2.93	2.00
35	0.0981816	0.51735	65	3	0.125	46.519274	10.26494	45.6	2761.0	179.0	22.53	261	200	783	2.93	2.00
36	0.09	0.5165	65	3	0.125	48.630176	9.9155285	47.7	3379.6	229.0	20.59	244	184	732	5.04	4.07
37	0.08	0.515	65	3	0.125	54.178391	9.4911297	53.1	4476.4	338.0	18.22	224	164	672	10.59	9.51
38	0.07	0.51255	65	3	0.125	68.653791	9.0504359	67.3	6200.3	593.2	15.84	204	144	612	25.06	23.69
39	0.065	0.5107	65	3	0.125	84.64842	8.8231482	83.0	7460.1	880.0	14.64	194	134	582	41.06	39.37
40	0.06	0.5082	65	3	0.125	109.444	8.5908675	107.3	9148.2	1395.2	13.43	184	123	552	65.86	63.67
41	0.0894442	0.5167	65	4	0.125	46.519274	11.426768	45.6	3427.4	222.2	20.47	243	183	972	2.93	2.00
42	0.08	0.51535	65	4	0.125	49.482031	10.961129	48.5	4469.6	308.2	18.23	224	164	896	5.89	4.90
43	0.07	0.51315	65	4	0.125	57.372836	10.452303	56.2	6185.5	494.5	15.85	204	144	816	13.78	12.64
44	0.065	0.5115	65	4	0.125	65.921808	10.189684	64.6	7436.8	683.2	14.65	194	134	776	22.33	21.01
45	0.06	0.50925	65	4	0.125	81.738902	9.9209885	80.1	9109.3	1037.6	13.45	184	124	736	38.15	36.52
46	0.0713653	0.52915	60	3	0.1875	44.251701	13.586476	43.4	4693.0	304.9	15.83	204	144	612	2.89	2.00
47	0.07	0.5288	60	3	0.1875	44.624658	13.484736	43.7	4912.2	321.9	15.51	201	141	603	3.26	2.37
48	0.06	0.5257	60	3	0.1875	50.064817	12.822704	49.1	7233.5	531.8	13.19	182	121	546	8.70	7.70
49	0.055	0.5233	60	3	0.1875	56.719095	12.461978	55.6	9030.7	752.1	12.01	172	111	516	15.35	14.22
50	0.05	0.5198	60	3	0.1875	70.535281	12.091499	69.1	11592.1	1200.6	10.83	162	101	486	29.17	27.76
51	0.0650933	0.5278	60	4	0.1875	44.251701	15.213664	43.4	5889.2	382.7	14.38	192	131	768	2.89	2.00
52	0.06	0.5261	60	4	0.1875	46.212217	14.807441	45.3	7222.5	490.1	13.19	182	121	728	4.85	3.92
53	0.05	0.5206	60	4	0.1875	57.322759	13.963146	56.2	11555.8	972.7	10.84	162	102	648	15.96	14.81
54	0.045	0.5158	60	4	0.1875	74.27812	13.522798	72.8	15359.1	1675.2	9.65	152	91	608	32.91	31.43
55	0.0927166	0.5317	60	3	0.125	44.251701	9.9667411	43.4	2515.2	163.4	20.75	246	185	738	2.89	2.00
56	0.09	0.5314	60	3	0.125	44.838417	9.8408507	43.9	2690.5	177.1	20.12	240	180	720	3.47	2.57
57	0.08	0.52995	60	3	0.125	48.629278	9.4320566	47.7	3571.6	255.0	17.81	221	160	663	7.26	6.29
58	0.07	0.5277	60	3	0.125	58.402125	8.9865335	57.2	4933.8	423.1	15.49	201	141	603	17.04	15.87
59	0.065	0.52605	60	3	0.125	69.057919	8.7567579	67.7	5925.5	600.9	14.32	191	131	573	27.69	26.31
60	0.06	0.52375	60	3	0.125	88.163899	8.5218236	86.4	7249.3	938.5	13.14	181	121	543	46.80	45.03
61	0.055	0.52055	60	3	0.125	116.83166	8.2813779	114.5	9075.7	1557.0	11.95	171	111	513	75.46	73.13
62	0.0844688	0.53095	60	4	0.125	44.251701	11.117868	43.4	3135.5	203.7	18.85	230	169	920	2.89	2.00
63	0.08	0.5303	60	4	0.125	45.418964	10.892861	44.5	3567.0	237.9	17.82	221	160	884	4.05	3.14
64	0.07	0.5282	60	4	0.125	50.788774	10.378594	49.8	4924.0	367.2	15.50	201	141	804	9.42	8.41
65	0.06	0.52465	60	4	0.125	67.065129	9.8687927	65.7	7264.0	715.3	13.16	182	121	728	25.70	24.36
66	0.055	0.5218	60	4	0.125	87.195912	9.5913291	85.5	9084.2	1163.1	11.98	172	111	688	45.83	44.09
67	0.0741161	0.5296	60	6	0.125	44.251701	12.99912	43.4	4294.2	279.0	16.46	210	149	1260	2.89	2.00
68	0.07	0.5287	60	6	0.125	45.499924	12.713148	44.6	4914.3	328.3	15.51	201	141	1206	4.13	3.22
69	0.06	0.5255	60	6	0.125	52.43698	12.088894	51.4	7239.0	557.4	13.18	182	121	1092	11.07	10.02
70	0.05	0.5194	60	6	0.125	78.882021	11.399569	77.3	11610.4	1344.8	10.82	162	101	972	37.52	35.94
71	0.0612811	0.5443	55	4	0.1875	41.989174	14.772019	41.1	5362.2	349.4	13.14	181	121	724	2.84	2.00
72	0.06	0.54385	55	4	0.1875	42.397929	14.688806	41.5	5669.1	373.0	12.85	179	119	716	3.25	2.41

Table E - 3

AIR CURTAIN DESIGN	Created: Warren T. Jones, Ph.D. 10/29/08 11:05 AM
Solutions Summary	Last Revision: 12/19/08 9:42 AM

Solution #	Max Speed of Sound Ratio c/c_w (-)	Non-Dim Height, z/H, at Max c/cw (-)	Depth of Manifold [H] (ft)	Number of nozzles per ft [n] (1/ft)	Diameter of nozzle exit [d] (in)	Manifold Pressure [Pm] (psia)	Diameter of manifold [Dman] (in)	Pressure at Manifold End [Pend] (psia)	Flow Rate (scfm)	Total Pneumatic HP at manifold (hp)	Rise Time (sec)	Manifold length (ft)	Manifold Position in front of array (ft)	Total Number of Nozzles (-)	Pressure Diff at Manifold Beginning (psi)	Pressure Diff at Manifold End (psi)
73	0.05	0.5387	55	4	0.1875	49.735396	13.878792	48.7	9081.8	700.9	10.58	160	99	640	10.59	9.60
74	0.045	0.53425	55	4	0.1875	60.69544	13.434915	59.5	12028.2	1132.9	9.42	150	90	600	21.55	20.34
75	0.04	0.52725	55	4	0.1875	87.555772	12.977102	85.8	16705.5	2269.7	8.24	140	80	560	48.41	46.66
76	0.0872689	0.5486	55	3	0.125	41.984127	9.6592836	41.1	2279.2	148.5	18.97	231	170	693	2.84	2.00
77	0.08	0.5476	55	3	0.125	44.032604	9.352379	43.2	2803.8	191.6	17.34	217	156	651	4.89	4.01
78	0.07	0.5455	55	3	0.125	50.52671	8.9230567	49.5	3880.9	304.3	15.09	198	137	594	11.38	10.37
79	0.06	0.54185	55	3	0.125	70.360592	8.4765726	69.0	5711.5	623.6	12.81	179	118	537	31.22	29.81
80	0.055	0.53895	55	3	0.125	92.893603	8.2339115	91.0	7131.8	1028.0	11.67	169	109	507	53.75	51.89
81	0.0795106	0.5478	55	4	0.125	41.984127	10.77518	41.1	2841.5	185.1	17.24	216	156	864	2.84	2.00
82	0.07	0.5459	55	4	0.125	45.467914	10.305313	44.6	3874.6	273.4	15.09	198	137	792	6.32	5.41
83	0.06	0.5426	55	4	0.125	56.187687	9.7896677	55.1	5695.5	496.6	12.83	179	118	716	17.04	15.92
84	0.055	0.54	55	4	0.125	69.577496	9.5090102	68.2	7103.8	767.0	11.69	169	109	676	30.43	29.04
85	0.05	0.5362	55	4	0.125	94.603972	9.2210876	92.7	9111.1	1337.5	10.53	159	99	636	55.46	53.57
86	0.045	0.5552	50	3	0.1875	62.260706	11.557789	61.0	9331.0	955.7	9.14	148	87	444	25.34	24.09
87	0.05	0.5596	50	3	0.1875	49.354617	11.907556	48.4	7016.5	569.7	10.26	157	97	471	12.43	11.45
88	0.06	0.5647	50	3	0.1875	40.742539	12.617456	39.9	4396.4	294.7	12.46	176	115	528	3.82	3.01
89	0.0630358	0.5657	50	3	0.1875	39.716553	12.799138	38.9	3870.7	252.9	13.12	181	121	543	2.79	2.00
90	0.0575204	0.56405	50	4	0.1875	39.716553	14.358813	38.9	4875.8	318.6	11.92	171	111	684	2.79	2.00
91	0.05	0.56015	50	4	0.1875	43.81422	13.750859	42.9	7002.6	504.7	10.27	157	97	628	6.89	6.02
92	0.045	0.55605	50	4	0.1875	50.792549	13.346952	49.8	9302.5	777.3	9.15	148	87	592	13.87	12.85
93	0.04	0.54965	50	4	0.1875	68.365575	12.885146	67.0	12853.7	1445.7	8.02	138	78	552	31.44	30.08
94	0.08	0.56865	50	3	0.125	40.142457	9.2519218	39.3	2162.2	142.8	16.80	212	152	636	3.22	2.42
95	0.075	0.5678	50	3	0.125	41.745418	9.0464459	40.9	2529.9	173.7	15.72	203	143	609	4.82	3.99
96	0.07	0.5667	50	3	0.125	44.376572	8.837555	43.5	2998.0	218.9	14.63	194	134	582	7.45	6.57
97	0.065	0.56525	50	3	0.125	48.889171	8.6248812	47.9	3606.8	290.1	13.53	185	124	555	11.97	10.99
98	0.06	0.56335	50	3	0.125	57.07104	8.4080712	55.9	4418.5	414.8	12.43	176	115	528	20.15	19.01
99	0.055	0.5607	50	3	0.125	72.95887	8.1622474	71.5	5501.9	660.4	11.33	166	106	498	36.04	34.58
100	0.05	0.55685	50	3	0.125	99.374244	7.9356371	97.4	7087.6	1158.7	10.21	157	96	471	62.45	60.46
101	0.074572	0.568	50	4	0.125	39.716553	10.421174	38.9	2559.9	167.3	15.63	202	142	808	2.79	2.00
102	0.07	0.56705	50	4	0.125	41.077618	10.206535	40.3	2994.1	202.3	14.63	194	134	776	4.16	3.33
103	0.06	0.56395	50	4	0.125	48.015269	9.7107367	47.1	4408.5	348.2	12.45	176	115	704	11.09	10.13
104	0.055	0.56155	50	4	0.125	56.533788	9.4266659	55.4	5484.7	510.1	11.34	166	106	664	19.61	18.48
105	0.05	0.5581	50	4	0.125	74.191358	9.1643398	72.7	7055.3	861.1	10.23	157	96	628	37.27	35.79
106	0.0589005	0.5901	45	3	0.1875	37.44898	12.404913	36.7	3495.2	229.1	11.78	170	109	510	2.75	2.00
107	0.05	0.5857	45	3	0.1875	42.571107	11.796489	41.7	5329.5	397.2	9.90	154	75	408	7.87	7.02
108	0.04	0.57525	45	3	0.1875	70.44672	11.078176	69.0	9792.8	1207.6	7.74	136	75	408	35.75	34.34
109	0.0537618	0.5882	45	4	0.1875	37.44898	13.933313	36.7	4413.5	289.3	10.70	161	100	644	2.75	2.00
110	0.05	0.58615	45	4	0.1875	39.082228	13.622592	38.3	5321.2	364.0	9.90	154	94	616	4.38	3.60
111	0.04	0.5764	45	4	0.1875	54.162768	12.793059	53.1	9754.3	924.8	7.75	136	75	544	19.46	18.38
112	0.0375	0.5721	45	4	0.1875	65.495485	12.554166	64.2	11693.0	1340.6	7.20	131	71	524	30.80	29.49

Table E - 4

AIR CURTAIN DESIGN	Created: Warren T. Jones, Ph.D. 10/29/08 11:05 AM
Solutions Summary	Last Revision: 12/19/08 9:42 AM

Solution #	Max Speed of Sound Ratio c/c_w (-)	Non-Dim Height, z/H, at Max c/cw (-)	Depth of Manifold [H] (ft)	Number of nozzles per ft [n] (1/ft)	Diameter of nozzle exit [d] (in)	Manifold Pressure [Pm] (psia)	Diameter of manifold [Dman] (in)	Pressure at Manifold End [Pend] (psia)	Flow Rate (scfm)	Total Pneumatic HP at manifold (hp)	Rise Time (sec)	Manifold length (ft)	Manifold Position in front of array (ft)	Total Number of Nozzles (-)	Pressure Diff at Manifold Beginning (psi)	Pressure Diff at Manifold End (psi)
113	0.035	0.5664	45	4	0.1875	83.210117	12.359883	81.5	14402.1	2097.8	6.64	127	66	508	48.51	46.85
114	0.0764369	0.5937	45	3	0.125	37.44898	9.0127348	36.7	1836.7	120.4	15.44	201	140	603	2.75	2.00
115	0.07	0.59245	45	3	0.125	39.469314	8.7527704	38.7	2282.1	157.7	14.09	190	129	570	4.77	3.98
116	0.06	0.58935	45	3	0.125	47.444082	8.3159294	46.5	3349.7	278.2	11.99	172	111	516	12.74	11.80
117	0.05	0.58345	45	3	0.125	76.781633	7.8609573	75.2	5371.6	722.0	9.86	154	93	462	42.08	40.55
118	0.045	0.5782	45	3	0.125	108.50122	7.6257986	106.3	7147.1	1357.4	8.78	145	84	435	73.80	71.63
119	0.0696558	0.59265	45	4	0.125	37.44898	10.08135	36.7	2302.7	151.0	14.03	189	128	756	2.75	2.00
120	0.06	0.58985	45	4	0.125	41.760923	9.6044154	40.9	3343.7	244.4	12.00	172	111	688	7.06	6.23
121	0.05	0.5845	45	4	0.125	58.010362	9.0786138	56.9	5352.5	543.5	9.88	154	93	616	23.31	22.15
122	0.045	0.57975	45	4	0.125	80.930775	8.8063192	79.3	7108.0	1007.0	8.80	145	84	580	46.23	44.61
123	0.04	0.60835	40	3	0.1875	53.994182	10.957167	52.9	7252.8	732.4	7.43	133	73	399	21.52	20.44
124	0.045	0.6142	40	3	0.1875	42.149864	11.326312	41.3	5257.0	414.4	8.46	142	81	426	9.67	8.83
125	0.05	0.618	40	3	0.1875	37.333925	11.685474	36.6	3981.9	278.0	9.47	151	90	453	4.86	4.11
126	0.0547881	0.62055	40	3	0.1875	35.181406	11.997706	34.5	3136.0	206.3	10.44	159	98	477	2.70	2.00
127	0.036	0.6024	40	4	0.1875	57.105438	12.31295	56.0	9770.7	1043.5	6.60	126	66	504	24.63	23.49
128	0.038	0.6062	40	4	0.1875	49.266343	12.508325	48.3	8390.4	773.1	7.02	130	69	520	16.79	15.80
129	0.04	0.60925	40	4	0.1875	44.266045	12.653509	43.4	7231.2	598.7	7.44	133	73	532	11.79	10.90
130	0.045	0.61475	40	4	0.1875	37.847879	13.079771	37.1	5247.4	371.4	8.46	142	81	568	5.37	4.61
131	0.047	0.6164	40	4	0.1875	36.521234	13.219603	35.8	4656.3	318.0	8.87	145	85	580	4.04	3.31
132	0.048	0.6171	40	4	0.1875	36.005634	13.311729	35.3	4411.8	297.1	9.07	147	87	588	3.53	2.81
133	0.0710592	0.6247	40	3	0.125	35.181406	8.6712722	34.5	1630.4	107.3	13.69	186	126	558	2.70	2.00
134	0.07	0.6245	40	3	0.125	35.447497	8.6226153	34.7	1689.9	112.0	13.47	184	124	552	2.97	2.26
135	0.065	0.62325	40	3	0.125	37.207997	8.4248908	36.5	2036.1	141.7	12.47	176	115	528	4.73	3.99
136	0.06	0.6216	40	3	0.125	40.342035	8.1996444	39.5	2482.6	187.3	11.47	167	107	501	7.86	7.06
137	0.055	0.61935	40	3	0.125	46.277932	7.9949465	45.4	3111.1	269.3	10.46	159	98	477	13.80	12.87
138	0.05	0.6162	40	3	0.125	58.495094	7.7606967	57.3	3979.6	435.4	9.45	150	90	450	26.02	24.85
139	0.045	0.61145	40	3	0.125	82.248153	7.5477458	80.6	5305.7	816.1	8.42	142	81	426	49.77	48.13
140	0.064765	0.6235	40	4	0.125	35.181406	9.7019234	34.5	2045.4	134.6	12.43	175	115	700	2.70	2.00
141	0.06	0.622	40	4	0.125	36.855422	9.470115	36.1	2479.1	170.9	11.48	167	107	668	4.38	3.64
142	0.05	0.617	40	4	0.125	46.683403	8.9632239	45.7	3968.7	346.5	9.46	150	90	600	14.21	13.27
143	0.045	0.6127	40	4	0.125	61.429316	8.7166705	60.2	5283.6	607.0	8.44	142	81	568	28.95	27.72
144	0.04	0.60585	40	4	0.125	90.781357	8.4332861	89.0	7313.3	1241.7	7.40	133	72	532	58.30	56.49
145	0.035	0.6412	35	3	0.1875	62.13753	10.492844	60.9	7748.6	966.6	6.06	122	61	366	31.88	30.64
146	0.0375	0.64635	35	3	0.1875	49.867873	10.665372	48.9	6334.6	634.2	6.56	126	65	378	19.61	18.61
147	0.04	0.65025	35	3	0.1875	42.82438	10.835685	42.0	5273.6	453.4	7.05	130	70	390	12.57	11.71
148	0.045	0.6557	35	3	0.1875	35.99639	11.169978	35.3	3813.5	275.6	8.02	138	78	414	5.74	5.02
149	0.05	0.65925	35	3	0.1875	33.16137	11.49652	32.5	2880.0	191.7	8.97	146	86	438	2.91	2.24
150	0.0657119	0.66455	35	3	0.125	32.913832	8.3156937	32.3	1434.3	94.8	11.94	171	111	513	2.66	2.00
151	0.06	0.6628	35	3	0.125	34.96675	8.0835878	34.3	1804.6	126.7	10.86	162	102	486	4.71	4.01
152	0.055	0.66075	35	3	0.125	38.463577	7.8738928	37.7	2255.1	174.1	9.91	154	94	462	8.21	7.44

Table E - 5

AIR CURTAIN DESIGN	Created: Warren T. Jones, Ph.D.	10/29/08 11:05 AM
Solutions Summary	Last Revision:	12/19/08 9:42 AM

Solution #	Max Speed of Sound Ratio c/c_w (-)	Non-Dim Height, z/H, at Max c/cw (-)	Depth of Manifold [H] (ft)	Number of nozzles per ft [n] (1/ft)	Diameter of nozzle exit [d] (in)	Manifold Pressure [Pm] (psia)	Diameter of manifold [Dman] (in)	Pressure at Manifold End [Pend] (psia)	Flow Rate (scfm)	Total Pneumatic HP at manifold (hp)	Rise Time (sec)	Manifold length (ft)	Manifold Position in front of array (ft)	Total Number of Nozzles (-)	Pressure Diff at Manifold Beginning (psi)	Pressure Diff at Manifold End (psi)
153	0.05	0.6578	35	3	0.125	45.534518	7.6604183	44.6	2893.3	264.5	8.96	146	86	438	15.28	14.37
154	0.045	0.6535	35	3	0.125	61.252839	7.442843	60.0	3840.0	472.2	7.99	138	77	414	31.00	29.77
155	0.0425	0.6505	35	3	0.125	73.849235	7.3325391	72.4	4495.5	666.5	7.50	134	73	402	43.59	42.12
156	0.04	0.64665	35	3	0.125	90.309053	7.2210861	88.5	5333.3	967.0	7.01	130	69	390	60.05	58.25
157	0.038	0.6427	35	3	0.125	107.37265	7.1084364	105.2	6145.9	1324.8	6.61	126	66	378	77.12	74.97
158	0.08	0.45215	100	3	0.1875	77.530347	14.749655	76.0	16592.5	1321.2	20.14	241	180	723	18.39	16.84
159	0.09	0.4541	100	3	0.1875	67.801897	15.412713	66.4	12497.9	870.3	22.80	263	203	789	8.66	7.30
160	0.1	0.45535	100	3	0.1875	63.604798	16.050135	62.3	9745.8	636.6	25.45	285	225	855	4.46	3.19
161	0.1052052	0.4558	100	3	0.1875	62.39229	16.388034	61.1	8672.8	555.7	26.82	297	237	891	3.25	2.00
162	0.07	0.4498	100	4	0.1875	83.402368	16.195516	81.7	22907.1	1962.1	17.49	218	158	872	24.26	22.59
163	0.08	0.4526	100	4	0.1875	69.345256	17.032353	68.0	16559.7	1179.4	20.16	241	180	964	10.20	8.81
164	0.09	0.45435	100	4	0.1875	63.979295	17.797875	62.7	12481.7	820.1	22.81	263	203	1052	4.83	3.56
165	0.0958903	0.4551	100	4	0.1875	62.39229	18.236028	61.1	10746.1	688.6	24.37	276	216	1104	3.25	2.00
166	0.1	0.45435	100	3	0.125	82.451387	10.697362	80.8	9790.3	829.0	25.41	285	225	855	23.31	21.66
167	0.11	0.45545	100	3	0.125	71.838043	11.125752	70.4	7857.6	579.7	28.06	308	247	924	12.69	11.26
168	0.12	0.4563	100	3	0.125	66.484545	11.522485	65.2	6422.6	438.5	30.72	330	269	990	7.34	6.01
169	0.13	0.45685	100	3	0.125	63.593894	11.907819	62.3	5343.2	349.0	33.37	352	292	1056	4.45	3.18
170	0.1367309	0.4572	100	3	0.125	62.39229	12.164634	61.1	4763.1	305.2	35.16	367	307	1101	3.25	2.00
171	0.08	0.451	100	4	0.125	114.29008	11.329055	112.0	16614.3	1950.1	20.10	240	180	960	55.15	52.86
172	0.09	0.4533	100	4	0.125	84.472198	11.862948	82.8	12542.6	1088.1	22.77	263	202	1052	25.33	23.64
173	0.1	0.4548	100	4	0.125	72.040292	12.353781	70.6	9770.2	722.9	25.43	285	225	1140	12.90	11.46
174	0.11	0.4558	100	4	0.125	66.214844	12.84836	64.9	7845.7	533.5	28.08	308	247	1232	7.07	5.75
175	0.1245854	0.4568	100	4	0.125	62.39229	13.510036	61.1	5883.5	377.0	31.94	340	280	1360	3.25	2.00
176	0.15	0.39905	200	3	0.1875	122.50531	19.746064	120.1	40107.6	2881.1	42.82	432	372	1296	18.92	16.47
177	0.175	0.4002	200	3	0.1875	110.7052	21.164454	108.5	28359.6	1841.0	50.34	496	435	1488	7.12	4.90
178	0.18	0.40035	200	3	0.1875	109.54388	21.420424	107.4	26580.9	1707.4	51.85	508	448	1524	5.95	3.76
179	0.19	0.4006	200	3	0.1875	107.81894	21.965031	105.7	23563.4	1489.7	54.89	534	474	1602	4.23	2.07
180	0.1905391	0.40065	200	3	0.1875	107.74376	21.985775	105.6	23397.4	1478.2	55.05	535	475	1605	4.15	2.00
181	0.15	0.39935	200	4	0.1875	114.13595	22.801421	111.9	40046.5	2680.2	42.84	432	372	1728	10.55	8.26
182	0.16	0.3998	200	4	0.1875	110.60441	23.480005	108.4	34668.9	2248.5	45.84	458	397	1832	7.02	4.80
183	0.17	0.4002	200	4	0.1875	108.37533	24.115153	106.2	30222.7	1920.6	48.85	483	423	1932	4.79	2.62
184	0.1738586	0.40035	200	4	0.1875	107.74376	24.364709	105.6	28747.5	1816.2	50.01	493	432	1972	4.15	2.00
185	0.13	0.39495	200	3	0.125	325.08378	12.342891	318.6	56118.2	10697.3	36.64	380	319	1140	221.49	214.99
186	0.15	0.39755	200	3	0.125	205.94944	13.14681	201.8	40323.9	4869.6	42.70	431	371	1293	102.36	98.24
187	0.175	0.3993	200	3	0.125	140.70459	14.093382	137.9	28433.6	2345.9	50.27	495	435	1485	37.12	34.30
188	0.2	0.40025	200	3	0.125	119.29639	14.982992	116.9	21041.9	1471.9	57.89	559	499	1677	15.71	13.32
189	0.225	0.40085	200	3	0.125	110.96905	15.83846	108.7	16146.8	1050.7	65.60	624	564	1872	7.38	5.16
190	0.2459976	0.4012	200	3	0.125	107.74376	16.542811	105.6	13217.2	835.0	72.17	680	619	2040	4.15	2.00

Table E - 6

AIR CURTAIN DESIGN	Created: Warren T. Jones, Ph.D. 10/29/08 11:05 AM
Solutions Summary	Last Revision: 12/19/08 9:42 AM

Solution #	Max Speed of Sound Ratio c/c_w (-)	Non-Dim Height, z/H, at Max c/cw (-)	Depth of Manifold [H] (ft)	Number of nozzles per ft [n] (1/ft)	Diameter of nozzle exit [d] (in)	Manifold Pressure [Pm] (psia)	Diameter of manifold [Dman] (in)	Pressure at Manifold End [Pend] (psia)	Flow Rate (scfm)	Total Pneumatic HP at manifold (hp)	Rise Time (sec)	Manifold length (ft)	Manifold Position in front of array (ft)	Total Number of Nozzles (-)	Pressure Diff at Manifold Beginning (psi)	Pressure Diff at Manifold End (psi)
191	0.15	0.39825	200	4	0.125	159.2735	15.199215	156.1	40277.1	3761.6	42.76	432	371	1728	55.68	52.50
192	0.175	0.3997	200	4	0.125	124.14648	16.274781	121.7	28374.3	2065.5	50.30	495	435	1980	20.56	18.07
193	0.18	0.3999	200	4	0.125	120.75809	16.488306	118.3	26642.8	1886.6	51.82	508	448	2032	17.17	14.75
194	0.19	0.40025	200	4	0.125	115.74869	16.907642	113.4	23610.0	1602.5	54.86	534	473	2136	12.16	9.84
195	0.2	0.40055	200	4	0.125	112.35767	17.317358	110.1	21050.2	1386.9	57.91	560	499	2240	8.77	6.52
196	0.21	0.40075	200	4	0.125	110.0131	17.703056	107.8	18837.2	1215.2	60.98	585	525	2340	6.42	4.22
197	0.22	0.40095	200	4	0.125	108.36182	18.110765	106.2	16995.9	1079.9	64.06	612	551	2448	4.77	2.61
198	0.2248209	0.40105	200	4	0.125	107.74376	18.289433	105.6	16171.7	1021.7	65.56	624	564	2496	4.15	2.00

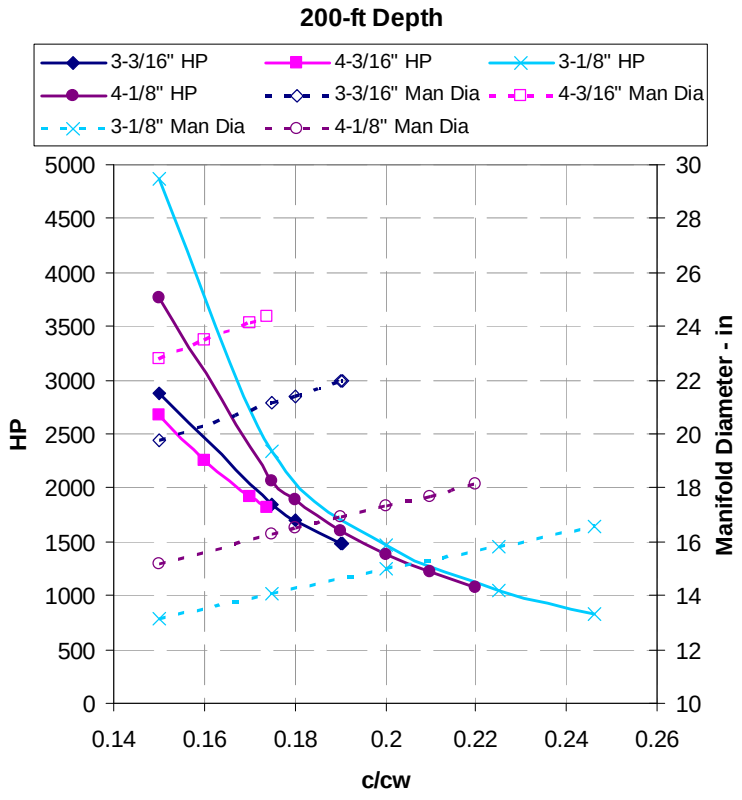

Figure E - 1

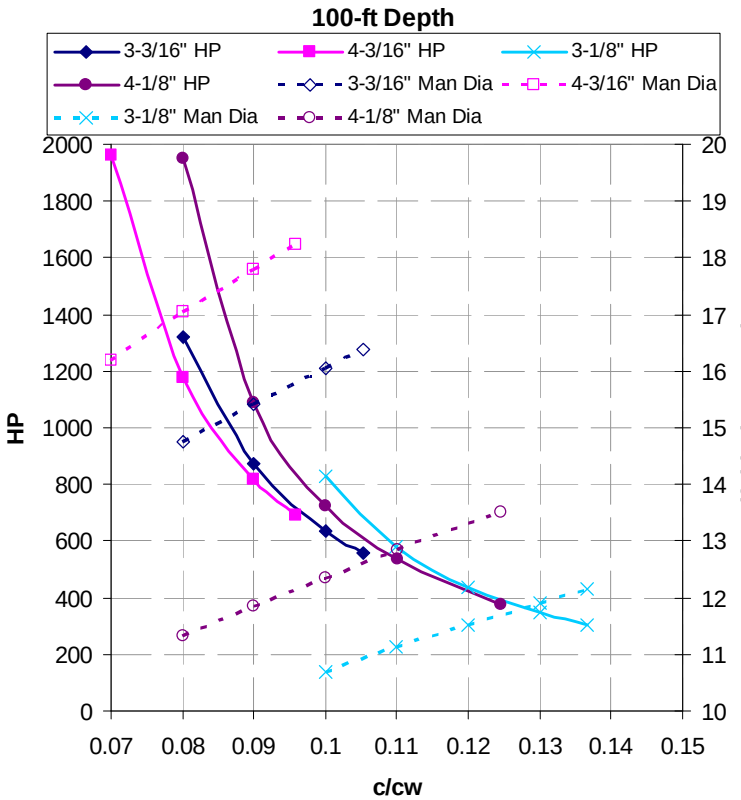

Figure E - 2

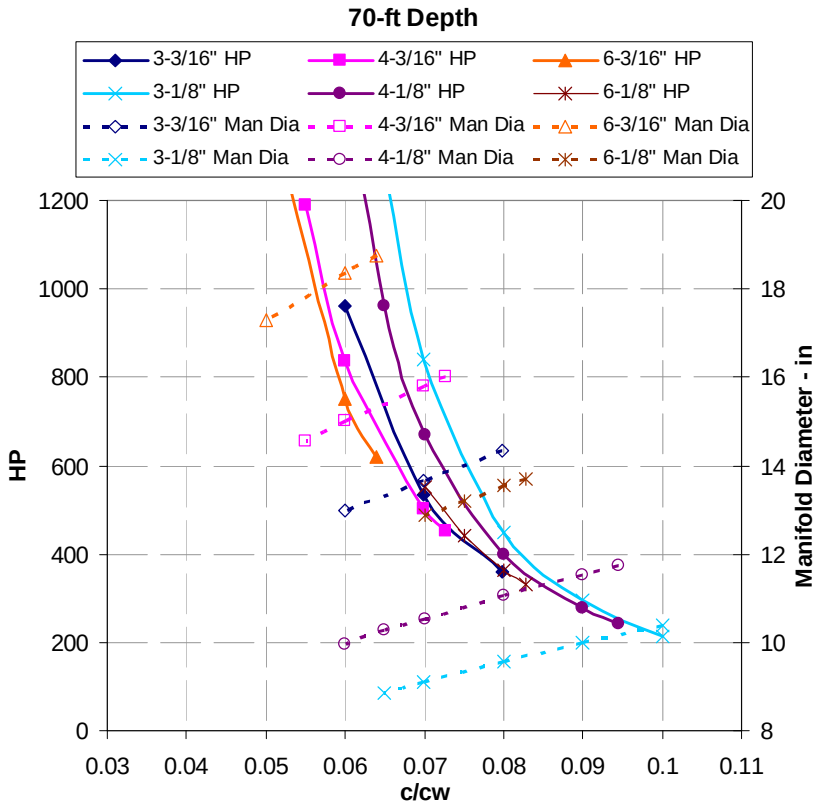

Figure E - 3

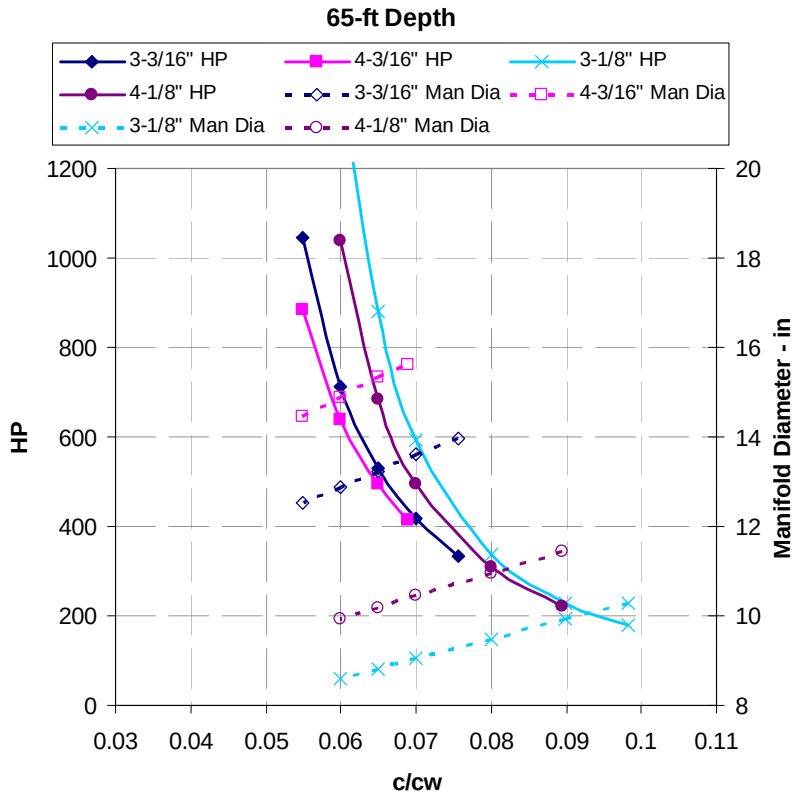

Figure E - 4

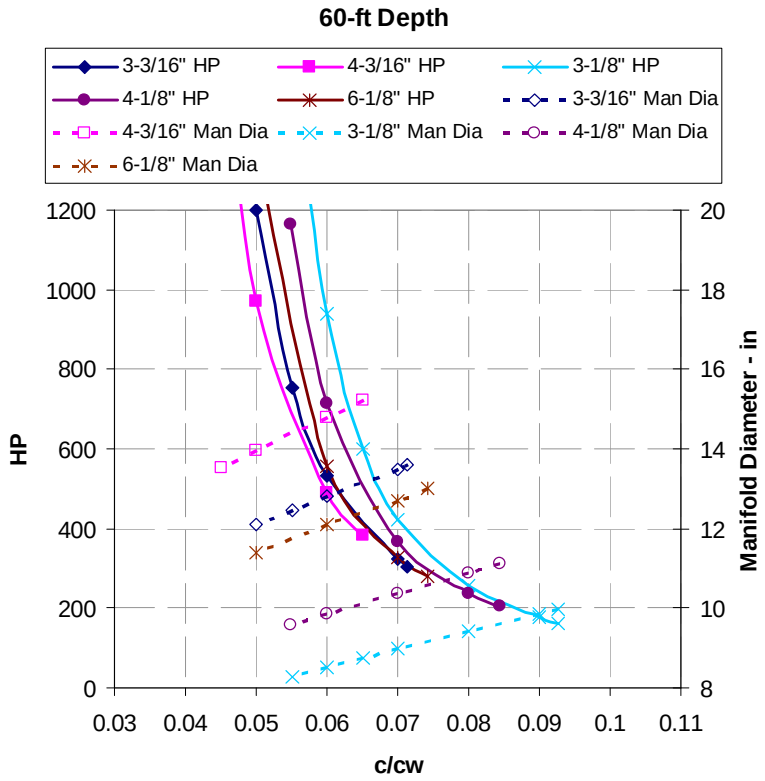

Figure E - 5

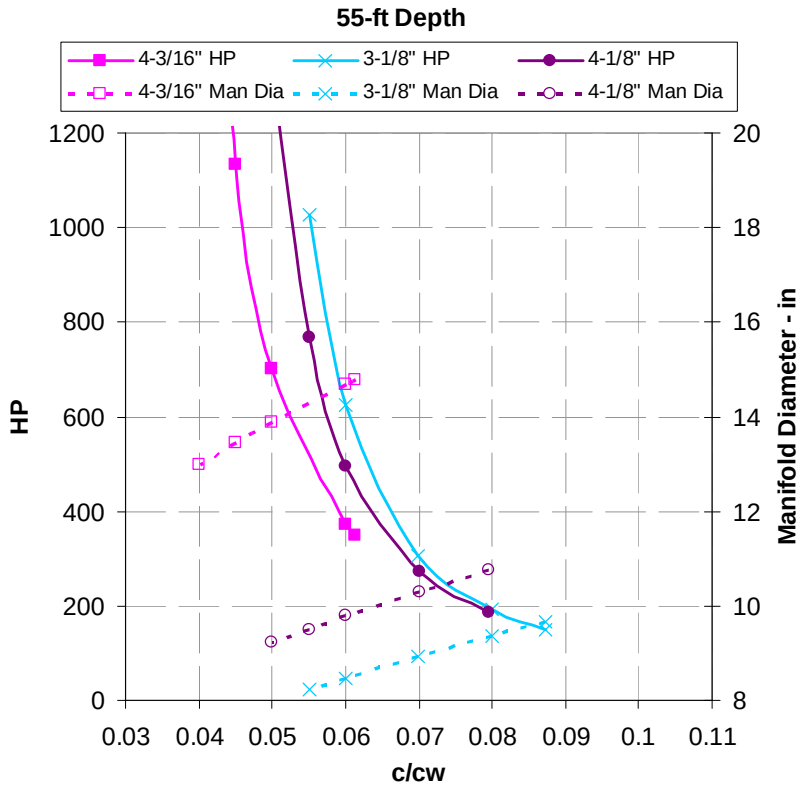

Figure E - 6

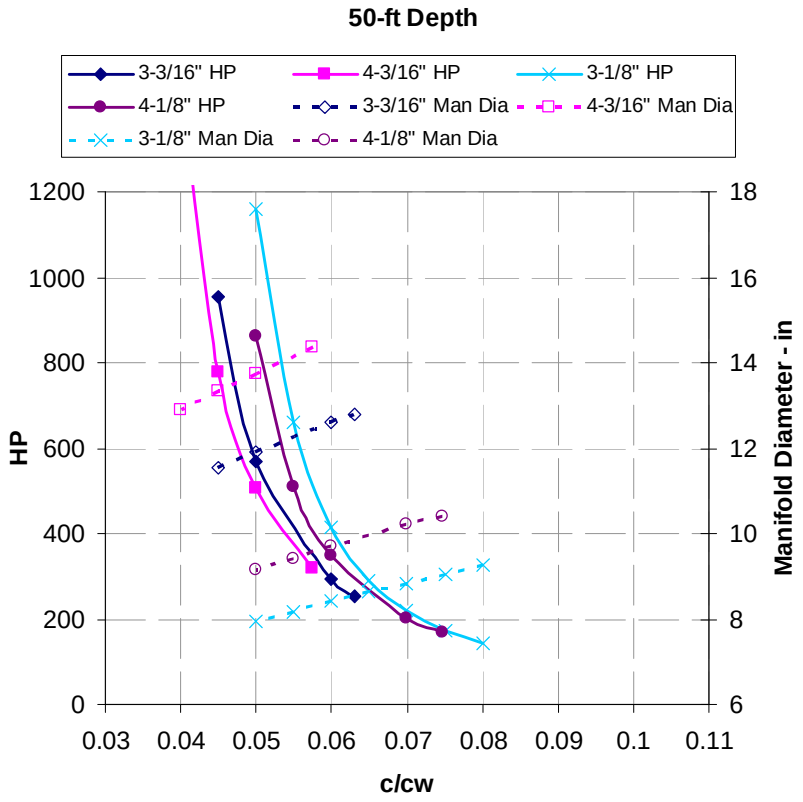

Figure E - 7

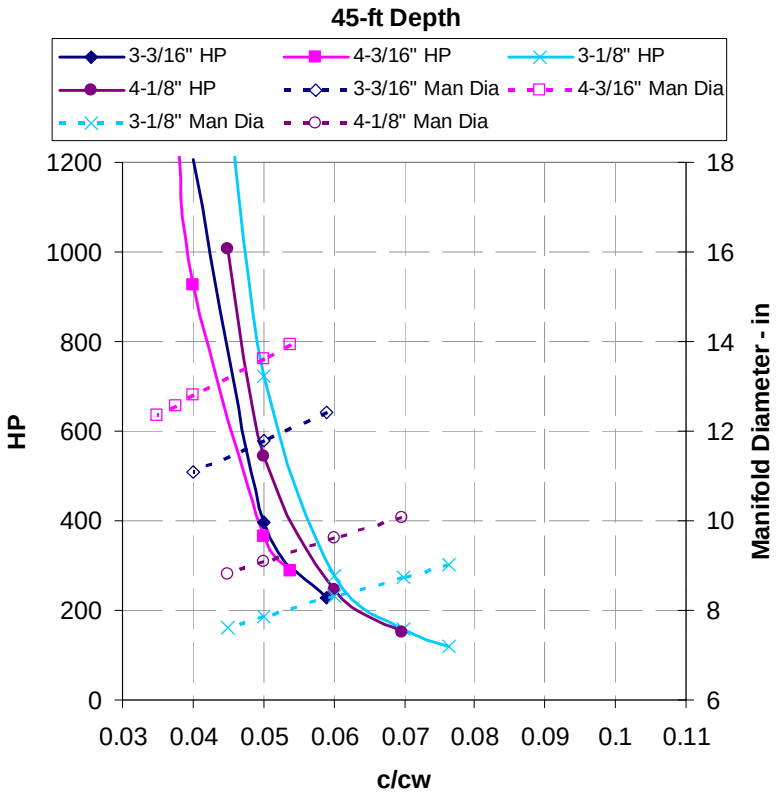

Figure E - 8

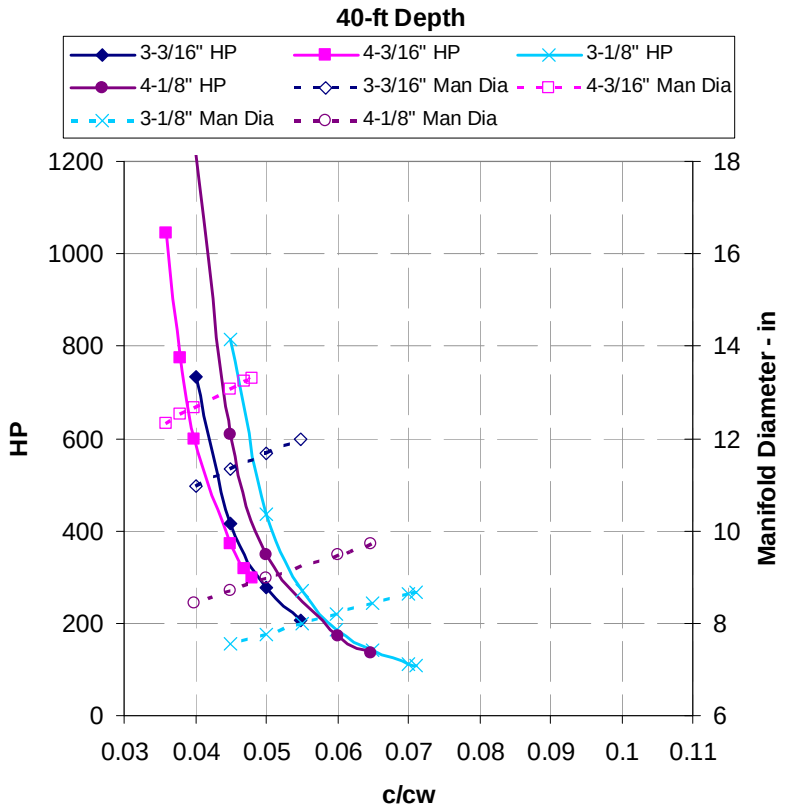

Figure E - 9

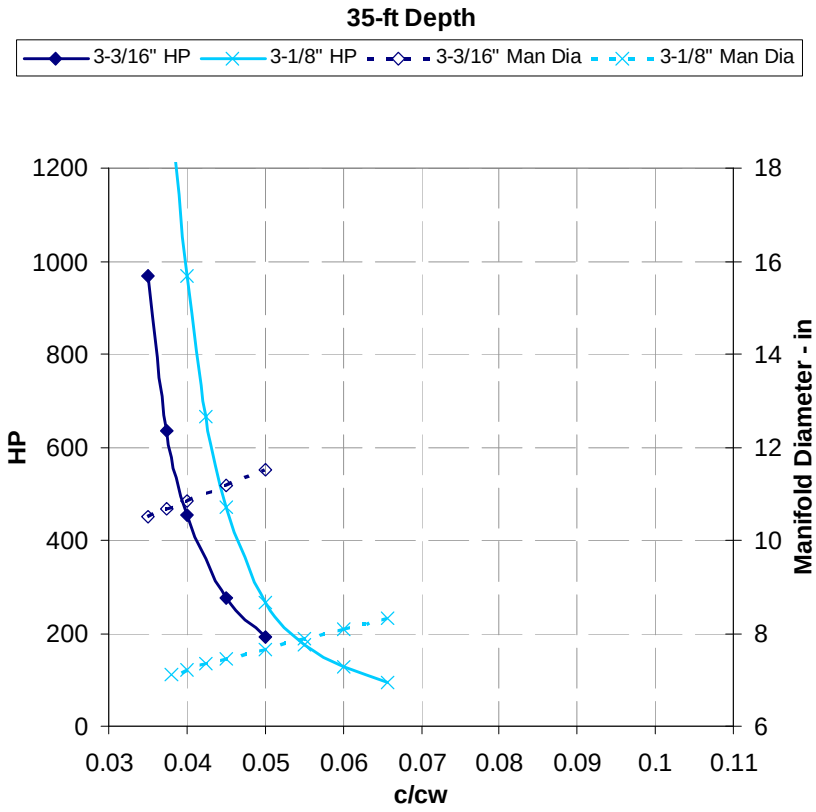

Figure E - 10

APPENDIX B

MODELING OF ACOUSTIC ATTENUATION OF AN AIR CURTAIN

Prepared By

JASCO Research Ltd.

For

Stress Engineering Services

Report Delivered to:
Ray R. Ayers, Ph.D., P.E.

Version 1.0
December 27, 2008

MODELING OF ACOUSTIC ATTENUATION OF AN AIR CURTAIN

Report Prepared by

David Hannay
JASCO Research Ltd

Version 1.0
December 27, 2008

1 BACKGROUND AND INTRODUCTION

Stress Engineering Services Inc is investigating the use of bubble curtains to reduce underwater sound pressure levels produced by airgun arrays that are commonly used as the seismic source for marine seismic survey programs. The acoustic modeling study described here was performed by JASCO Research Ltd to estimate the effectiveness of a specific air curtain configuration for absolute reduction of sound levels.

Airguns produce underwater sounds by rapidly releasing highly compressed air into the surrounding water. The pressurized bubble is initially small but starts to increase in size before undergoing damped oscillations. The resulting acoustic pressure wave is proportional to the pressure variation within the oscillating bubble. It has a high initial primary pressure peak corresponding to air release followed by a series of secondary peaks associated with the subsequent volume minima of the oscillating bubble. The secondary peaks are referred to as bubble pulses and these are undesirable from a seismic imaging perspective. The period between bubble pulses increases with the volume of the airgun chamber and airgun arrays use this feature to suppress bubble pulses by simultaneously firing multiple airguns with different volumes. The primary pulses occur at the same time so their pressures add coherently while the bubble pulses do not.

Airgun arrays are typically configured with the airguns laid out in one or more "strings" comprising sequences of in-line deployed airguns. Multiple strings are often towed side-by-side to provide a 2-dimensional array with all airguns on a constant depth plane. Planar airgun arrays produce highest sound pressure levels in the downward direction because the pressure pulses from all airguns add coherently only in that direction. However, high levels of sound are produced in all directions and this sound can lead to disturbance of nearby marine mammals. Air curtains have been proposed as a method of reducing sound levels in certain directions from airgun arrays. Air curtains have recently been employed to reduce sound levels produced by pile driving activities. That application is relatively more straightforward because the piles are stationary. The manifolds to be used for producing air curtains on the sides of airgun arrays will have to be towed on either side of the array at a depth greater than the airguns. The released air bubbles will move vertically upward due to buoyancy and horizontally due to water flow relative to the airgun array. Figure 1 depicts the relative positions of the manifolds and air curtains relative to a 3-string airgun array with 5 airguns in each string.

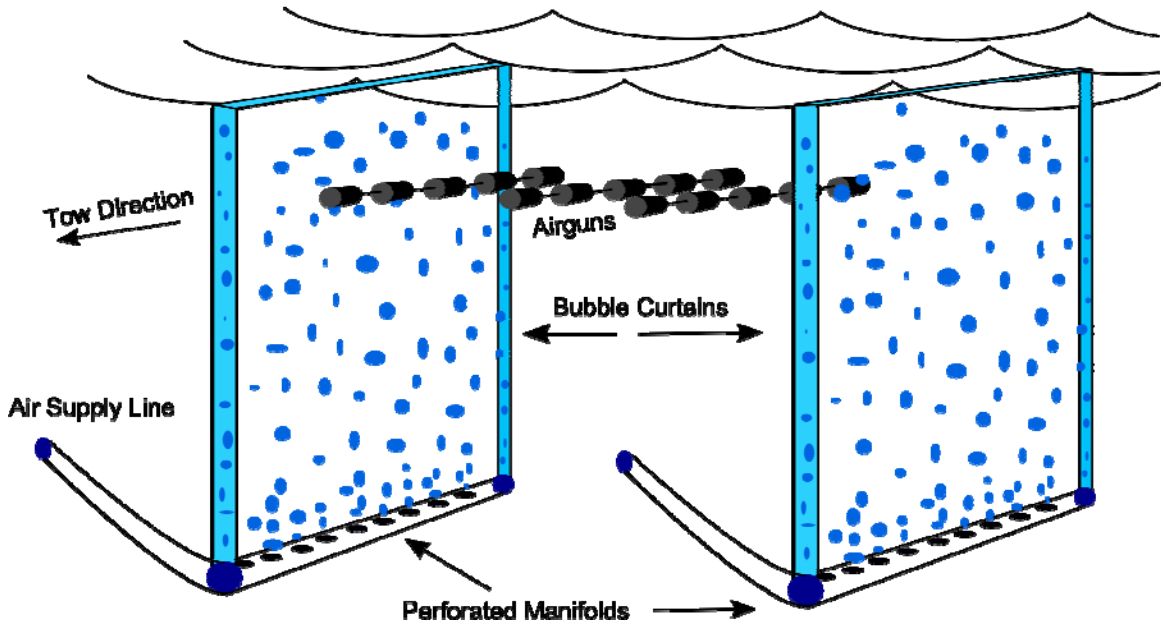

Figure 1: Positions of manifolds and curtains relative to a towed airgun array.

2 PURPOSE

The purpose of this acoustic modeling study is to predict the absolute pressure reduction as a function of sound frequency that could be achieved by a specific air curtain configuration. The specific configuration is described by two 201 foot (61.3 m) - long manifolds deployed on either side of the airgun array and towed at 60 feet (18.3 m) depth. This scenario was chosen based on fluid-dynamic modeling by Warren Jones (Figure 2) that predicted the fractional volume of water that would occur as a function of depth in the region above the manifolds. The bubble density decreases perpendicularly across each curtain according to a square exponential decay function. The distance perpendicular to a vertical plane passing through the manifold axis at which the bubble density reaches 1/e (~0.37) of its on-axis density is 2.4 m at 15.2 m depth and 0.58 m at 3.7 m depth.

AIR CURTAIN DESIGN	Created: Warren T. Jones, Ph.D.	12/4/08 10:02 AM
Solution #64	Last Revision	12/11/08 2:07 PM

Max Speed of Sound Ratio c/c_w (-)	Depth of Manifold [H] (ft)	Number of nozzles per ft [n] (1/ft)	Diameter of nozzle exit [d] (in)	Manifold Pressure [Pm] (psia)	Diameter of manifold [Dman] (in)	Pressure at Manifold End (psia)	Flow Rate (scfm)	Total Pneumatic HP at manifold (hp)	Rise Time (sec)	Manifold length (ft)	Manifold Position in front of array (ft)	Total Number of Nozzles (-)	NumSteps (-)
0.07	60	3	0.125	58.40212	8.986533	57.23408	4933.793	423.1036	15.4867557	201	141	603	20000

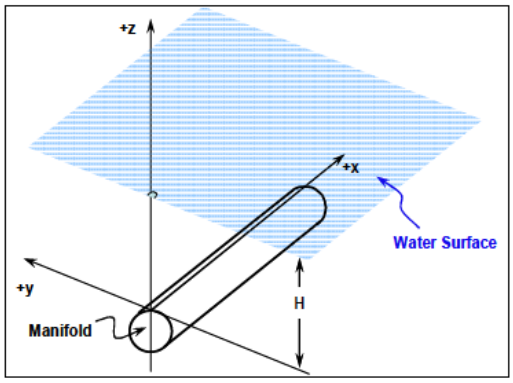

z (ft)	Avg s (-)	sm (-)	b (ft)	λb ft
0	1			
3	0.110072	0.13759	0.348	0.4698
6	0.061522	0.076902	0.696	0.9396
9	0.04353	0.054412	1.044	1.4094
12	0.034204	0.042755	1.392	1.8792
15	0.028539	0.035673	1.74	2.349
18	0.024764	0.030956	2.088	2.8188
21	0.022099	0.027623	2.436	3.2886
24	0.020141	0.025176	2.784	3.7584
27	0.018668	0.023334	3.132	4.2282
30	0.017543	0.021928	3.48	4.698
33	0.016681	0.020851	3.828	5.1678
36	0.016027	0.020033	4.176	5.6376
39	0.015542	0.019427	4.524	6.1074
42	0.015203	0.019003	4.872	6.5772
45	0.014993	0.018741	5.22	7.047
48	0.014905	0.018631	5.568	7.5168
51	0.014936	0.01867	5.916	7.9866
54	0.015089	0.018862	6.264	8.4564
57	0.015376	0.019219	6.612	8.9262
60	0.015812	0.019765	6.96	9.396

Average volume fraction of air = $\bar{s}$

$$s_m(z) = 1.25\,\bar{s}(z)$$
$$b = 0.116z, \quad \lambda = 1.35$$
$$s(z,y) = s_m(z)\exp\left[-y^2/(\lambda b)^2\right]$$

Figure 2: Fluid dynamic model of air curtain bubble density and volume fraction versus depth and distance off curtain axis. Modeling results provided by Warren T. Jones.

3 APPROACH

Sound propagation and back-scattering in bubbly water has been studied extensively in problems encountered in acoustic oceanography and ultrasonic imaging (Leighton 1994). Even a very small fractional volume of air bubbles in water can significantly change the sound speed. The primary reason for this effect is that the compressibility of bubbly water is much greater than for regular water. Sound pressure waves incident on the boundaries of bubbly water layers can be reflected strongly due to the large change in sound speed and acoustic impedance across the boundaries. Bubbles also can absorb energy from acoustic pressure waves if the natural frequency of bubble oscillation is similar to that of the incident pressure wave. The natural resonant frequency of bubbles depends on their radii and depth. The latter affect generally is important at low frequencies only for large bubble sizes; bubble diameters corresponding to resonant frequencies 100 Hz and 500 Hz respectively are 3 cm and 6 mm. It is quite possible that these large bubble sizes could be produced by the air curtain system considered here.

Sound attenuation due to excitation of individual bubble oscillations is complex and depends on the distribution of bubble sizes in the bubbly liquid region. Although resonance absorption is likely an important effect, we have neglected it in this initial examination. Here we only consider the macroscopic effect of reduced acoustic impedance in the bubbly layer on the

reflection and transmission coefficients through the layer. Leighton shows that when the frequency of the incident acoustic wave is much less than the bubble oscillation frequency then the sound speed C in the bubbly layer can be computed according to

$$C = C_w \left(1 + \frac{\{VF\}}{2} \frac{C_w^2 \rho_w}{C_a^2 \rho_a} \right)^{-1} \qquad \text{Eq.1}$$

where C_w is the water sound speed, ρ_w is the water density, C_a is the air sound speed, ρ_a is the water density and VF is the fractional volume occupied by air bubbles.

The specific approach taken here is to model the reflection and transmission coefficients as a function of frequency through a homogenous bubble layer that has reduced sound speed and density. The specific assumptions made here were:

1. Bubble layer thickness of 1.5 m was chosen based on the distance at which the density factor had decreased to 1/e of its on-axis value. This was based on the decay function value at 5 m depth (corresponding to common airgun array operating depth).
2. Bubble layer fractional air volume of 0.028 is used. It is the fluid-dynamic model predicted value at 5 m depth.
3. Bubble layer sound speed was computed using Eq. 1 with the following parameter values: C_w = 1500 m/s, ρ_w = 1020 kg/m^3, C_a = 343 m/s, ρ_a = 1.2 kg/m^3 and VF = 0.028. Eq. 1 gives C = 6.6 m/s but to be conservative we have increased the value by an order of magnitude; the value for sound speed in the bubble layer used for this study is 66 m/s.
4. Bubble layer density was chosen based on the sum of the products of relative fractions of water and air at 5 m depth and their respective densities. This gives 991 kg/m^3.

A one-dimensional problem was considered in which a plane acoustic wave of frequency f is incident on the bubble layer from angle θ as shown in Figure 3.

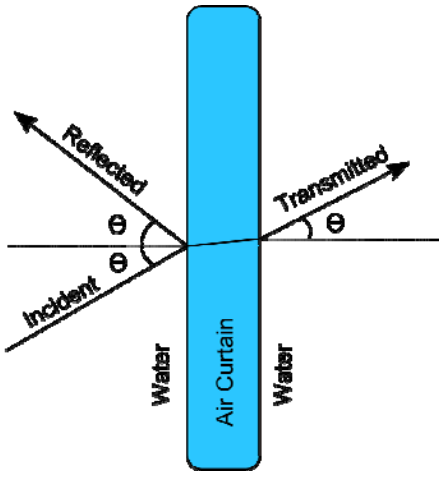

Figure 3: Diagram of Incident, Reflected and Transmitted Acoustic Paths.

The transmission coefficient T represents the ratio of amplitudes of the transmitted wave to the incident wave. This coefficient in decibels indicates how much signal attenuation will be produced by the air curtain. The transmission coefficient was computed using the well-known theoretical formula for sound transmission through a fluid layer having different acoustic impedance than the fluid on either side (e.g. Jensen et al. 2000 and Brekhovskikh 1960). This is an exact formulation for fluid layers. The acoustic impedances of the water and air curtain layers were computed from their respective sound speeds and densities and from the angle of propagation in each layer. The angles of propagation were computed from Snell's law.

4 RESULTS

The transmission loss through the bubble curtain was computed as a function of frequency using the method described in Section 3. The results for incident angles 0 degrees, 30 degrees, 60 degrees and 89 degrees are shown in Figure 4. The 89 degree result is labeled as 90 degrees.

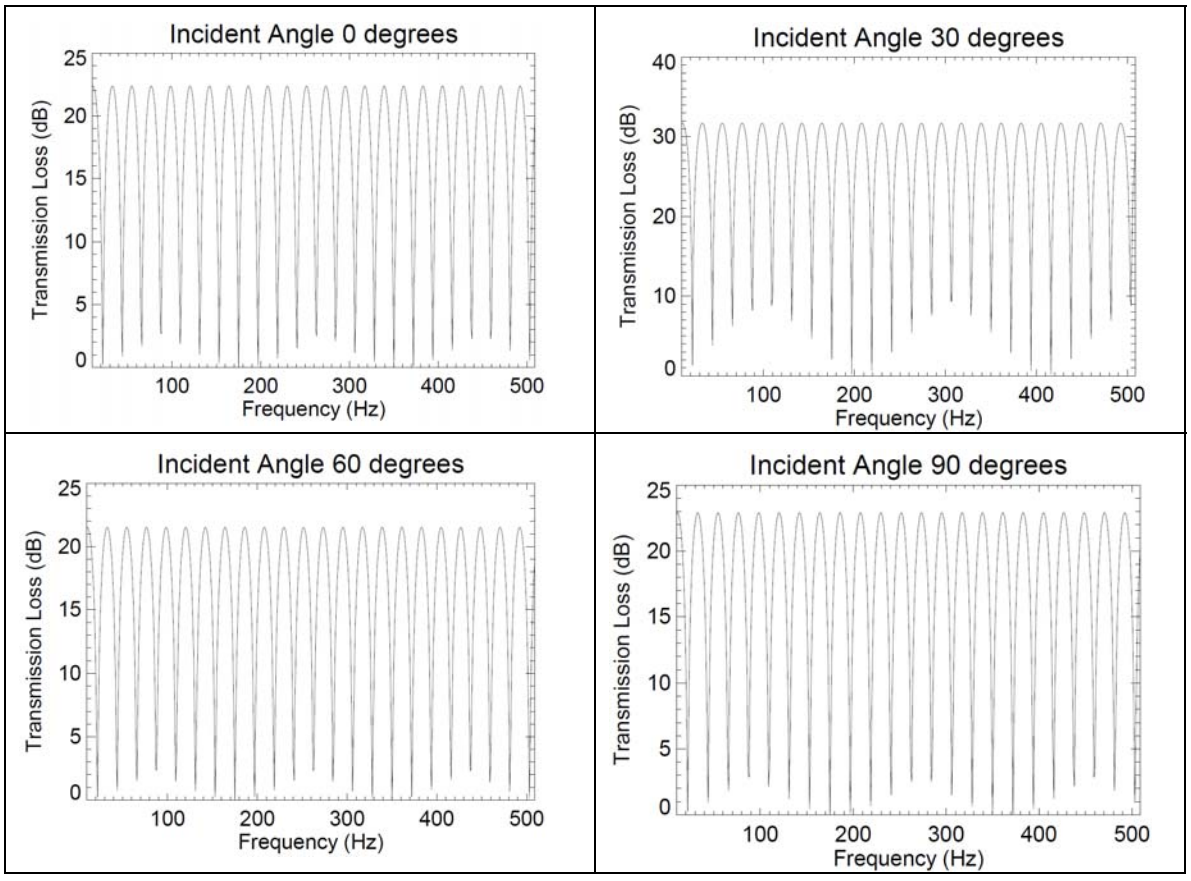

Figure 4: Transmission loss incurred by sound propagation through the air curtain bubble layer for four angles of incidence.

5 SUMMARY

Figure 4 shows the predicted acoustic transmission loss for sound transmission through the bubble curtain configuration described in Section 2 with several additional assumptions presented in Section 3. The acoustic transmission loss was predicted as a function of frequency for frequencies up to 500 Hz and for incident angles onto the bubble curtain layer of 0 degrees, 30 degrees, 60 degrees and 89 degrees. The results are plotted in Figure 4. Transmission loss values versus frequency were observed between 0 dB and 32 dB for the four incident angles tested. All four incident angles showed similar frequency variation whereby the transmission loss function cycled between 0 dB to the maximum (22 dB to 32 dB) with a period of 22 Hz. This frequency corresponds with ½-wavelength layer effect; the wavelength in the air curtain layer at 22 Hz is 3 m which is twice the layer thickness. The frequency of the loss minima do not change appreciably with incident angle because the wave propagation angle in the low speed bubbly layer is near perpendicular to the boundaries for all incident angles. We also examined the maximum loss value as a function of angle. The maxima for the four angles presented in Figure 4 were between 22 dB and 32 dB. The transmission loss maxima however can have greater variation than apparent at the four angles examined. Transmission loss at 11 Hz, and likely multiples of that frequency, ranged from 22 dB to 65 dB when incident angle was stepped through 1 degree increments between 1 and 89 degrees.

Insofar as sound level reduction is concerned, the bubble curtain scenario examined here could reduce the spectral levels for most frequencies by more than 10 dB. The absolute reduction appears to vary cyclically with frequency but there was not a trend with frequency. This result is likely due to our assumption of no absorptive losses within the bubble curtain layer. Losses incurred by exciting individual bubble resonances were not addressed in this study and those would be in addition to the impedance loss mechanism considered here. Those resonant losses would be frequency dependent and influenced by the similarities between bubble resonant frequencies and the airgun array sound frequency spectrum. The bubble resonant frequencies are dependent on the bubble size distribution.

6 LITERATURE CITED

Leighton, T.G. The Acoustic Bubble. San Diego: Academic Press, 1994. 613 p.

Brekhovskikh, L.M. Waves in Layered Media. New York: Academic Press, 1960. 561 p. [Acoustics Institute, Academy of Sciences, USSR]

Jensen, F.B., W.A. Kuperman, M.B. Porter, H. Schmidt. Computational Ocean Acoustics. New York: Springer Verlag, 2000.

APPENDIX C

TECHNICAL MEMO 08-035

Seismic Array Directionality Study

Jesse Spence

July 28, 2008

NCE JOB No. J08-040

Prepared for:
Stress Engineering Services, Inc.
13800 Westfair East Dr.
Houston, TX 77041
Attention: Mr. Ray Ayers

Prepared by:
NOISE CONTROL ENGINEERING, Inc.
799 Middlesex Turnpike
Billerica, MA 01821
978-670-5339
978-667-7047 (fax)
nonoise@noise-control.com
http://www.noise-control.com

TABLE OF CONTENTS

LIST OF FIGURES

0.0 EXECUTIVE SUMMARY

Noise Control Engineering (NCE) has performed a study to identify possible methods of reducing lateral sound propagation from air gun arrays. The methods investigated here include 1) use of a longitudinally-oriented air bubble curtain on both sides of the air gun array, 2) use of a barrier made of a low acoustic impedance material in a similar configuration to item 1, and 3) use of a parabolic reflector to focus sound downwards. This study has been performed using the Comsol™ finite element modeling software which contains an integrated acoustics module for modeling wave propagation around complex structures.

All three concepts appear to have merit and may be capable of reducing lateral transmission of sound. In general, the effectiveness of any of these approaches is dependent on the air gun array details, such as gun sizes, depth in the water, and configuration. Such factors must be taken into account when assessing the performance or making recommendations regarding optimal configurations of a barrier or reflector. Furthermore, the models used in this study are idealized, and the results should be taken as approximate. While the results indicate that all of the approaches are worth further consideration, testing a prototype is recommended to get a better determination of real-world effectiveness. This testing will also allow for feasibility studies of non-acoustic issues which are not addressed in detail in this report.

A summary of the results for each treatment is provided below.

Bubble Curtain Barrier

The air bubble curtain concept is shown in Figure 2. In deep water, it has been shown that reductions in sound with a bubble barrier are possible at 100 Hz and above for angles greater than 50 degrees relative to the vertical axis (i.e. near the water surface) for receivers that are located on the side of the air gun array (‘lateral’ or ‘transverse’ direction). Reductions of 5-25+ dB have been seen in some cases, though the performance is frequency dependent and does not necessarily get better at higher frequencies.

The effectiveness of the barrier is dependent on various parameters such as depth, distance from centerline, and air content. It has been shown that maximum effectiveness at higher frequencies can be achieved by locating the barrier as close to the air gun array as possible. Deeper barriers will also improve performance; though there will be diminishing returns below a certain depth. The bubble curtain should contain at least 10% air by volume. Barrier thickness does not appear to be a dominant factor in performance.

A longitudinal barrier will not significantly change the directivity of the array on centerline (fore/aft direction). For air gun arrays that have larger air guns near the front, the barrier effectiveness appears to be good for transverse propagation and propagation at forward azimuth angles (i.e. angles in the forward direction in the plane of the water surface). Effectiveness will drop off more rapidly for aft azimuth angles. The barrier length should generally be made as long as possible to maximize effectiveness, though some effectiveness is possible even for barriers that are short relative to the length of the air gun array.

Amplifications of sound should also be expected at some angles over certain frequency ranges. The specific angle where amplifications occur depend on the specific frequency, barrier configuration, and air gun arrangement, though amplifications as high as 20 dB have been seen.

There is also a potential for a reduction in sound at frequencies below 100 Hz directly beneath the array. While most frequencies below 100 Hz were largely unaffected by the barrier, some configurations showed reductions of sound as high as 12 dB directly below the array at specific frequencies (i.e. 30 Hz). This is an important result as these frequencies are useful in identifying geological features beneath the sea floor.

If the barrier is used in shallow water (~20-30 meters) then the reflections off the sea floor will act to reduce the effectiveness of the barrier. If the bottom is assumed to be 'perfectly rigid,' all frequencies are seen to have significant reductions in effectiveness, and some frequencies are not attenuated at all. For realistic sea floors it is expected that the reduction in performance would not be quite this dramatic, though the results will depend on the specific makeup of the sea floor and the amount of sound that is absorbed.

Low Impedance Material Barrier

It is possible to use closed cell foam materials in place of an air bubble curtain for the above barrier design, or for the parabolic reflector. Soft foam materials such as nitrile, neoprene, EPDM, etc. should work well from an acoustical perspective, and can be rolled for efficient retrieval, storage, and deployment. However, these materials may create added drag due to oscillatory lateral motion as they are pulled through the water (i.e. motion similar to a flag blowing in the wind). Additional structures are likely to be necessary in order to support these materials and to ballast the barrier into position.

Rigid closed cell foams such as polyurethane foam can also be used for these applications, though the specific properties should be assessed prior to use. Rigid foams will have the advantage of maintaining their shape in the water, potentially requiring less hardware to maintain position. However, hard foams will be more difficult to deploy and retrieve.

The modeling of the air bubble barrier (and reflector, see below) indicates that the acoustic effectiveness is not affected by the thickness of the barrier. However, it is reasonable to assume that if a foam material is used then there will be some thickness below which effectiveness will drop off. By analyzing the particle velocity in a material that has a specific acoustic impedance 30 times less than water, it has been estimated that the minimum required thickness of the barrier would be 1 inch assuming a sound pressure level of 210 dB re 1μPa at the barrier. Higher sound pressure levels may require thicker materials. Testing is recommended to confirm this assumption.

Parabolic Reflector

The parabolic reflector concept has a potential for large reductions in sound, particularly at vertical angles greater than 70 degrees. Compared to the effectiveness of the vertical barriers discussed above, the reflector appears to provide similar or greater reductions in sound over a larger vertical angle. A concept sketch of this design is provided in Figure 26. The air gun array has been modified for this design; a single longitudinal line of air guns is used instead of

multiple lines as is commonly used. Note that this configuration would provide additional longitudinal (centerline) directivity relative to a multiple line array if the same number of air guns is used.

The reflector is seen to provide an increase in output directly below the array of up to 10 dB for most frequencies, though the lowest frequencies (5, 30 Hz) can have reductions in sound of up to 17 dB.

The shape of the reflector has been selected so that the air gun array is located at the focus of the parabola. This means that arrays located closer to the water surface will tend to require less surface area for a given performance. For arrays located deeper in the water the size of the reflector may be a practical limitation. If air bubbles are used to make the reflector, the hoses used to create the air bubble curtain must be oriented laterally (transverse), and many rows of hoses must be used in order to maintain the parabolic shape over the entire array. This may prove difficult in practice. A solid material may be preferable in this case, and would also provide similarly large sound level reductions. Such a reflector would likely need to be assembled in sections to cover the entire length of the array.

As was found for the barrier designs, the effectiveness in shallow water is significantly compromised as a result of bottom reflections. If the sea floor is absorptive then this reduction in performance may not be as dramatic.

1.0 INTRODUCTION

Noise Control Engineering (NCE) has performed a study of various potential methods to reduce lateral propagation of sound from an air gun array used for seismic exploration. The purpose of this study is to identify feasible approaches for blocking lateral sound propagation to protect marine life that may exist near seismic survey operations. The study focuses on three approaches: 1) use of a longitudinally oriented air bubble curtain on both sides of the air gun array, 2) use of a low acoustic impedance material as a curtain in a similar configuration to item 1, and 3) use of a parabolic reflector to focus sound downwards. This study has been performed using the Comsol™ finite element modeling software which contains an integrated acoustics module for modeling wave propagation around complex structures.

Section 2 of this report discusses the models and results of the air bubble curtain analysis. Section 3 discusses possible materials that could be used for a barrier. Section 4 discusses the model and results of the parabolic reflector analysis.

2.0 AIR BUBBLE CURTAIN

2.1 Background

Air bubbles have been used in many applications to block underwater sound from pile driving and explosives [1]. The principle mechanism driving sound attenuation is the impedance mismatch between the water and the bubble curtain's air-water mixture. Reference [2] provides measurements of acoustic wave speeds in an air-water mixture for various levels of air saturation. A plot showing theoretical and measured results is provided in Figure 1. From this curve it is seen that introducing 10% air by volume reduces the speed of sound from approximately 1500 m/s to 45 m/s. This results in an impedance drop (density * speed of sound) from 1.5e6 rayls to 4.5e4 rayls, a factor of 33. This large impedance difference results in a strong reflection of sound waves at the bubble curtain boundary, and transmission through the bubble curtain is minimized.

Bubble curtains used for mitigating sound from pile driving and explosives must extend through the entire water column and completely surround the noise source in order to achieve any effectiveness (applications are limited to shallow water). Attenuations can vary depending on the specifics of the installation and ground conditions, but reductions in peak pressure, RMS pressure, and energy of 5-20+ dB have been documented [1].

Creating a bubble curtain that extends through the entire water column for a moving seismic source is not a practical endeavor. However, an attempt to use a bubble curtain as a barrier for a seismic source has been documented in Reference [3]. A sketch of the concept design is provided in Figure 2. The original intention of this design was to reduce interference at the receiving hydrophone array from shallow water acoustic modes; the seismic signal was being degraded by reinforcement of the reflected signal (in the water) at some frequencies. It was suggested in [3] that this approach may also be beneficial for reducing sound impacts on marine life.

Barriers have been used extensively on land for industrial and residential noise control [4]. The use of a barrier for underwater purposes is similar in concept, although some differences exist. If a bubble curtain is used, the barrier itself will be a pressure release surface rather than a hard

surface. Similarly, the 'ground' plane is a hard surface in air applications where it is a pressure release surface in water. These differences will change the way sound propagates in the medium, and will have impacts on the effectiveness of the barrier as is discussed in later sections. It is also worth noting that the speed of sound is very different in air vs. water, and therefore the effective frequency ranges will be different as well for a given geometry. The current study investigates the feasibility of the air curtain barrier approach with expected sound reductions at different frequencies.

2.2 Modeling

An arbitrary though practical array design was selected as a basis for this analysis, as shown in Figure 3 (based on Reference [5]). The air gun volumes are shown in this figure. It is indicated in Reference [3] that the acoustic pressure of an air gun is related to the cube root of the volume. The air gins are assumed to be positioned 3 meters below the waterline. The seismic vessel itself was not included in this analysis in order to reduce model size.

Several models were created as part of this analysis. The initial study was performed using two-dimensional models in order to decrease model size and allow for faster solution times and parameter investigation. While this analysis ignores the fore-aft component of the propagation, longitudinal barrier extent, and longitudinal details of the array, it does provide insight into appropriate parameters for the bubble curtain.

Examples of some 2-D models are shown in Figures 4 and 5. Figure 4 represents an array in deep water where bottom reflections are of secondary importance and Figure 5 represents an array in shallow water. All models use half symmetry along the vertical-CL plane. The air gun array was modeled as two point (line) sources. Given the relative sizes (pressure output) of the air guns on centerline vs. off centerline in Figure 3, the centerline air gun pressure was assigned to be 1.08 times the pressure of the off centerline air gun. This relationship holds for the forward three air gun sets and deviates slightly for the aft three.

The water was modeled with a density of 1000 kg/m^3 and a speed of sound of 1500 m/s. Some variation in these values will occur for different locations (resulting from temperature, depth, etc.), though these variations are small relative to the size of the model, and the expected differences in directivity results are small over short distances. The top surface of the model was set to be a pressure release surface. The outer portion of the model is a "Perfectly Matched Layer" (PML), which is a construct of Comsol™ that is used to accurately model an 'infinite' boundary (i.e. no reflection occurs beyond the inner surface of the PML).

The barrier itself was modeled using various properties, locations, and sizes. The speed of sound and density of the barrier was modeled using various data points from Figure 1. Locations off centerline ranged from 9 meters to 20 meters (note that the half width of the modeled array is 8 meters), and the depth ranged from 9 to 20 meters. Barrier thickness ranged from 0.0254 meters (1 inch) to 0.3 meters (12 inches), which is assumed to be the practical extent in practice. The air curtain was assumed to have uniform thickness throughout its depth. This is likely not to be the case as some spreading or movement is expected as the bubbles approach the water surface, though the extent of this spreading is not known. When modeled, the sea floor was assumed to

be a hard, reflecting surface. While this is obviously an approximation, the results from this analysis are instructive.

A harmonic (steady state) analysis was performed at discrete frequencies[1]. The analysis frequencies for all 2-D models are 5, 30, 60, 100, 200, 400, and 600 Hz. Sound Pressure Level (Lp) results were extracted at a large distance from the model center approximating the far field level. Results were compared to the sound pressure level that occurs without a barrier, and a 'barrier effect' was created for both shallow- and deep-water models.

Some 3-D models were created as well, though these models were limited in frequency range due to their large model size. An example model is shown in Figure 6. Only deep-water models were analyzed in 3-D. The overall modeling approach was the same as for the 2-D models, though the full array shown in Figure 3 was modeled at discrete points with the appropriate (relative) source pressures. The longitudinal extent of the barrier was also modeled and the effects of modifying this extend were investigated.

2.3 Results

2.3.1 2-D Deep-Water

Before discussing the results of barrier effectiveness, it is important to establish the sound radiation from the modeled array without the barrier. Figure 7 shows the sound pressure level from the array (at a distance of 50 meters from the model center) vs. angle, with 0 degrees being vertical and 90 degrees being the water surface. The results have been normalized to the level at 0 degrees. It is clear that the directivity is strongly dependent on frequency[2]. This is the expected result from an array of acoustic sources. However it is also important to note that even at low frequencies there is an apparent directivity because of the pressure release at the water surface. Another important aspect of these curves is the strong interference effects at the higher frequencies. The specific angles where the peaks and dips occur are related to the specific array layout and measurement distance. Changing these parameters will change the details of these curves, but the overall character would remain.

A 'baseline' barrier design has been defined for the purposes of this report as a barrier with the following properties: 12 meter depth, 12 meters off centerline, 0.1 meter thick, 45 m/s speed of sound, 900 kg/m^3 density. This roughly corresponds to injection of 10% air by volume into the water. The effect of adding this barrier is shown in Figure 8 for various frequencies. Note that positive values on this graph represent a reduction in sound level. Several items can be initially identified from this data:

- There is minimal effect at very low frequencies at all angles (5 Hz). 60 and 100 Hz show small changes at angles near 0 degrees, and have some variation (<10 dB) at larger angles, both positive and negative.
- At 200 and 400 Hz there is a 10-30+ dB reduction at angles greater than 60 degrees. Smaller increases and decreases in sound are seen at lower angles.

[1] Although an air gun is inherently transient, a harmonic analysis is performed here to reduce analysis time and model complexity. On a frequency basis, the results should be the same as if a transient analysis is performed.
[2] Note that for a simple source in air with a hard floor, the directivity would be uniform with angle at all frequencies.

- At 30 Hz there is a 13 dB reduction of sound at 0 degrees. This gradually changes to a 0 dB reduction near 90 degrees.
- At 600 Hz there is a minimum 5 dB reduction in sound at angles between 71 and 87 degrees. There is also a 27 dB increase in noise at 56 degrees.

The non-effect at 5 Hz is to be expected because the wavelengths are very long at this frequency relative to the size of the barrier. At 30 Hz there is a reduction in sound directly below the array because of an interaction with the barrier. This interaction can be seen in Figure 9. The barrier itself is capable of supporting sound waves, and so there are certain wavelengths that will travel well within the barrier. This will cause effects similar to those seen in Figure 9 (i.e. local maxima and minima along the length of the barrier), leading to reductions in sound even at low frequencies. This is also the reason for the small differences in level at 0 degrees for other frequencies including 5, 60, and 100 Hz. This effect will occur to varying degrees at different frequencies for any barrier/array configuration; the specific amount of sound increase or decrease will depend on the details of the geometry and air gun array.

At higher frequencies (200 Hz and above) the curves begin to develop sharp peaks and dips. Note that the directivity of the array without a barrier also contains peaks and dips at these frequencies corresponding to constructive and destructive interference at the specific measurement locations (see Figure 7). Because these peaks and dips exist without a barrier, the barrier effectiveness curves will also have peaks and dips. A sharp dip in effectiveness, which may seem to indicate an amplification of sound, may result simply because the sound waves from the elements of the array destructively add at that location *without the barrier*, but add constructively with the barrier. The same can be said for sharp effectiveness peaks.

For reference, an example plot of the sound field at 600 Hz is provided in Figure 10a for the baseline barrier model. A comparison of the sound pressure level at 600 Hz with and without the baseline barrier is provided in Figure 10b. It is clear that in some cases, such as at 30 degrees, the destructive interference dips have shifted. This will cause an apparent performance decreases and increases near those angles. Since the spatially 'quick' variations are location specific, it is prudent to smooth sharp peaks and dips seen in Figure 8 such as the dip seen for 600 Hz at 56 degrees and the peak seen for 200 Hz near 76 Hz. Though not performed explicitly here, this smoothing allows for a general determination of the barrier effectiveness.

Using this approach, the following can be said about the baseline curtain design:

- At 200 Hz, there is an increase in sound of approximately 0-10 dB between the angles of 0-45 degrees, a decrease in sound of 0-10 dB between 45 and 60 degrees, and a 10 dB minimum decrease in sound between 60 and 90 degrees.
- At 400 Hz, there are small changes (positive and negative) from 0 to 52 degrees, and a 10-25 dB decrease in sound at larger angles.
- At 600 Hz, there are small changes (positive and negative) from 0 to 52 degrees, an increase in sound of approximately 8 dB near 55-67 degrees, and a 5+ dB decrease in sound at angles greater than 70 degrees.
- At 30 Hz there is a 13 dB reduction of sound at 0 degrees. This gradually changes to a 0 dB reduction near 90 degrees.

- There is generally minimal effect for other frequencies below 100 Hz, although some amplification is seen for large angles at 60 Hz. At 100 Hz the sound is reduced and amplified by less than 10 dB, depending on the angle.

Overall there appears to be some reduction in sound at frequencies above 100 Hz for angles over 70 degrees. However, some increases in sound at these higher frequencies can occur at smaller angles. Furthermore, frequencies in the range of useful seismic data (below 100 Hz) can be affected by the barrier.

When the barrier depth is changed, the effects noted above can be amplified or decreased. Increasing barrier depth improves the higher frequency attenuation at larger angles, but also amplifies the increase in sound at smaller angles. The deeper barrier also increases the reduction of sound at 30 Hz. A shallow barrier has the opposite effect. Figures 11 and 12 show the effectiveness for barriers with 20 and 9 meter depth, respectively (all other parameters are the same as for the baseline design). It is interesting to note that while changing the depth from 12 meters to 9 meters results in a large reduction in performance, the increase in performance by going from 12 meters to 20 meters is not as dramatic.

Changing the location of the barrier relative to centerline can also have an affect on performance. Figures 13 and 14 show the effectiveness for barriers located at 9 m OCL and 20 m OCL, respectively (all other parameters are the same as for the baseline design). Modifying the barrier location seems to increase barrier performance at some frequencies above 100 Hz while decreasing it for others. Again, this is due to the varying path lengths from the sources (and around the barrier) for a given receiver. Taking the aggregate performance for all frequencies above 100 Hz, the barriers positioned at 9 meters and 12 meters from the array have similar performance, with the 9 meter barrier having slightly better performance. The performance of the barrier positioned 20 meters from the array is certainly degraded. It is also worth noting that the 30 Hz reduction in sound seen with the 12 meter barrier is reduced for angles near 0 degrees. For this reason the 9 meter barrier would likely be preferable in this case.

Reducing the amount of air in the bubble curtain will reduce its performance. Figure 15 is a plot of the barrier effectiveness when the air content is dropped to 2% (density = 980 kg/m^3, speed of sound = 150 m/s). Comparing this barrier with the baseline barrier, the high frequency attenuation at large angles is seen to have decreased. Interestingly, the 30 Hz reduction at 0 degrees has been replaced by a similar attenuation at 60 Hz. This again is due to the sound waves within the barrier itself. Increasing the air content to 30% (density = 700 kg/m^3, speed of sound = 30 m/s) produces a large improvement at 400 Hz relative to the baseline case (where performance is already good) but minimal change at all other frequencies.

The effects of barrier thickness were also investigated. Figure 16 is a plot of the effectiveness of a barrier with a 0.0254 meter (1 in) thickness. All other parameters are identical to the baseline. Comparing this graph to the baseline effectiveness it is seen that there are only minor differences; the specific shape of the effectiveness curve at 400 Hz is different, but the overall trend is the same. The same can be said for the reduction in sound at 30 Hz. Other thicknesses showed similarly small impacts on the overall effectiveness. This implies that the thickness of

the barrier is not a dominant factor for barrier effectiveness, and that variations in thickness through the height of the barrier will only have minor impacts.

Taking the above results into account, an 'optimized' barrier was modeled (note that this is optimized for this array). Figure 18 shows the effectiveness of a barrier that is 9 meters from centerline, 20 meters deep, with 10% air by volume, 0.1 meters thick. The effectiveness is generally 10 dB or more at vertical angles of 70 degrees or more at 100 Hz and above. There is an amplification of sound at 400 Hz for vertical angles between 33 and 58 degrees, and the output at 30 Hz is reduced by 15 dB directly below the array. However, the overall performance of this barrier is significantly better than for the baseline case.

2.3.2 2-D Shallow-Water

The baseline curtain design discussed in the above section was modeled in 20 meter and 30 meter water depths. For both models the ocean floor was assumed to be a hard surface (i.e. perfect reflector). While this is certainly not the case in reality, it is assumed that this is something of a worst case approximation. The sea floor is likely to be closer to a hard 'pressure doubler' surface than a pressure release surface (such as the water surface), and some attenuation at certain frequencies is also possible. The specific properties of the sea floor will vary depending on location. The use of a hard surface for the sea floor is an approximation that should allow for general investigations to determine the effect of the presence of the sea floor.

As was the case for the deep-water models, the sound pressure level due to the array alone without a barrier can have significant variations that are dependent on location. This is due to the reasons given in the above section, as well as the existence of the ocean floor. An example plot of the sound pressure level at 600 Hz for the 30 meter water depth case is provided in Figure 18. Because of this, the sharp variations in barrier effect seen for the deep water case also exist here.

Figures 18 and 19 show the effectiveness of the baseline barrier in 20 and 30 meter water depths. Note that these graphs are plotted against water depth instead of angle as was the case for the previous graphs. All results are taken at a distance of 60 meters from centerline (i.e. measurement positions are along the right hand vertical edge of the model). At this distance the 30 meter water depth corresponds to a 63 degree angle and the 20 meter water depth corresponds to a 71 degree angle.

At 400 Hz, the reduction in sound is roughly 10 dB for both the 20 and 30 meter water depths, which is less effective relative to the deep water case (Figure 8). At 200 and 600 Hz there is, on average, no effectiveness for either depth. The overall reduction in effectiveness is primarily due to the scattering of sound from the bottom, and the modal pattern that arises. Because the bottom is modeled as a hard surface this is likely to be a worst case performance, but does indicate that the barrier effectiveness can be compromised by the presence of the sea floor.

It is interesting to note that at the 20 meter depth the 30 and 60 Hz frequencies are attenuated by 10 dB along the vertical plane at the right side of the model (representing the propagating sound wave). However, the sound pressure level directly below the array (not shown here) has also

been reduced by 10-20 dB. At 30 meters the 30 Hz sound is attenuated by approximately 10 dB as seen in the deep water case.

2.3.3 3-D Deep-Water

The number of finite elements required to model a 3-D space is very large compared to a 2-D space. Because of this, the frequency range that can be analyzed in 3-D is significantly smaller than for two-dimensional models[3]. To help reduce model size, the barrier was modeled at a distance of 9 meters from centerline as opposed to 12 meters in the 2-D baseline case. Furthermore, the barrier was modeled as a pressure release surface for all 3-D models. This is an approximation that appears to be valid for most frequencies assuming the bubble curtain has at least 10% air by volume. Figure 21 is a plot of the 2-D model baseline case vs. an identical model using a pressure release surface. At 100 and 200 Hz (and other frequencies not shown here) the results are very close. At 30 Hz the results do differ, but this is a result of the wave propagation within the barrier in the baseline model as discussed in Section 2.3.1. The current 3-D analysis focuses on waves at 100 and 200 Hz.

A comparison of the sound pressure level at 100 Hz between the 2-D and 3-D models is provided in Figure 22. This 3-D model uses a barrier that is 34 meters long with the other parameters the same as the 2-D baseline barrier with the exceptions noted above. The results of the 3-D model were taken along the transverse axis at the center of the array. The results are similar, and the small differences can be attributed to the differences in the modeling of the air gun array. Note that the air gun array is not symmetrical in the fore/aft direction, and therefore will not have exactly the same radiation pattern as a line source. This result is seen to verify the general findings of the 2-D modeling with regards to the effectiveness of the barrier and the effects of varying the barrier parameters. This result also underlines the fact that the specific performance of any barrier will be directly linked to the air gun array setup itself.

The effect of changing the barrier length was investigated, and the effective area of sound reduction in the fore/aft direction was analyzed. Sound pressure levels were extracted along the transverse or 'lateral' direction as well as along +/-45 degrees azimuth angles relative to the water surface, as shown in Figure 23[4]. Barriers with lengths of 34 meters, 20 meters, and 14 meters were modeled. The barrier was always centered longitudinally at the middle of the air gun array. Note that the array length is 15 meters.

The results at 100 Hz are presented in Figure 24. Of particular note is the fact that there is only moderate variation between the 34 and 20 meter barriers, and the 14 meter barrier actually appears to perform the best at this frequency. The barrier effectiveness is roughly 10 dB or more at (vertical) angles of 60 degrees or more (i.e. near the water surface) for the lateral and forward 45 degree azimuth angles. The large dip in the aft 45 degree azimuth line at the 63 degree

[3] A rule of thumb of 8 elements per wavelength has been used here. With fewer elements, the highest frequency capable of analysis is reduced.

[4] For the purposes of this report, spherical coordinates are used to identify locations in the 3-D model. The 'azimuth angle' refers to the angle away from the transverse direction in the plane of the water. 0 degrees azimuth would refer to the 'lateral' direction in Figure 22. The 'vertical angle' is the angle away from the vertical axis, with 0 degrees being directly below the air gun array. The center of the coordinate system is the middle of the air gun array at the water surface.

vertical angle is due to a destructive interference dip in the sound pressure field without a barrier that gets smoothed over when the barrier is present. Ignoring this dip, the larger two barriers have no effectiveness at the aft 45 degree azimuth angle, though the smallest barrier seems to provide a 10 dB reduction of sound for vertical angles greater than 75 degrees.

To analyze the effectiveness at 200 Hz, a ¼ model was created. This model encompasses the forward three rows of the air gun array (see Figure 3), and assumes the array is symmetrical in the fore/aft direction. This simplification was necessary in order to be able to acquire results at this frequency. The effectiveness of the three barriers is provided in Figure 25. In this case the longer barrier clearly provides more attenuation than the shorter barriers both laterally and at a 45 degree azimuth angle, particularly at the higher vertical angles. As the barrier is made smaller the effectiveness is reduced. It is interesting to note that the effectiveness is greater at the 45 degree azimuth angle than it is in the lateral direction.

These results indicate that longer barriers will be more effective at some frequencies, though short barriers, even barriers that are shorter than the air gun array, could provide increased attenuation at some frequencies. However, after comparing Figures 23 and 24 it can be said that a longer barrier will likely provide an overall increased performance. This is good because it would be difficult to make a bubble curtain with sharply defined vertical forward and aft edges, particularly when the array and bubble curtain is moving. Rather, it is easier to make a long bubble curtain relative to the air gun array size. However, the above result may be useful if a foam material is used for the barrier instead of air bubbles (see Section 3).

The results of the 3-D models also show that because the air gun array output is biased towards the forward end the barrier effectiveness is also biased for forward azimuth angles. Aft azimuth angles do not appear to perform as well. Although not shown here, the directivity in the longitudinal direction is essentially unchanged for any barrier, and thus the effectiveness of the barrier will drop off at some azimuth angle. The specific angle where this occurs will be dependent on the specific air gun array.

2.4 Conclusions – Bubbler Barrier

It is clear that some attenuation of laterally propagating sound from an air gun array can be achieved through the use of a longitudinally oriented air bubble curtain. For the modeled array, sound level reductions at frequencies of 100 Hz and above are on the order of 5-25+ dB for large vertical angles (i.e. closer to the water surface) where receivers are located on the side of the air gun array (‘lateral’ or ‘transverse’ direction). For air gun arrays that are biased at the forward end (i.e. larger air guns are placed at the front of the array) the barrier effectiveness will be greater at forward azimuth angles and less at aft azimuth angles. The barriers do not significantly change the radiation pattern on centerline. Barrier length in the forward/aft direction should generally be made as long as possible or practical to maximize effectiveness.

For the specific air gun array modeled here, attenuations were seen to begin at roughly 50 - 70 degrees relative to the vertical axis, depending on frequency. The angle where effectiveness begins will depend on the barrier depth and distance from centerline. Barriers that are very close to the air gun array show the best performance, significantly so even when compared to a barrier that is moved only a few meters away. Deep barriers will have better performance, though there

appears to be diminishing returns past a certain depth (12 meters for the array modeled here). The angles of effectiveness will also depend on the specific air gun array characteristics, including geometry, relative size of the air guns, and depth in the water.

The air content should be as high as is practical, with 10% air by volume being a good minimum design. Barrier thickness was not seen to be a dominant factor in performance for practical sizes.

It is important to note that increases in sound level have been noted for some frequencies and angles as a result of the use of a bubble curtain. This amplification appears to be generally limited to angles closer to vertical, though the specific angle and amount of amplification will depend on the specific frequency and barrier/air gun array characteristics. For example, the baseline barrier modeled here showed an approximate 8 dB increase in sound between the vertical angles of 54 and 67 degrees (2-D model). Amplifications as high as 20 dB have been noted for some of the modeled barriers. These amplifications occur at certain angles because the sound radiation from the air gun array *without the barrier* is reduced when there is destructive interference between the array elements and the water surface. When the barrier is added the sound level may in fact be relatively smooth at these frequencies, but when compared to the sound level without the barrier there is a relative amplification.

It cannot be generally said that higher frequencies are attenuated more than low frequencies because of the specific geometry and pressure release surfaces that exist[5]. For the array modeled here, the baseline barrier produced 27 dB of reduction at 400 Hz for a vertical angle of 75 degrees while at 600 Hz only 6 dB of reduction was seen. These effects were nearly reversed when the barrier was moved closer to the array. Again, actual barrier attenuations will be dependent on the specifics of the array and barrier.

Another important result is the possible reduction in sound of low frequencies (<100 Hz) directly below the array. While most frequencies below 100 Hz were largely unaffected by the barrier, some configurations showed reductions of sound as high as 12 dB directly below the array at specific frequencies (e.g. 30 Hz). This is an important result as these frequencies are useful in identifying geological features beneath the sea floor.

If the barrier is used in shallow water (~20-30 meters) then the reflections off the sea floor will act to reduce the effectiveness of the barrier. Using a 'perfectly rigid' approximation for the sea floor all frequencies were seen to have significant reductions in effectiveness. No reduction in sound was seen at some frequencies that otherwise show some sound reduction in deep water. For realistic sea floors it is expected that the reduction in performance would not be quite this dramatic, though the results will depend on the specific makeup of the sea floor and the amount of sound that is absorbed.

Given the fact that the performance of any barrier is strongly dependent on the air gun array configuration, it is suggested that some modeling be performed to help optimize the location and size of the barrier for maximum effectiveness. This modeling will also help to identify and

[5] This is generally true for hard in-air barriers.

minimize amplification of unwanted sound at large vertical angles as well as identifying any possible reduction of sound below 100 Hz under the array.

3.0 LOW IMPEDANCE BARRIER MATERIALS

While bubble curtains have been shown in the literature to be effective at blocking sound propagation, they can sometimes be difficult to work with [1]. Set-up is critical, and includes properly locating air hoses and getting the air pressure and flow correct, among other factors. Bubble curtains are also susceptible to currents; if the bubble curtain is not contiguous then reductions in performance can result. Marine fouling can also be an issue, clogging the holes in the hoses and reducing performance. While it is certainly possible to successfully use air bubble curtains in practice, a more consistent alternative may be desirable.

Reference [6] shows that closed cell foam attached to the interior of a steel pipe can be used as an effective barrier against pile driving noise. The sound level reduction was seen to be similar to if not better than an air bubble curtain. Reference [7] indicates that large attenuations can be gained in similar applications through the use of closed cell foam alone (no steel backing). It is believed that the underwater noise attenuation that occurs is a result of the fact that the foam has integrated air (or gas) pockets. As is the case at the surface of the water, the water-air interface poses a large impedance mismatch, causing a reflection. To a first order approximation, the closed cell foam acts to put air into the water and keep it in place, thus becoming as an acoustic barrier.

It can be argued that the material lattice that makes up the foam will provide some impact on the acoustic reflectivity or transmissibility of the foam as a whole. To investigate this it is possible to determine the specific acoustic impedance of the foam and compare it to the water to see if there will be a sufficient impedance mismatch. As noted before, air is a pressure release material relative to water. The specific acoustic impedance of air (density * speed of sound) is 415 rayls, and the specific acoustic impedance of water is 1.5e6 rayls, or 3500 times greater. It was shown in Section 2 that injecting 10% air by volume into water creates a fluid with an impedance that is 33 times lower than water, and this still approximates a pressure release surface. Thus, in order for a foam material to work in this application, it should have an impedance that is at least 30 times less than water.

Neoprene and nitrile foams have been used in several applications as an underwater acoustic decoupling materials on vessels [1, 8]. Rubatex Corporation (www.rubatex.com) manufactures a nitrile foam R-437 with a density of 160-352 kg/m^3, tensile strength of 1200 kPa, and low water absorption. The pressure required to compress this material to 25% of its thickness is approximately 76 kPa. After using this figure to calculate an approximate Young's modulus, the compressive wave speed in the material is calculated to be on the order of 20 m/s. This yields a specific acoustic impedance of 5000 rayls, which is 300 times less than water. As a result, this material appears to be appropriate for use as an underwater sound barrier.

Other foams such as neoprene, EPDM, and hybrids also appear to be appropriate for this purpose. These foams are all relatively limp and are capable of bring rolled and stored on a vessel. However they may also create increased drag if placed in the ocean due to oscillating lateral motion similar to a flag in wind. They will also need to be ballasted down to maintain the

appropriate depth. A metal backing plate or other supporting structure may be desirable here, acting both as ballast and structural support.

A hard or quasi-rigid foam, as used in References [6, 7], may be another option that would be more likely to hold its shape in the water, thereby reducing drag. Reference [9] presents material properties of some polyurethane foams with densities ranging from 120 to 320 kg/m^3. The compressive Young's modulus is shown to increase with increasing density. The highest density foam has a specific acoustic impedance for compressive waves that is only 6 times less than water, while the lowest density foam is 30 times less than water. However, bending waves will likely be most important here, and the calculated specific acoustic impedance using the bending wave speed is much less than that of water. Therefore, from an acoustic perspective, polyurethane closed cell hard foams should also be appropriate for this application, though lower density foams may provide a slight acoustic advantage. Other rigid foams may be appropriate as well, though their material properties should be analyzed to determine their specific acoustic impedance. From a non-acoustic perspective, hard foams may be more difficult to deploy and retrieve than soft foams.

It was shown in Section 2 that the barrier thickness, when varied between 1 and 12 inches, did not significantly influence effectiveness. However, in the limit of vanishing thickness the effectiveness would go to zero. Therefore at some thickness there will be a reduction in performance. The model assumes that the overall shape of the barrier does not change. In water, the particle motions resulting from sound levels expected from an air gun are much less than 1 mm. However, in a material with an acoustic impedance 30 times less than water the particle motions can be more significant. At a level of 210 dB re 1μPa, a 30 Hz wave will cause particle motions on the order of 3 mm, and at 10 Hz the motion will be 10 mm. It is reasonable to believe that the thickness of the barrier should be much more than the expected particle motion within the barrier. For the above case, a minimum thickness of 25 mm (1 inch) should be sufficient, though physical testing is recommended.

It is noted that in both Reference [6, 7] the thickness of the (hard) closed cell foam was 2-16 inches. A thicker barrier should not compromise acoustical effectiveness, though non-acoustic factors such as space, weight, and costs would be affected. Stiffness is also a consideration, as noted above.

4.0 PARABOLIC REFLECTOR

4.1 Background

Parabolic reflectors are commonly employed to focus waves of various types at a central point. Parabolic reflectors are used in various applications, such as with microphones on the side of a football field where the broadcasting network is trying to hear the grunts of the players on the field. The reflector takes the otherwise omni-directional microphone and creates a highly directional receiver. If a source were placed at the apex of the reflector instead of a microphone then the radiation would also be highly directive.

It may be possible to apply this concept to air gun arrays as well. A concept sketch is provided in Figure 26. In this design a barrier is located above the air gun source in the shape of a parabola with the intention of focusing sound in the downward direction. The sketch is a lateral

cross section, and shows a single row of sources (air guns). Because there is only a single row of air guns, the array could be made longer than in a typical air gun array while retaining the same number of air guns. This would increase longitudinal directivity, while the reflector would increase lateral directivity.

Initially the barrier is assumed here to be an air bubble curtain, similar to what was used in Section 2 of this report. Based on the results of Section 2, it is clear that the air bubble curtain would approximate a pressure release surface, which creates a reflection with inverted phase, as long as the air content is greater than 10% by volume[6]. A reflector made from a solid material is considered here as well.

4.2 Modeling

A 2-D finite element model was created in Comsol™ to model the air gun array and reflector. The model and analysis approach is similar to the 2-D models built to model the air bubble curtain described in Section 2, with the major differences being the modeling of the reflector and the different array geometry. Because the reflector is oriented in the lateral direction, it is assumed that the entire area above the reflector is an air-water mix. A screen capture of one model is provided in Figure 27. Note that in practice in order to achieve a consistent reflector shape over the entire air gun array multiple hoses will be needed along the length of the array. Both deep and shallow water applications were modeled here.

The air gun array was varied between 3 and 6 meter depths. The reflector was created so that the air guns were located at the focus of the parabola, using the following equation:

$$Depth = \frac{1}{4a} x^2$$

where a is the distance between the array and the water surface and x is the distance from centerline. The reflector was made to coincide with the water surface at x = 0. This means that the width of the reflector was always 4a at the depth of the array (dimension b in Figure 26). The reflector size was varied by changing the largest distance from centerline. For the 3 meter deep array, the reflector was varied between x_{max} = 9 - 15 meters (18 - 30 meter total width), corresponding to reflector depths of 6.75 - 18.75 meters, respectively. For the 6 meter depth array the reflector shape was wider and shallower. The size was varied between x_{max} = 12-20 meters, corresponding to reflector depths of 6 and 16.7 meters, respectively.

The air bubble reflector was assumed to have 10% air by volume, yielding a density of 900 kg/m^3 and a 45 m/s speed of sound. A pressure release surface was also modeled separately for comparison purposes (water was assumed to exist directly over the reflector in this case).

[6] Creating an acoustically hard surface in water is difficult and may not be practical for this application. For example, if a metal sheet were used instead of an air bubble layer, the impedance would be controlled by the bending wave speed of the plate. This speed is very low at the frequencies of interest, and the characteristic impedance would not be sufficiently greater than the impedance of water.

4.3 Results

As was noted in Section 2, the array directivity without a reflector must be established in order to determine the effectiveness of the reflector. A plot of the normalized output of the 3 meter deep array vs. vertical angle is provided in Figure 28. It is noted that the directivity of this array is slightly more uniform than the array modeled in Section 2 because there is only a single line of air guns. However, it is important to note the large dips in output at certain angles for higher frequencies – these dips will create apparent increases in sound when the reflector is used, as discussed in Section 2.

Figures 29, 30, and 31 present the effectiveness of three reflector configurations for the 3 meter deep array. In comparing these figures it is clear that a larger reflector will be more effective at reducing lateral propagation than a smaller reflector. For the largest reflector, reductions in sound of 30-40 dB are seen at 400-600 Hz at vertical angles above 70 degrees; however at 100 and 200 Hz the reductions in sound are only on the order of 0-5 dB for these angles. For the 'medium' sized reflector the reduction in sound is more consistent, with 20+ dB reductions seen for 200-600 Hz at vertical angles greater than 70 degrees. Even the small reflector shows 10-15 dB reductions at frequencies above 100 Hz for vertical angles greater than 70 degrees. Furthermore, the vertical angle where reductions begin is seen to be approximately 30 degrees for the large reflector and 40 degrees for the medium and small reflectors.

Directly below the array, nearly all frequencies have a 0-10 dB increase in sound, which is advantageous to seismic exploration. The exceptions here are at 5 and 30 Hz, where 0-17 dB reductions are seen depending on the specific reflector size.

Similar results are seen for the 6 meter deep array, though in general the reductions in sound are not as great. Figure 32 shows the effectiveness of a reflector that is 24 meters wide but only 6 meters deep (depth being controlled by the equation in Section 4.2). Because the reflector does not extend below the array the effectiveness is minimal. A larger reflector will have greater effectiveness, but the width will become very large before an appreciable depth is achieved (a 12 meter deep reflector would require a total width of 44 meters).

Figure 33 shows the effectiveness of the 'medium' sized reflector used with the 3 meter deep array in water that is 30 meters deep. As was discussed in Section 2, the sea floor was assumed to be a hard reflecting surface. Similar to what was shown in Section 2, the ability of the reflector to reduce lateral sound levels is significantly reduced. In this case the sound is actually amplified by roughly 10 dB at 200 and 600 Hz.

Lastly, if the reflector is modeled as a simple pressure release surface the results are similar to those seen for the air bubble reflector. Figure 34 provides the effectiveness of the medium size reflector applied to a 3 meter deep air gun array when modeled with a pressure release surface. These results are seen to be similar, though not identical, to those of Figure 30. The pressure release surface could be considered to be a rough model of a solid material containing air pockets, as discussed in Section 3. Thus, it can be said that instead of an air bubble reflector, a solid material could be used to create the reflector.

4.4 Conclusions - Reflector

The parabolic reflector has a potential for large reductions in sound, particularly at vertical angles greater than 70 degrees. Compared to the effectiveness of the vertical barriers modeled in Section 2, the reflector appears to provide similar or greater reductions in sound over a larger vertical angle. The reflector is seen to provide an increase in output directly below the array of up to 10 dB for most frequencies, though the lowest frequencies (5, 30 Hz) can have reductions in sound of up to 17 dB. It is noted again that if the number of air guns used is held constant, a single line array can have greater directivity in the longitudinal direction (on centerline) than an array with 3 rows of guns, further improving the performance of this arrangement.

However, the size of the reflector may be a practical limitation, particularly for arrays positioned deeper in the water. If an air bubble curtain is used, the hoses used to create the air bubble curtain must be oriented laterally (transverse), and many rows of hoses must be used in order to maintain the parabolic shape over the entire array. This may prove difficult in practice. A solid material may be preferable in this case, and would also provide similarly large sound level reductions. Such a reflector would likely need to be assembled in sections to cover the entire length of the array. Possible candidate materials have been discussed in Section 3.

As was found for the vertical barriers of Section 2, the effectiveness in shallow water is significantly compromised as a result of bottom reflections. If the sea floor is absorptive then this reduction in performance may not be as dramatic.

REFERENCES

1. J. Spence et.al., "Review of Existing and Future Potential Treatments for Reducing Underwater Sound from Oil and Gas Industry Activities," NCE Report 07-001, December 31, 2007.
2. G. Costigan, P.B. Whalley, "Measurements of the speed of sound in air-water flows," *Chemical Engineering Journal* **66** (1997) 131-135.
3. E. Sixma and S. Stubbs, "Air Bubble Screen Noise Suppression Tests in Lake Maracaibo," Sociedad Venezolana de Ingenieros Geofisicos *Congreso Venezolano de Geofisica*, 1996.
4. L. Beranek, *Noise and Vibration Control*, McGraw Hill, New York, 1971.
5. B. Dragoset, "Introduction to Air Guns and Air-Gun Arrays," *The Leading Edge,* August 2000, pp.892-897.
6. J. Laughlin, "Underwater Sound Levels Associated with Driving Steel and Concrete Piles near the Mukilteo Ferry Terminal," Report for WSF Mukilteo Test Pile Project, March 2007.
7. K. Lucke, "Protecting Sensitive Ears Underwater from Impulsive Sounds," Presentation at the *Workshop and Review of Noise Reduction Technologies Capable of Reducing Underwater Acoustical Footprints*, Burlington MA, June 2007.
8. M.J. Coughlin et.al., "Design of a Hull Coating to Reduce Interior Propeller Cavitation-Induced Noise for the PGG 511 Class Patrol Gunboat," Bolt, Beranek, and Newman Technical Memorandum No. W473, April 1979 (not commercially available).
9. M. Thompson, I. McCarthy, and L. Lidgren, "Compressive and Shear Properties of Commercially Available Polyurethane Foams," *Transactions of the ASME*, Vol. 125, October 2003, pp.732-734.

FIGURE 1: Theoretical and Measured Sound Speed in Air-Water Mixture vs. Air Content [2]

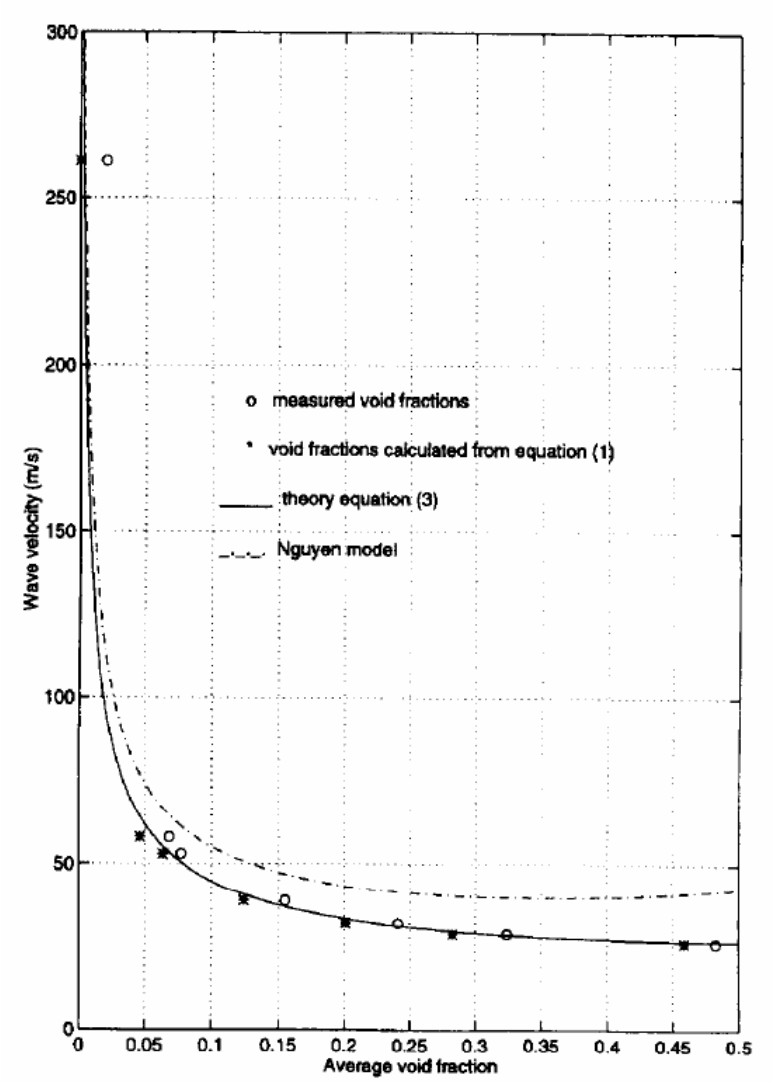

FIGURE 2: Underwater Air Curtain Barrier Concept [3]

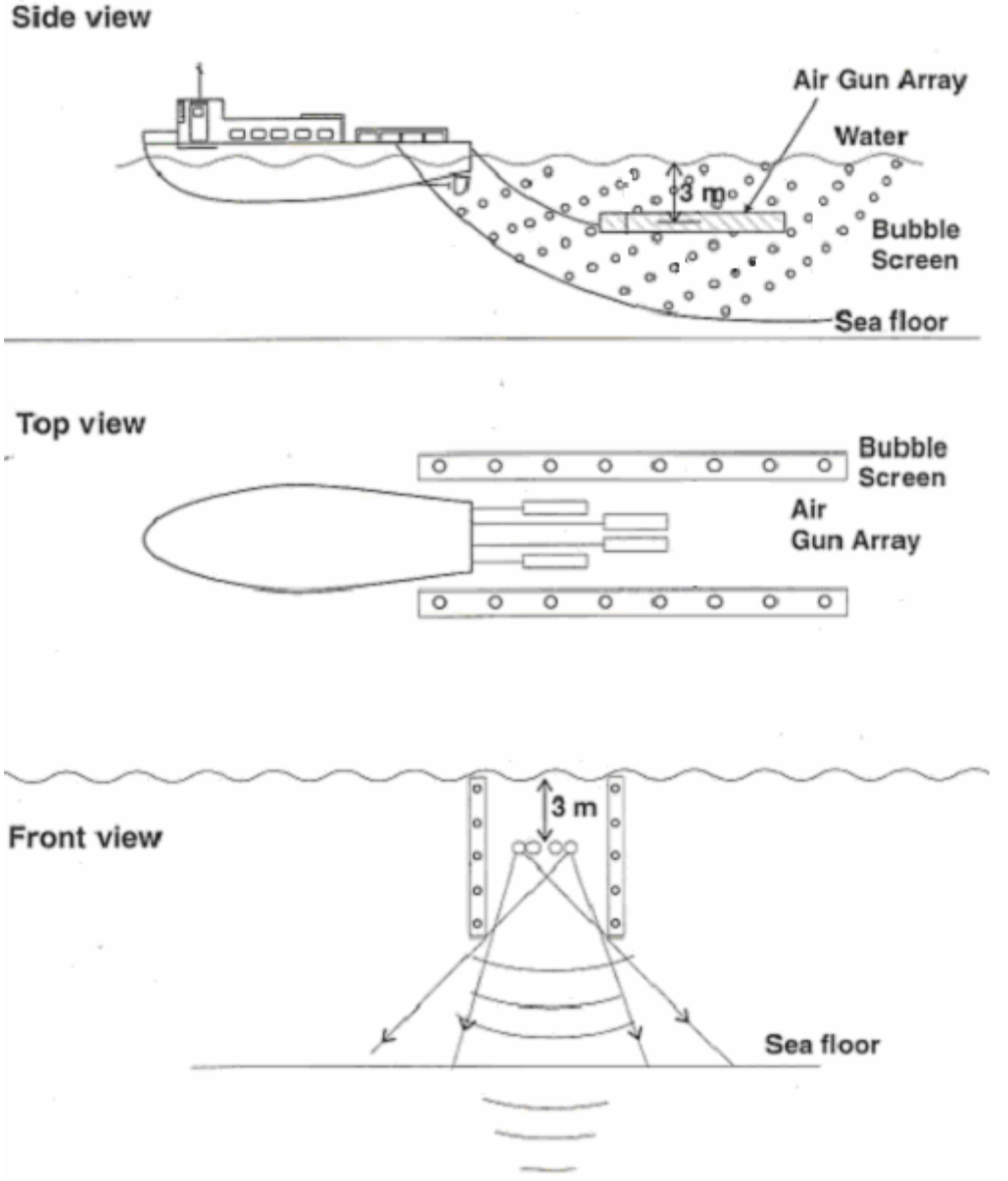

FIGURE 3: Example Array Design (from [5])
Air Gun Volumes are Indicated

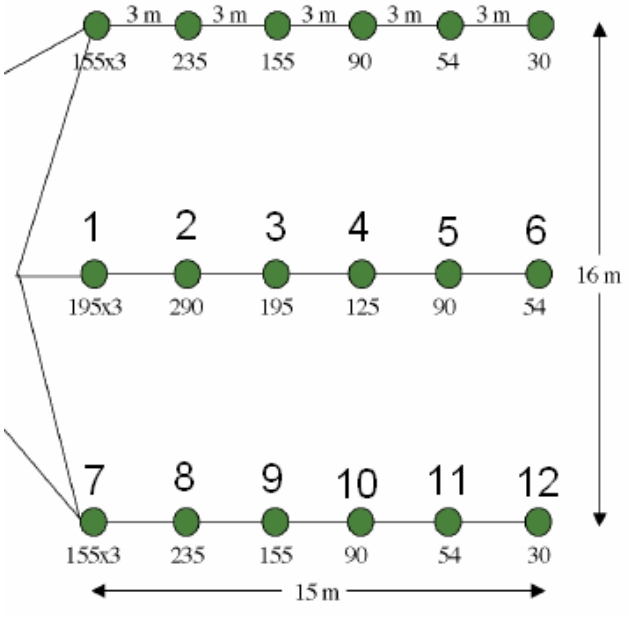

FIGURE 4: Example 2-D Deep Water Model

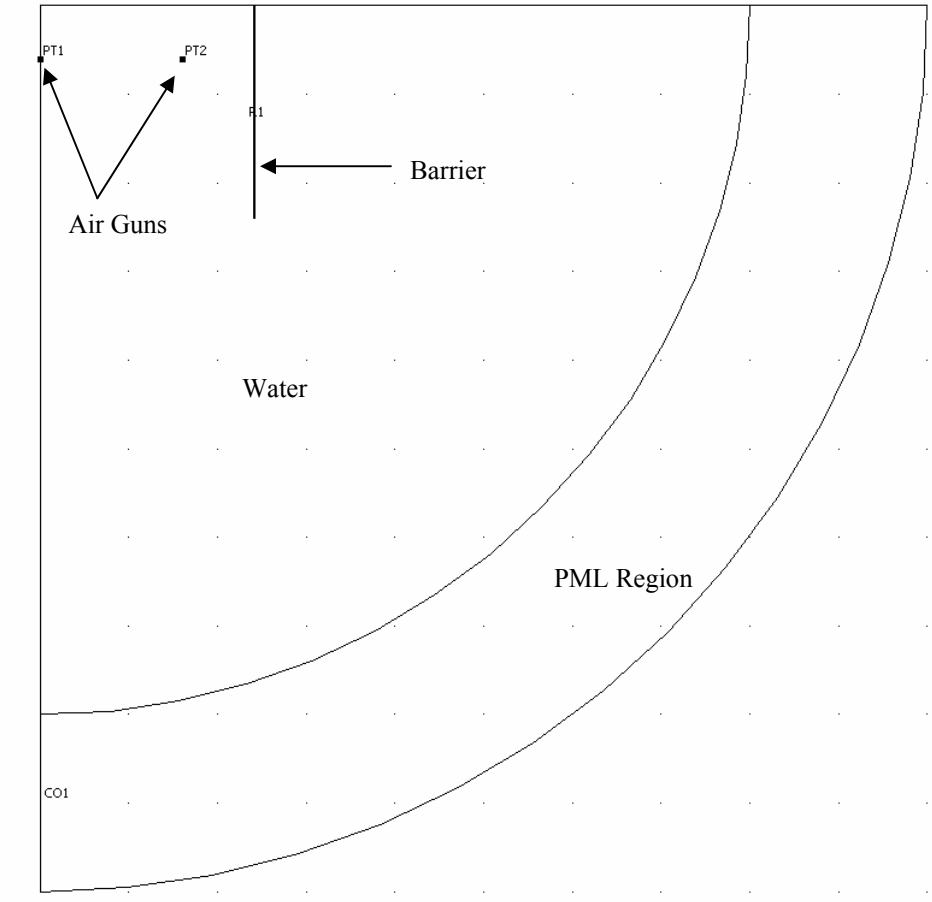

FIGURE 5: Example 2-D Shallow Water Model

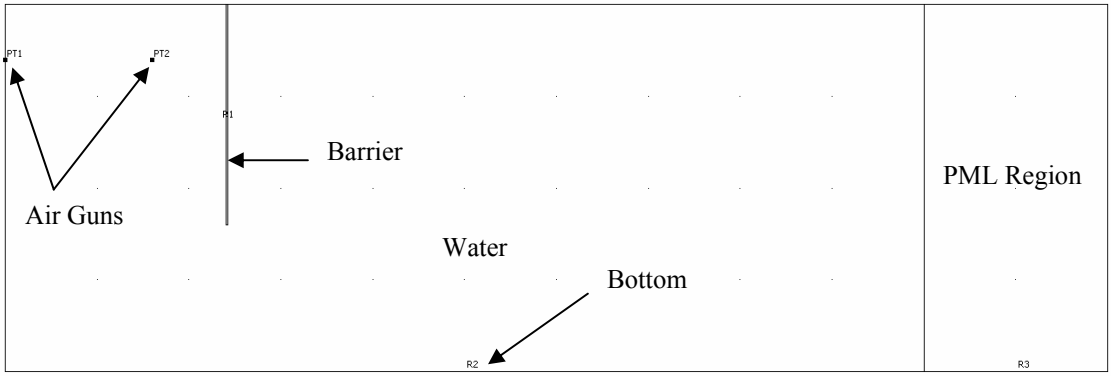

FIGURE 6: Example 3-D Deep Water Model

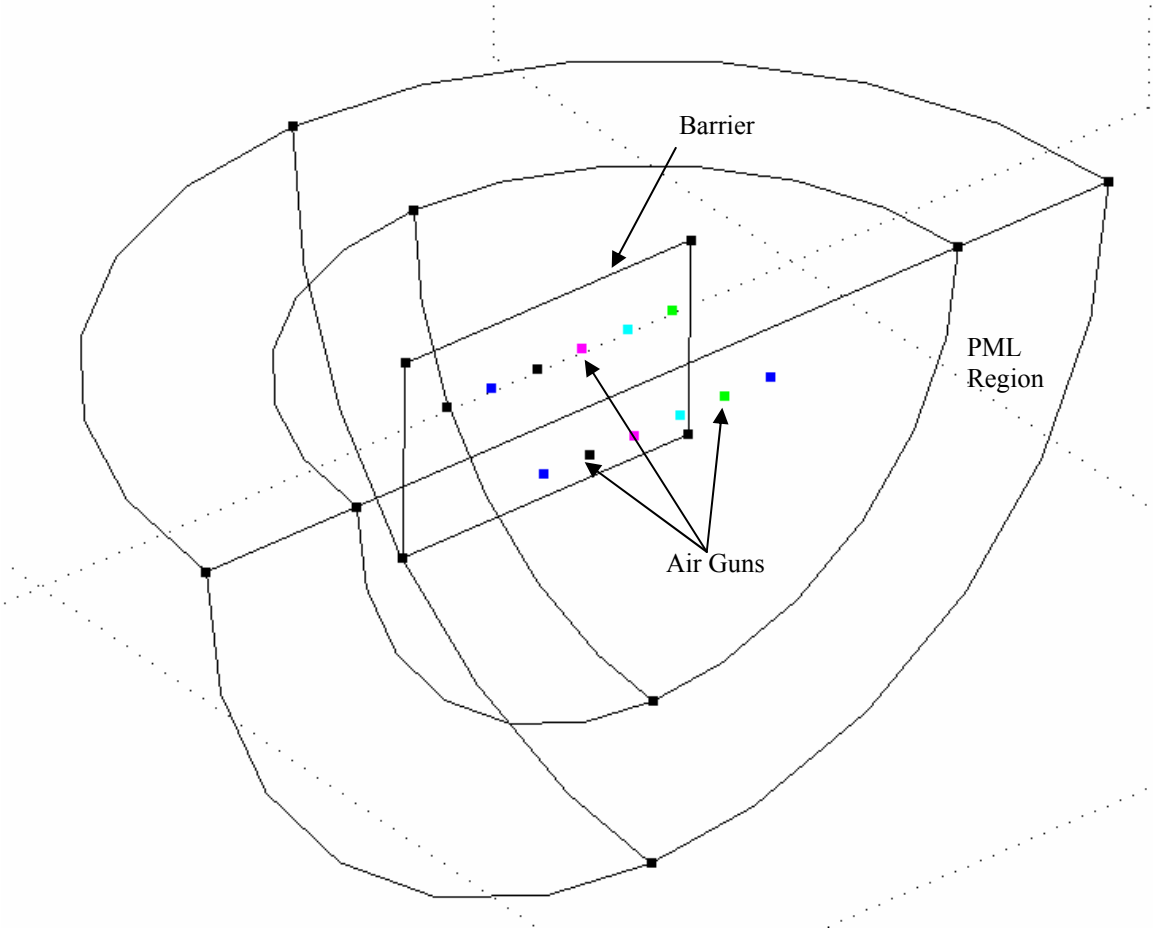

FIGURE 7: Directivity for 2-D Deep Water Model, No Barrier

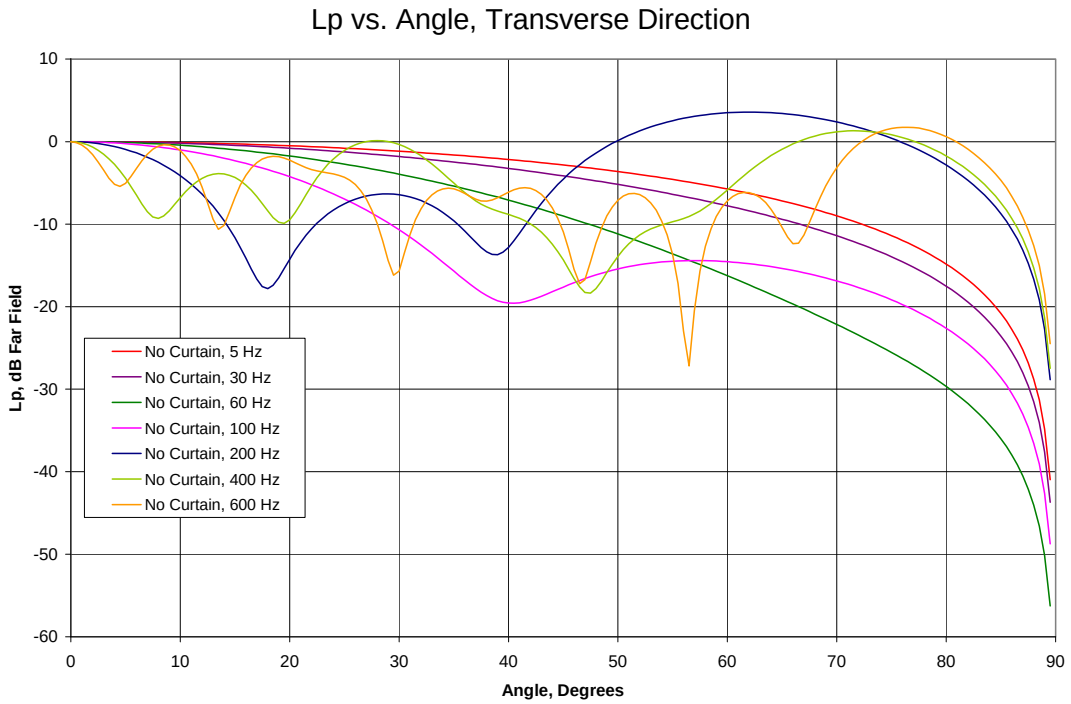

FIGURE 8: Barrier Effect for 2-D Deep Water Model, Baseline Barrier

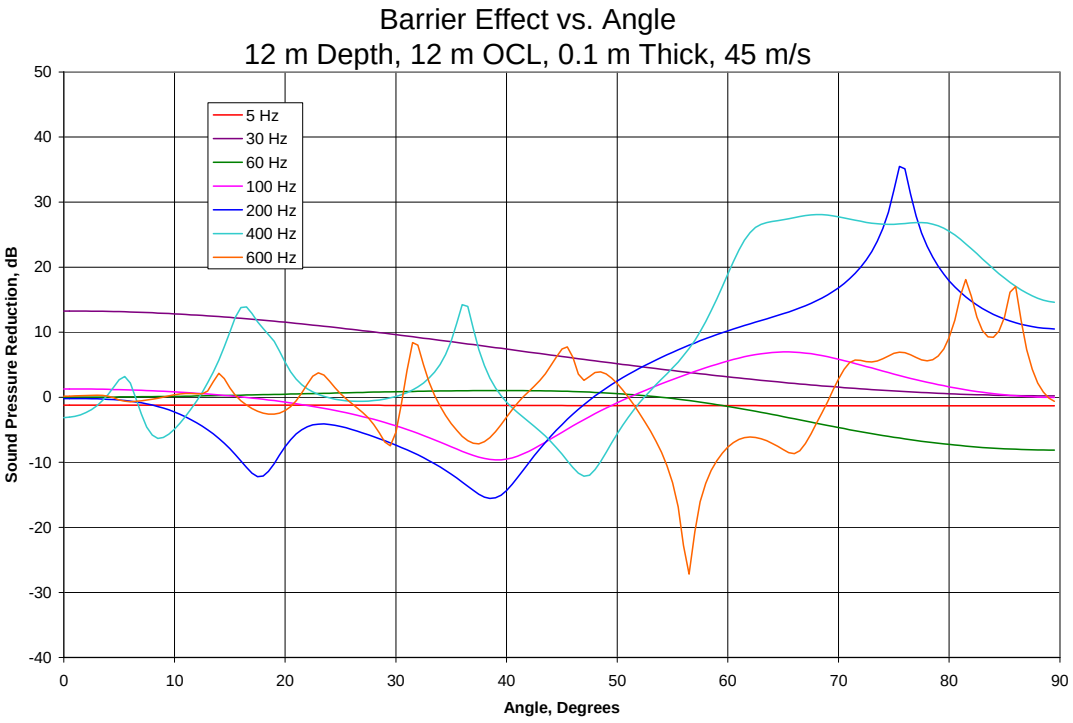

FIGURE 9: Lp in dB, 2-D Deep Water Model, Baseline Barrier, 30 Hz
Note absolute level is arbitrary

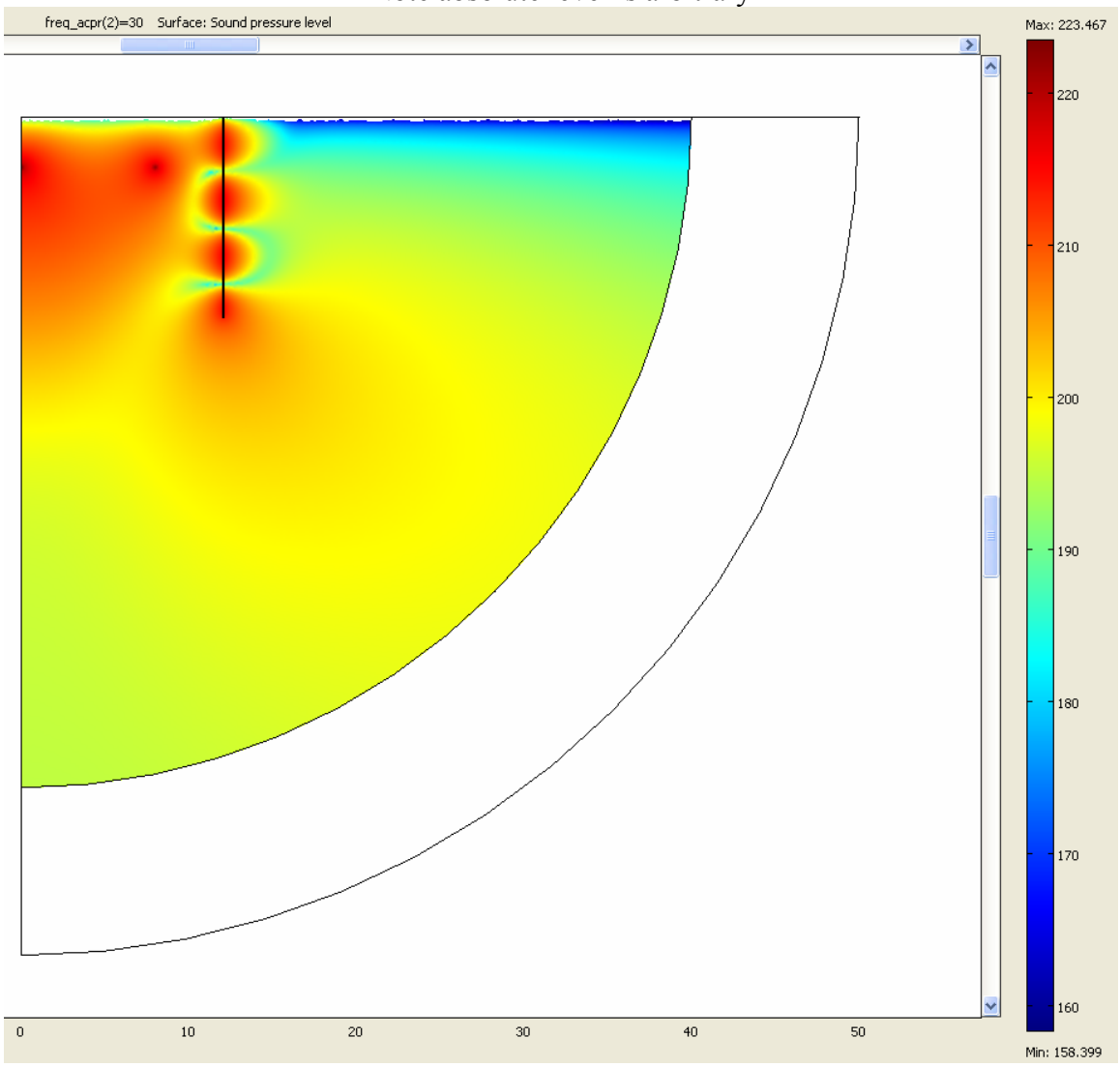

FIGURE 10a: Lp in dB, 2-D Deep Water Model, Baseline Barrier, 600 Hz
Note absolute level is arbitrary

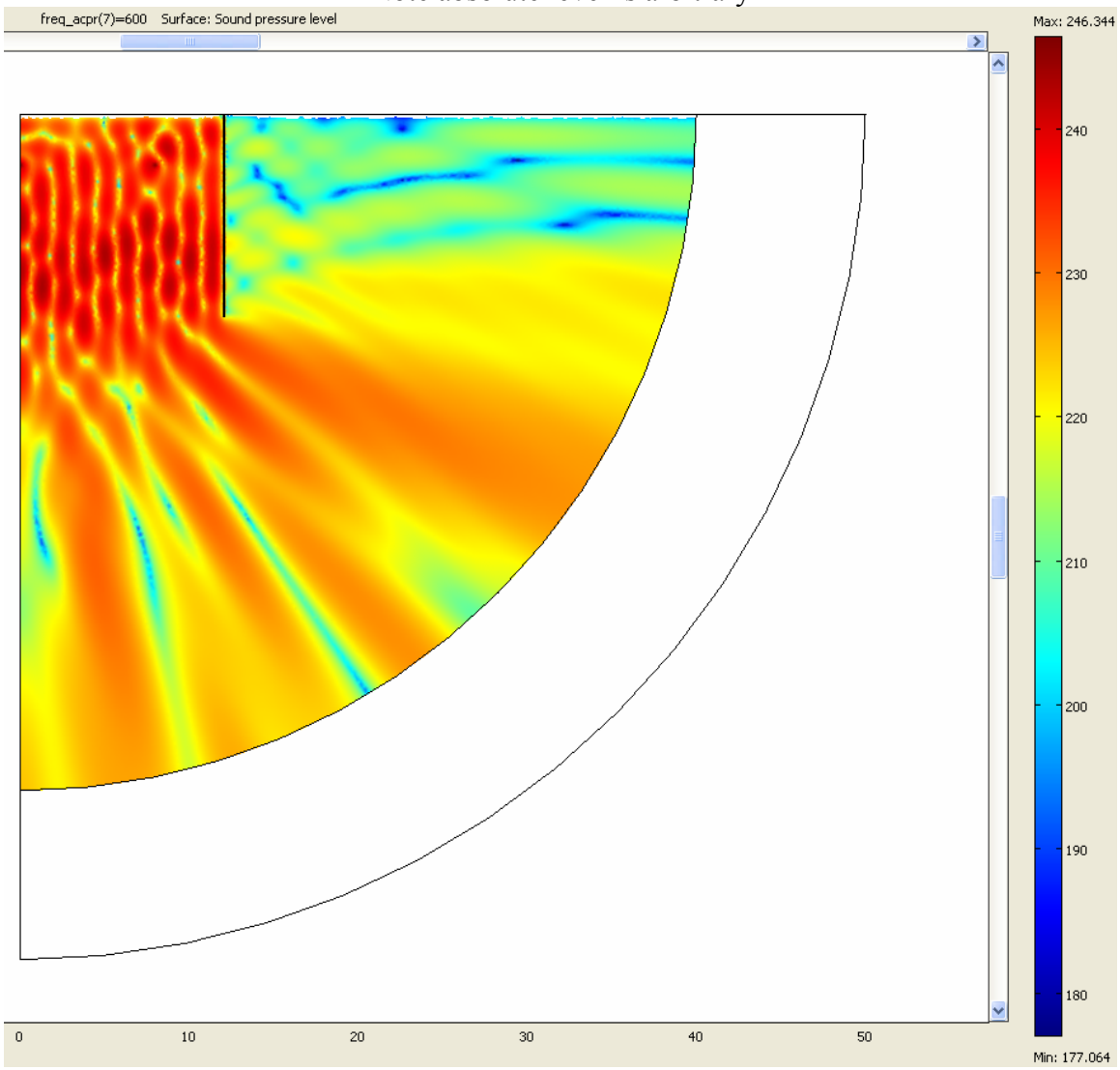

FIGURE 10b: Comparison of Lp for Baseline Barrier vs. No Barrier, 600 Hz, 2-D Deep Water Model

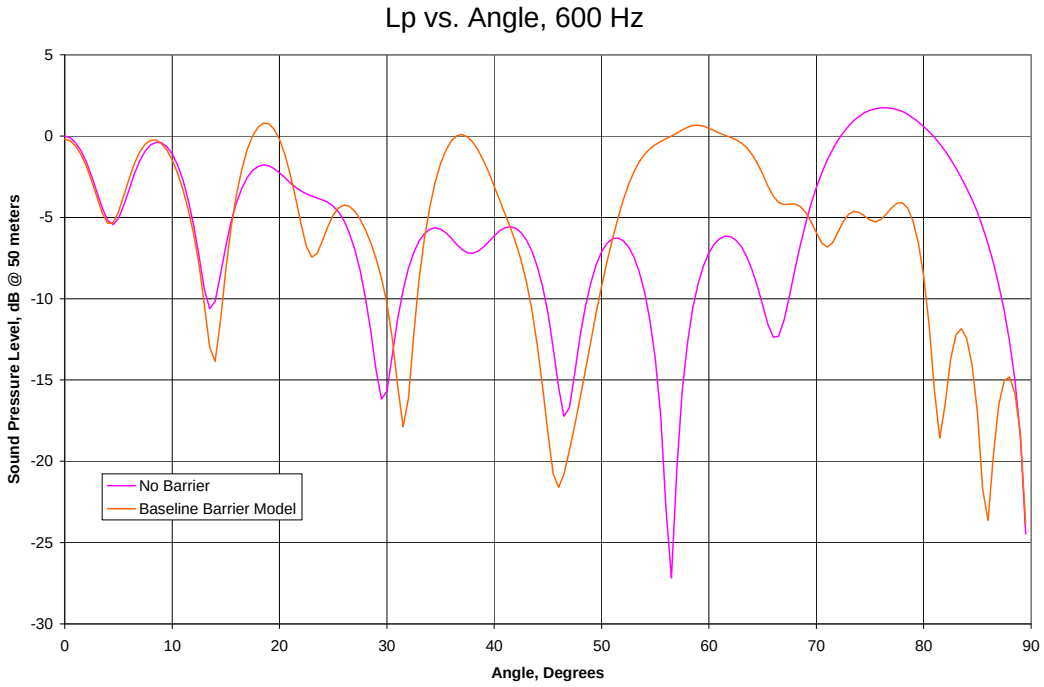

FIGURE 11: Barrier Effect for 2-D Deep Water Model, Deep Barrier

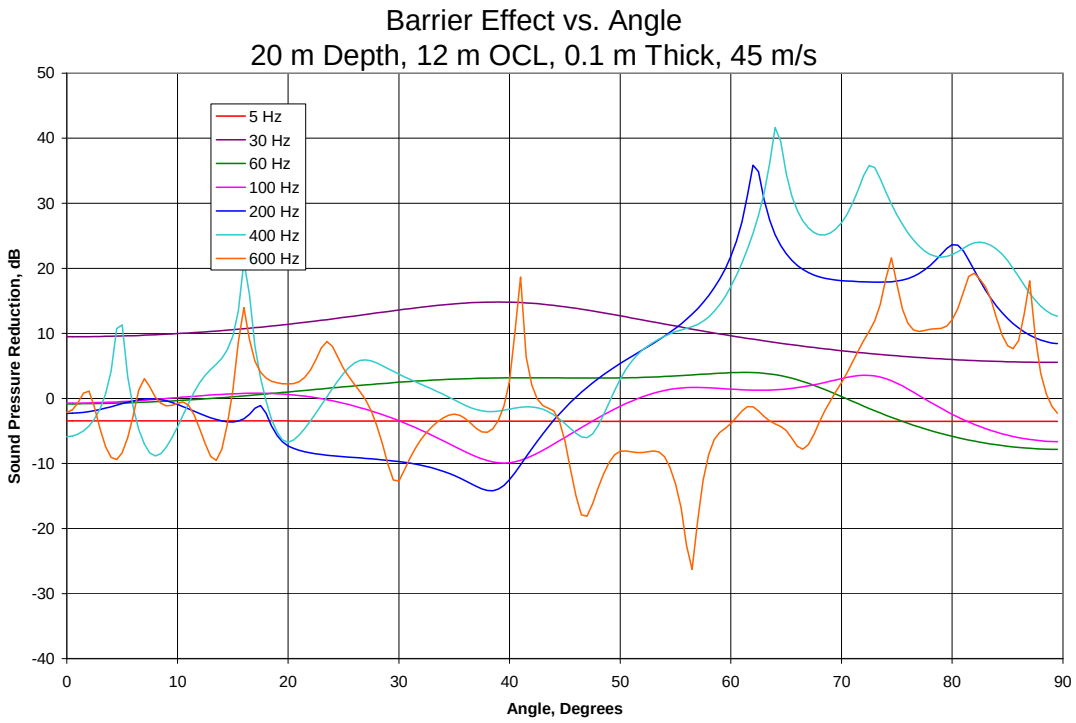

FIGURE 12: Barrier Effect for 2-D Deep Water Model, Shallow Barrier

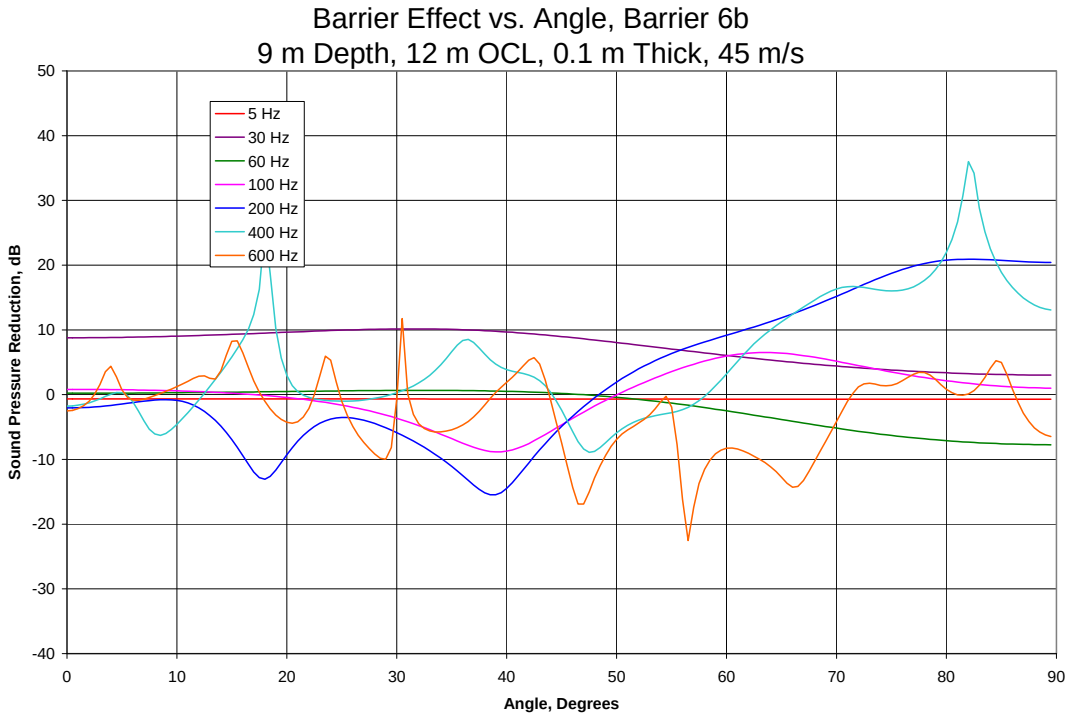

FIGURE 13: Barrier Effect for 2-D Deep Water Model, Close Barrier

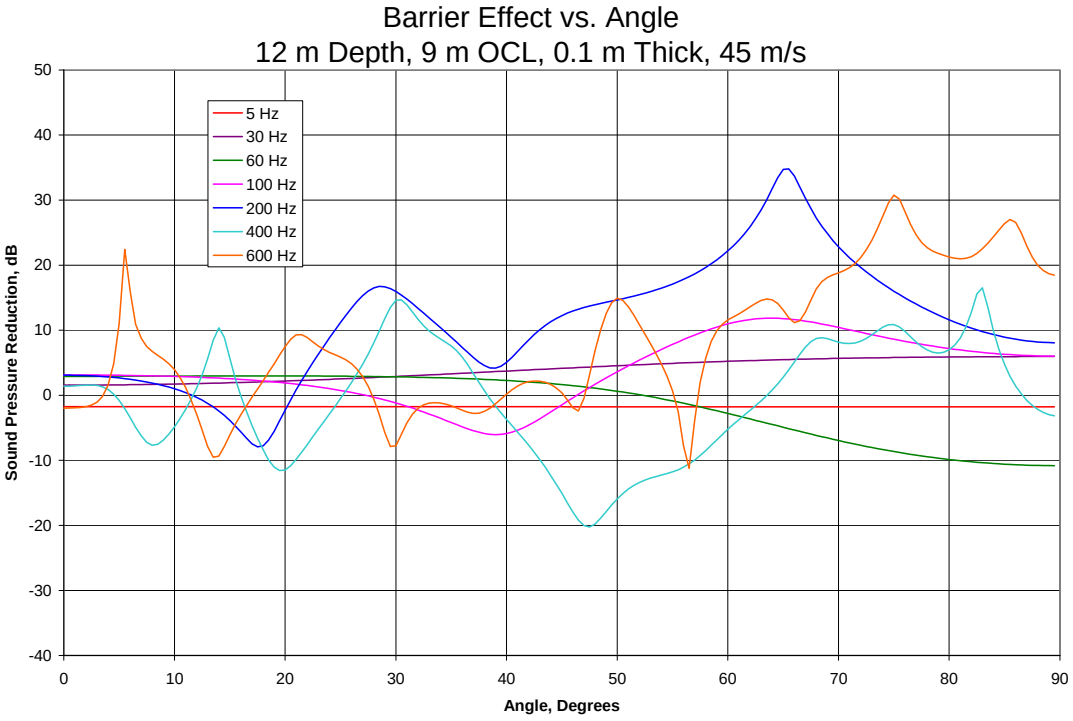

FIGURE 14: Barrier Effect for 2-D Deep Water Model, Far Barrier

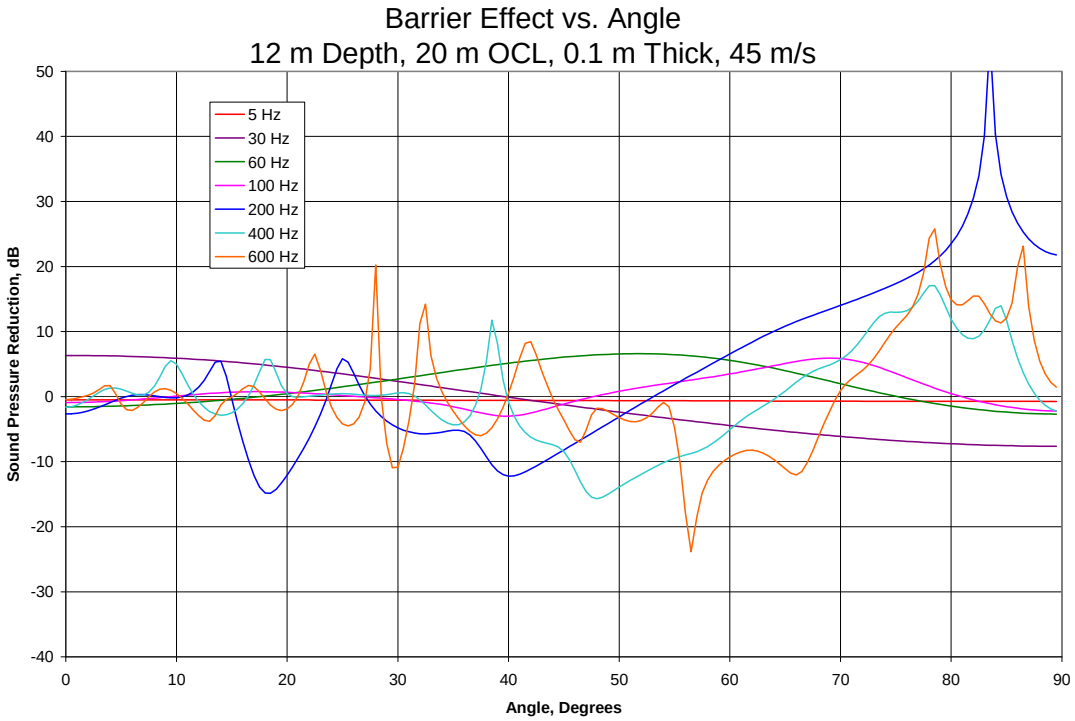

FIGURE 15: Barrier Effect for 2-D Deep Water Model, Low Saturation Barrier

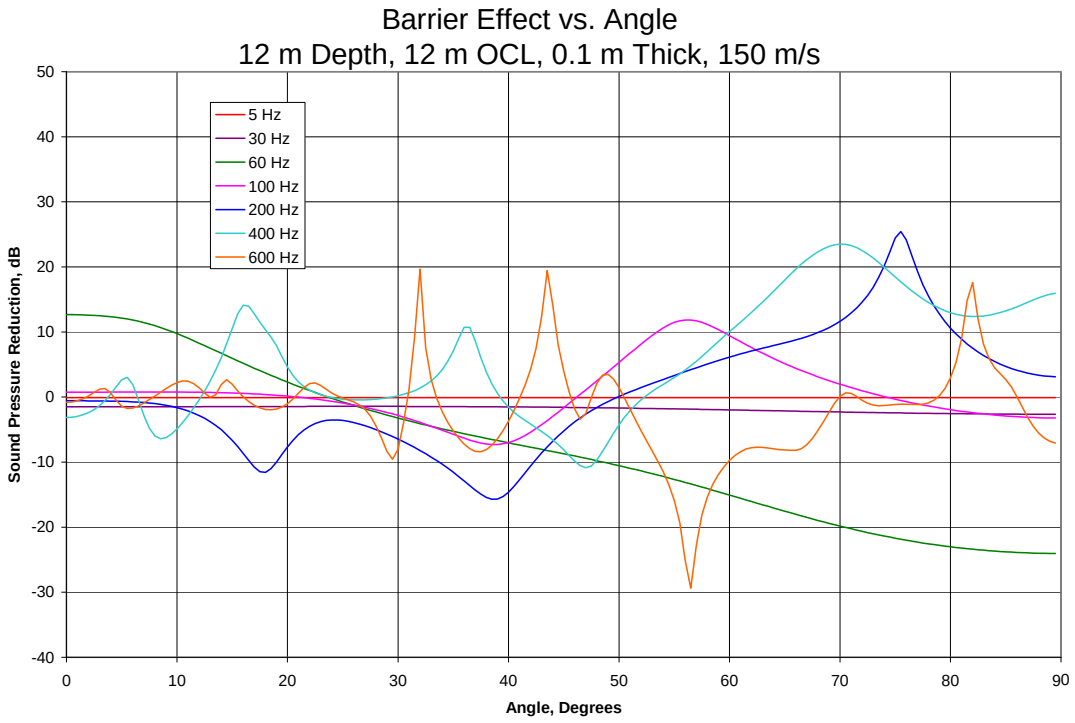

FIGURE 16: Barrier Effect for 2-D Deep Water Model, Thick Barrier

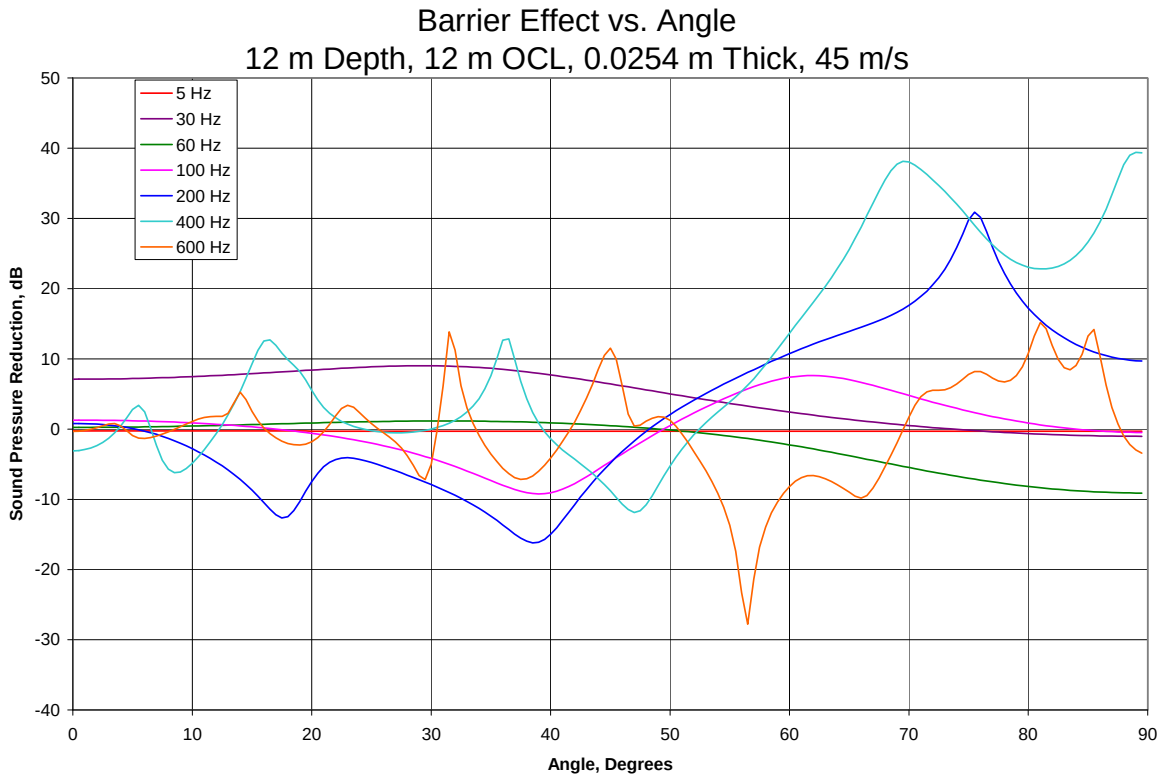

FIGURE 17: Barrier Effect for 2-D Deep Water Model, Optimized

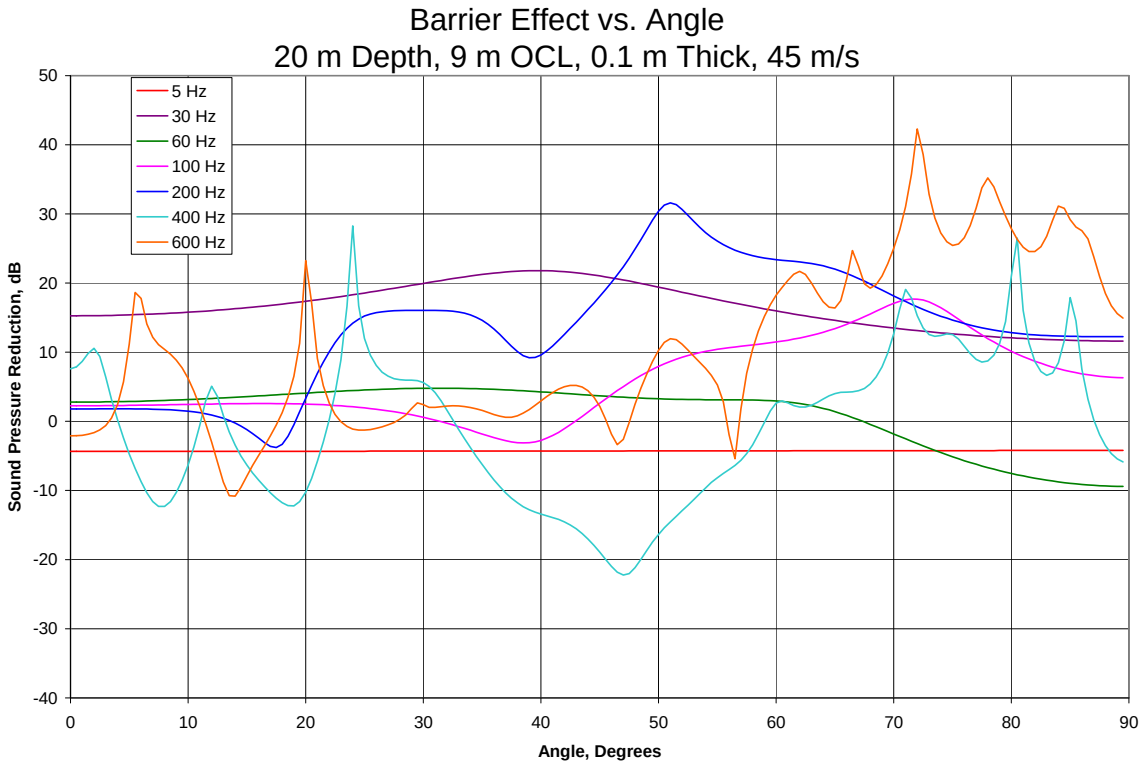

FIGURE 18: Sound Level in dB, 2-D Shallow Water (30 meter) Model, No Barrier, 600 Hz

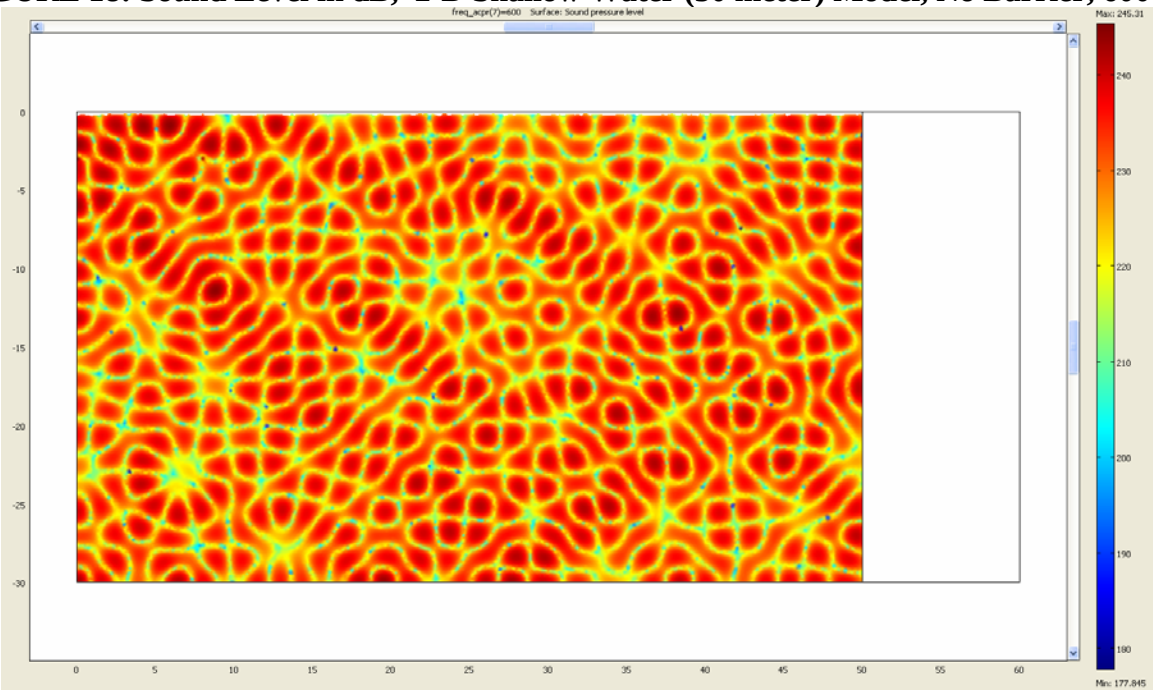

FIGURE 19: Barrier Effect for 2-D Shallow Water Model, 20 meter Depth

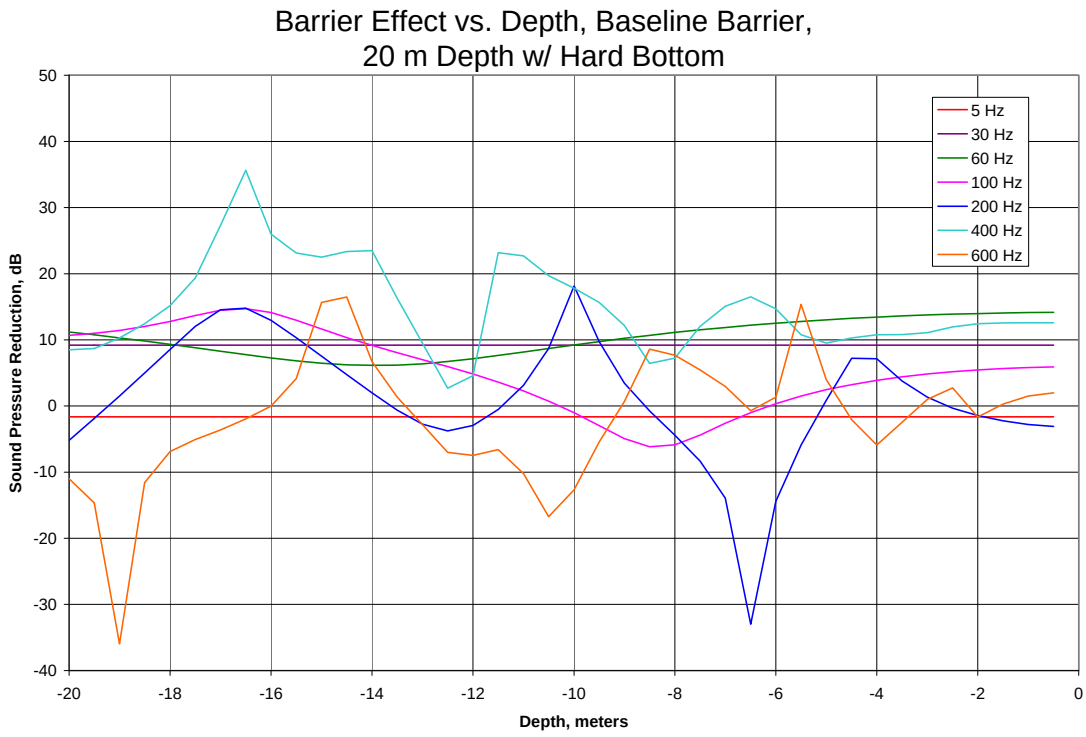

FIGURE 20: Barrier Effect for 2-D Shallow Water Model, 30 meter Depth

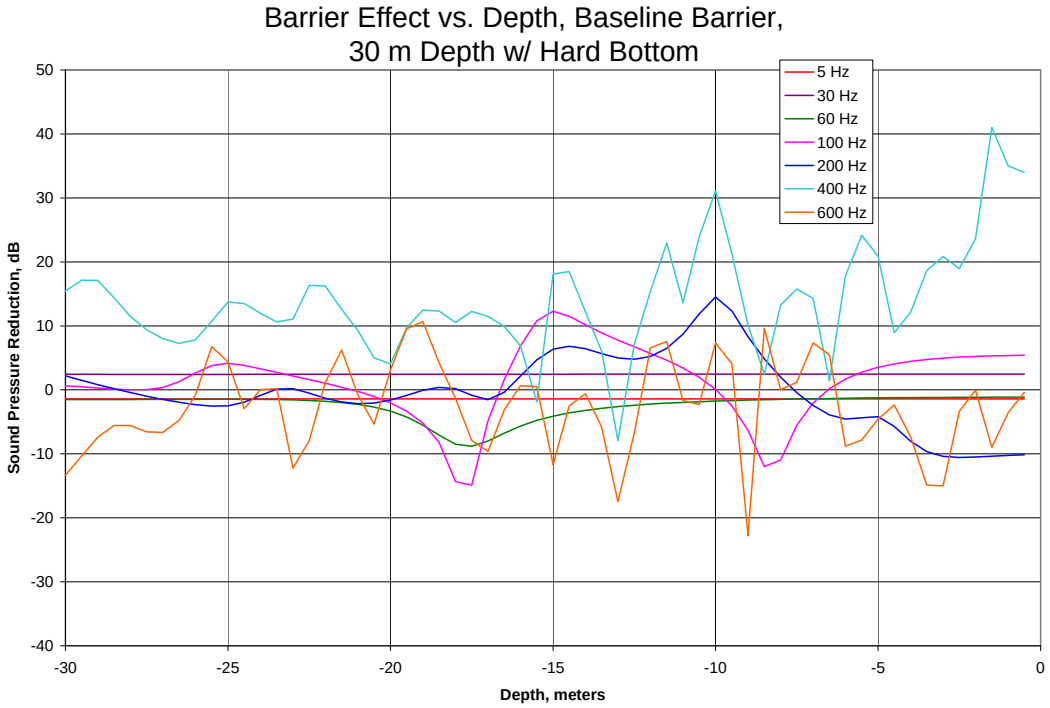

FIGURE 21: 2-D Model Results for Baseline Barrier vs. Pressure Release Surface

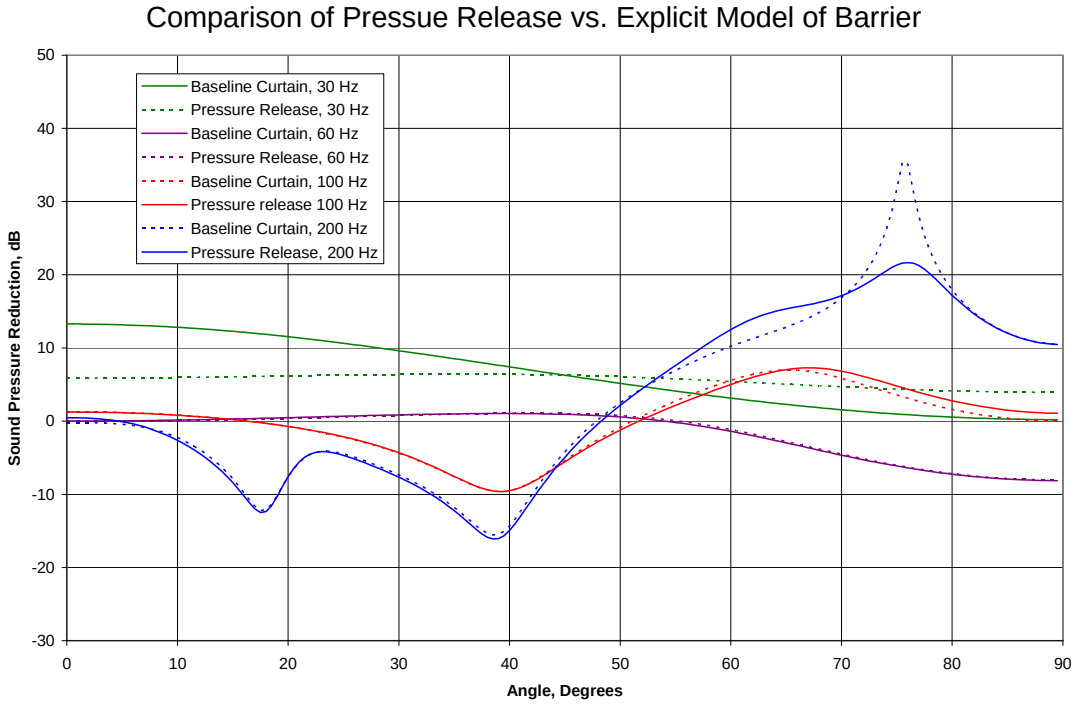

FIGURE 22: Comparison of 3-D vs. 2-D Model Results

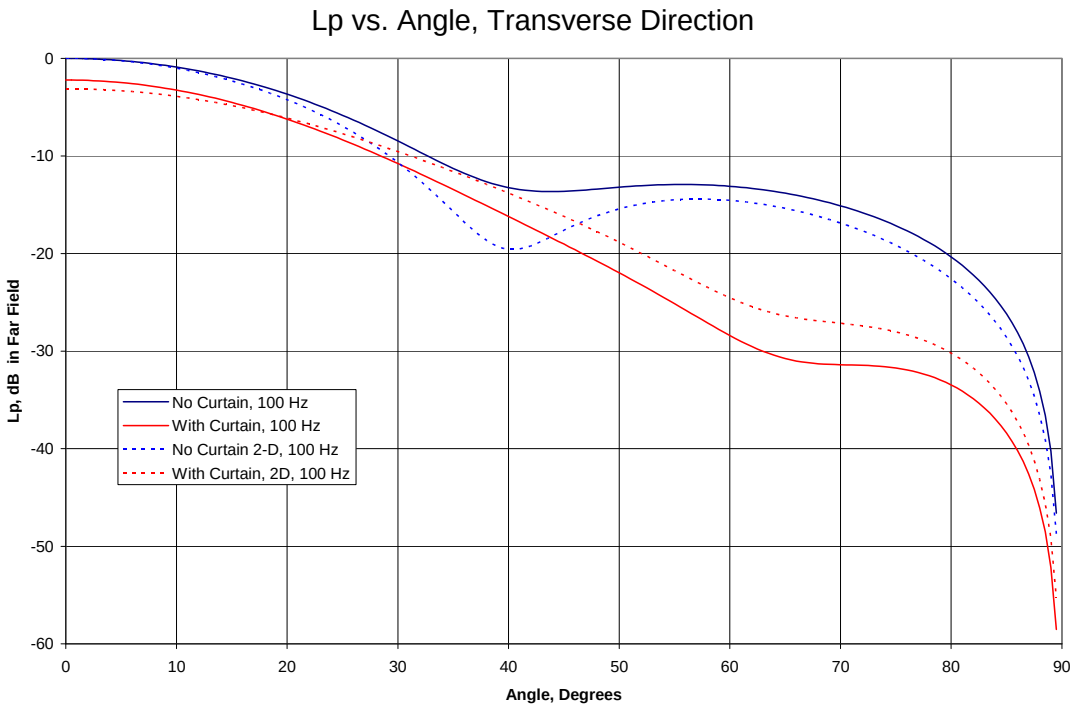

FIGURE 23: Plot of Results Extraction Locations

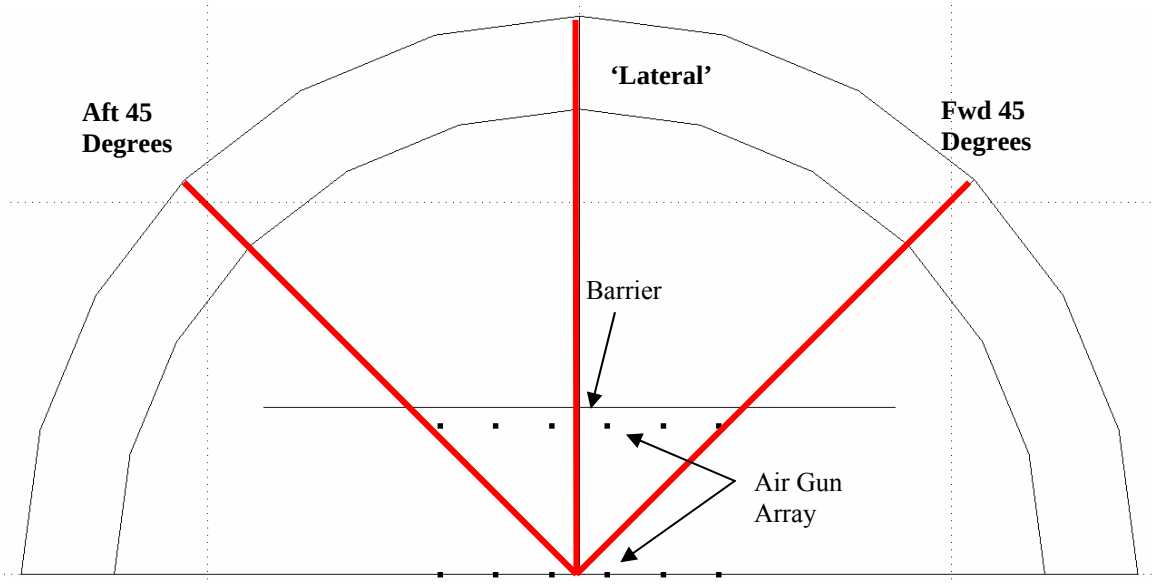

FIGURE 24: Barrier Effect for 3-D Model, 100 Hz

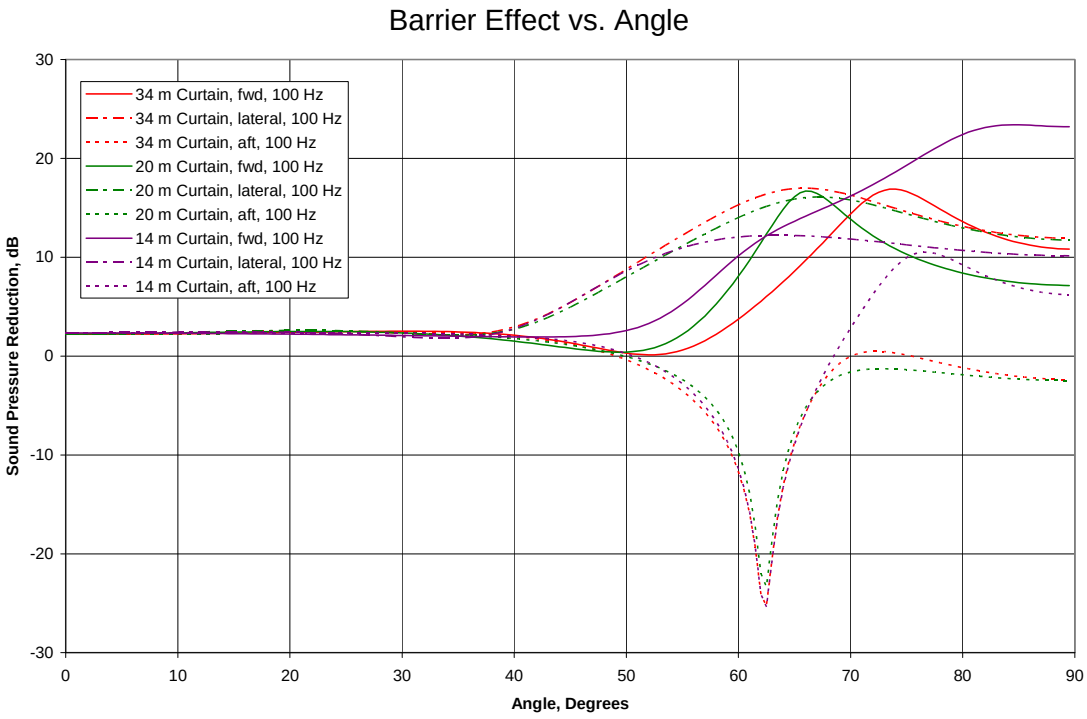

FIGURE 25: Barrier Effect for 3-D Model, 200 Hz

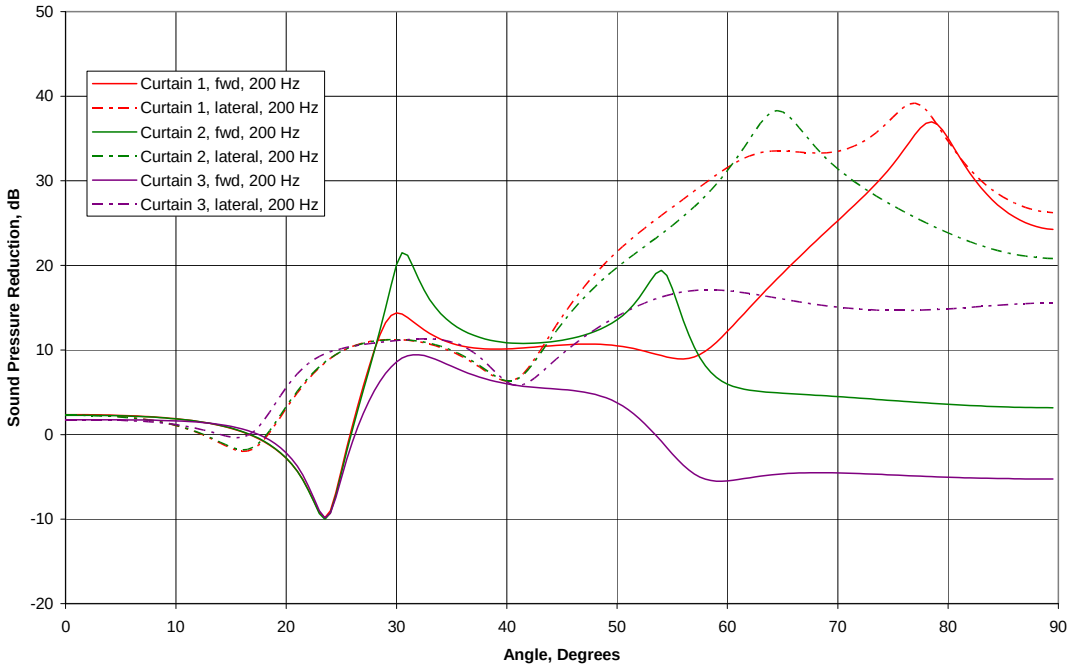

FIGURE 26: Concept Sketch of Parabolic Reflector

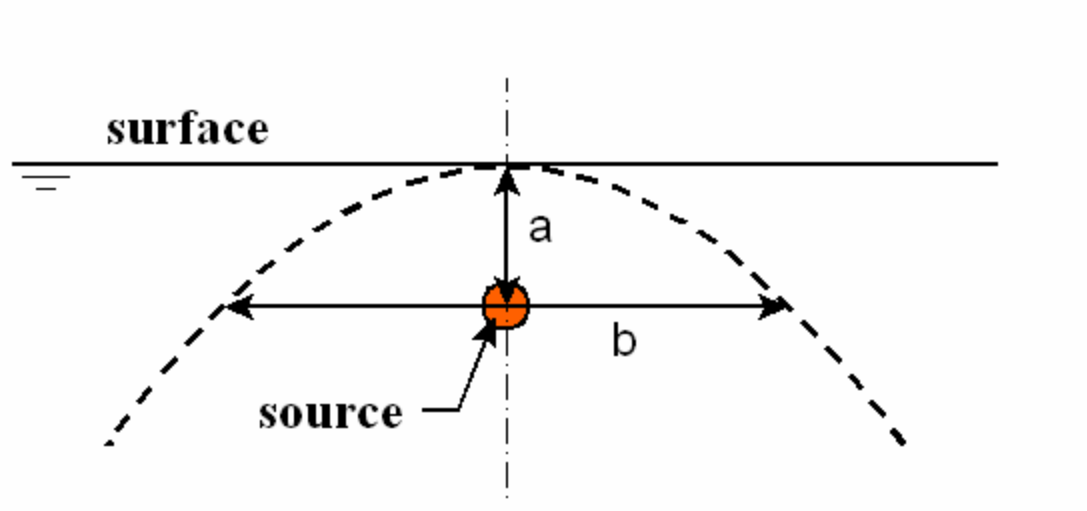

FIGURE 27: Example Parabolic Reflector Model

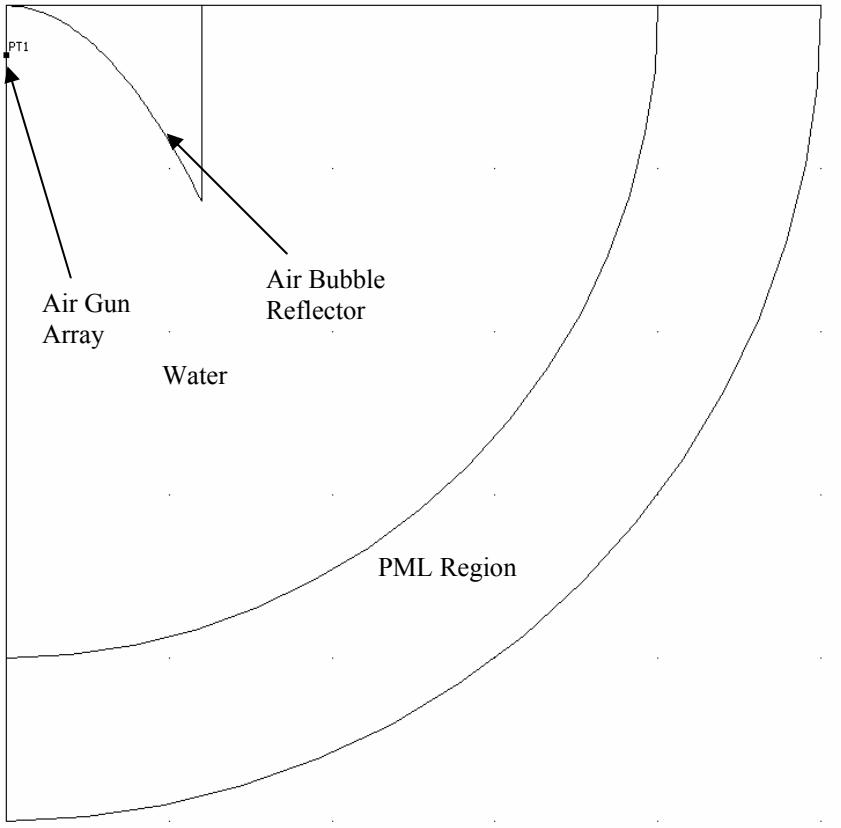

FIGURE 28: Lateral Directivity for Single Line Air Gun Array, 3 Meter Depth, No Reflector

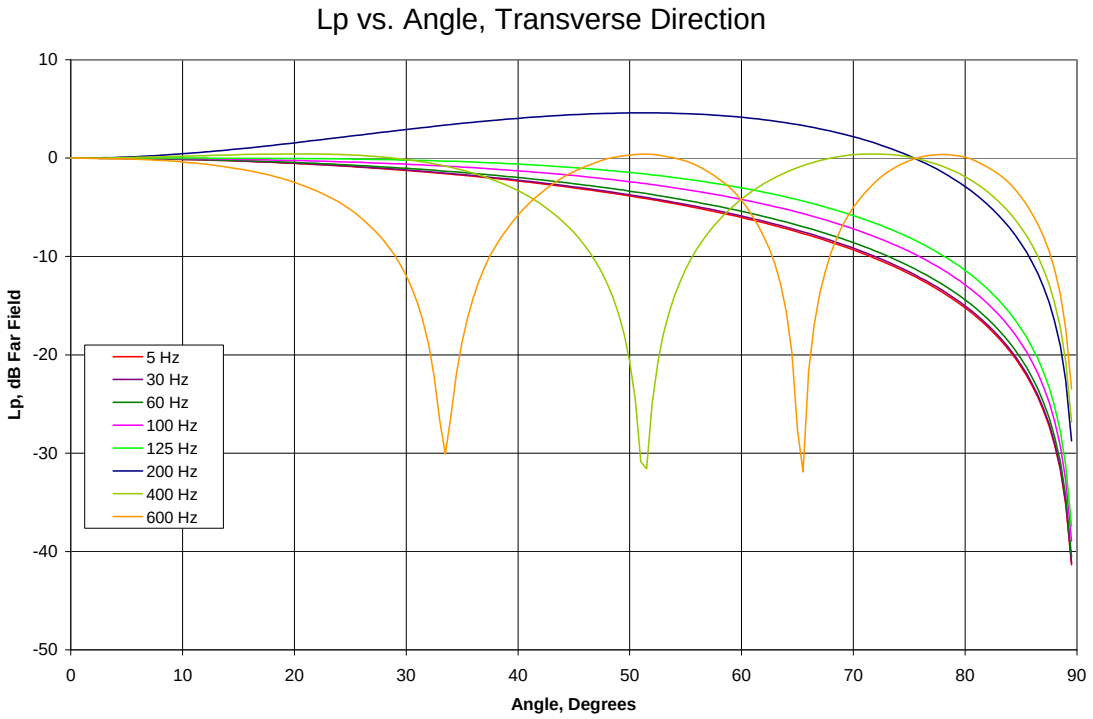

FIGURE 29: Reflector Effectiveness, 3 Meter Deep Array, Large Reflector

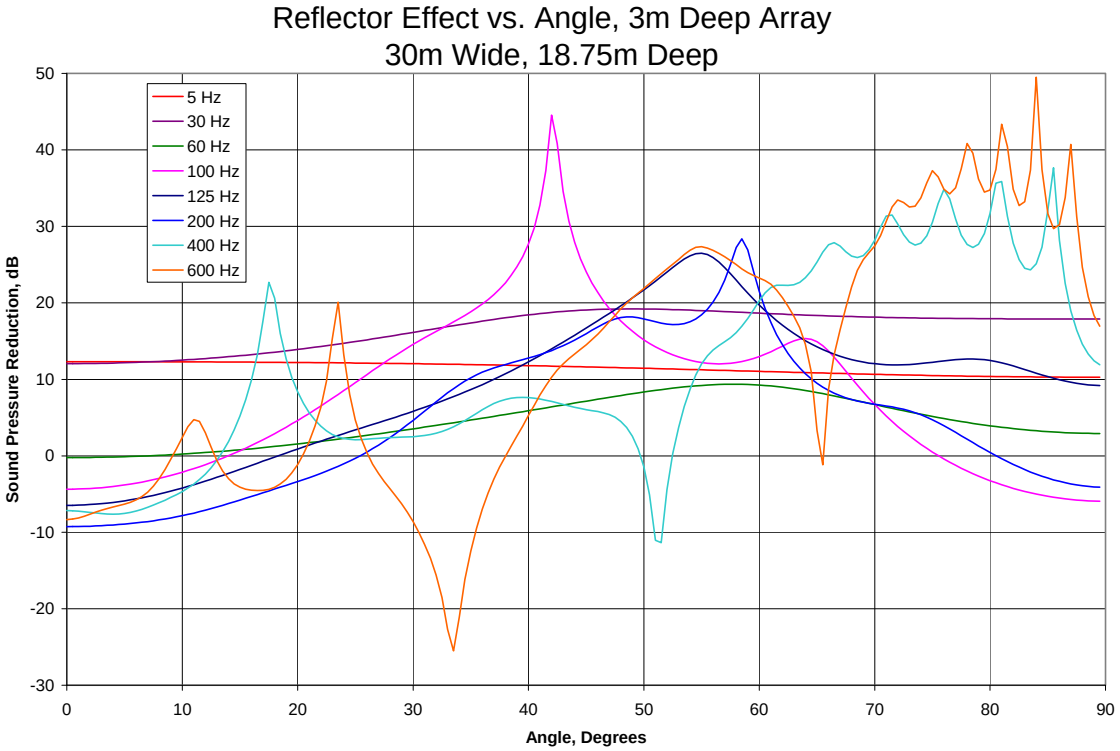

FIGURE 30: Reflector Effectiveness, 3 Meter Deep Array, Medium Reflector

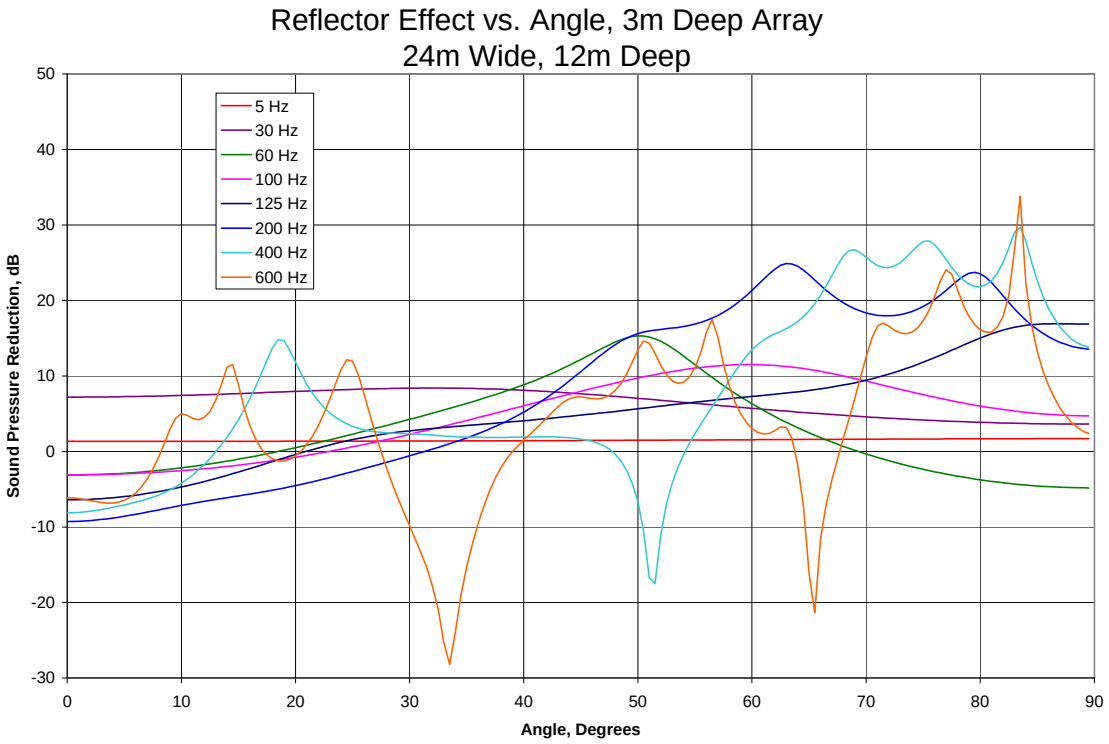

FIGURE 31: Reflector Effectiveness, 3 Meter Deep Array, Small Reflector

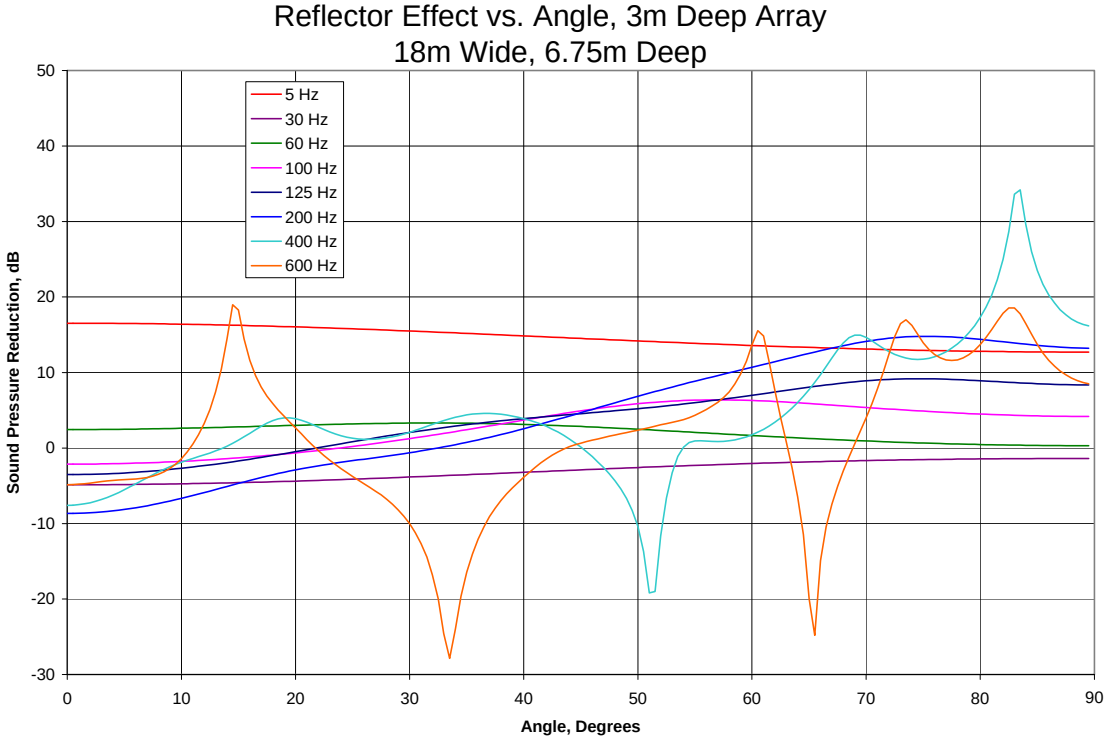

FIGURE 32: Reflector Effectiveness, 6 Meter Deep Array, Small Reflector

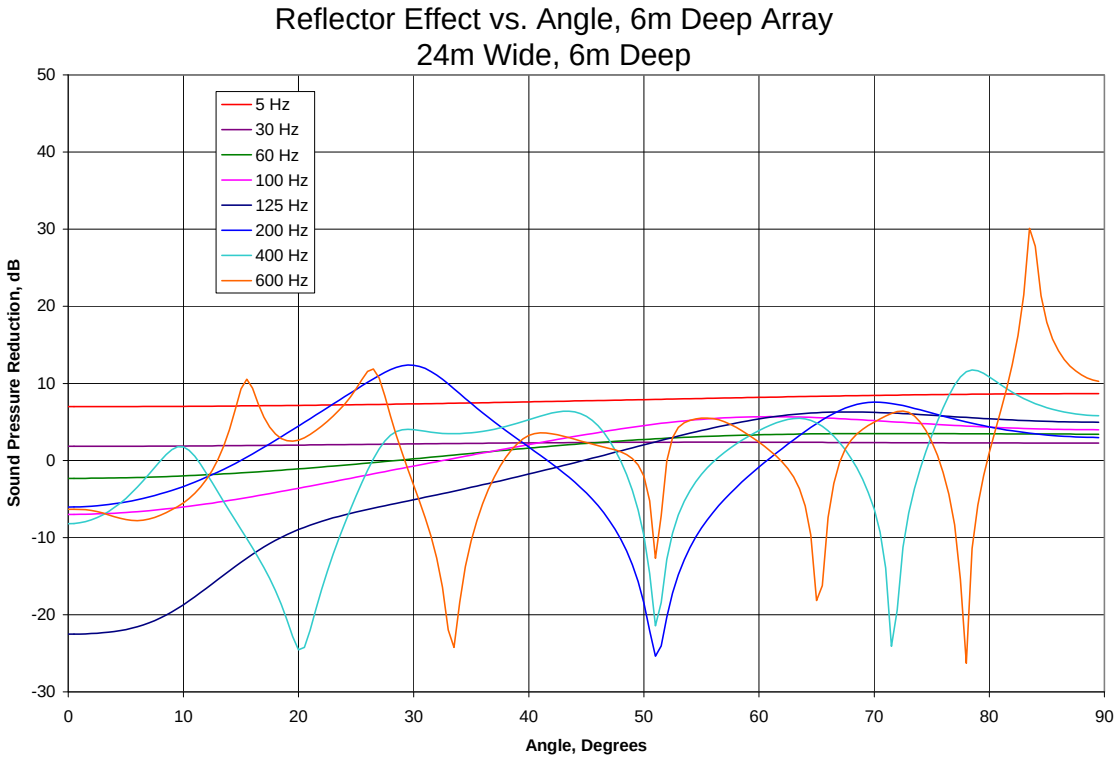

FIGURE 33: Reflector Effectiveness, 3 Meter Deep Array, Medium Reflector, 30 Meter Deep Water (Shallow)

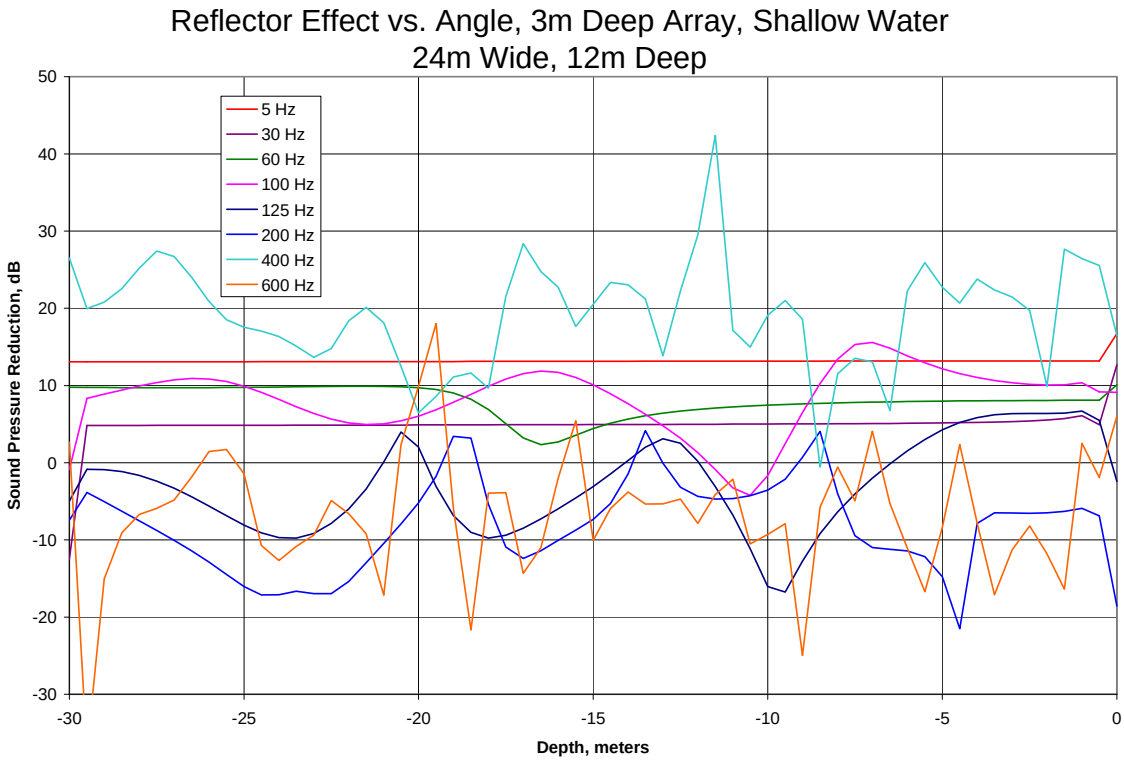

FIGURE 34: Reflector Effectiveness, 3 Meter Deep Array, Medium Reflector, Pressure Release Surface